DOE/ET-0058/3

WiFFEW

PE-16 Swelling

Alloy Development for Irradiation Performance

Quarterly Progress Report

JULY-SEPT 78 ~~January-March, 1978~~

May 1979

U.S. Department of Energy
Assistant Secretary for Energy Technology
Office of Fusion Energy

DOE/ET-0058/3
uc-20, 20c

Alloy Development for Irradiation Performance

Quarterly Progress Report
~~January-March, 1978~~

May 1979

U.S. Department of Energy
Assistant Secretary for Energy Technology
Office of Fusion Energy
Washington, DC 20545

Available from:

National Technical Information Service (NTIS)
U.S. Department of Commerce
5285 Port Royal Road
Springfield, Virginia 22161

Price: **Printed Copy: $ 6.50**
Microfiche: $ 3.00

FOREWORD

This report is the third in a series of Quarterly Technical Progress Reports on *"Alloy Development for Irradiation Performance"* (ADIP), which is one element of the Fusion Reactor Materials Program, conducted in support of the Magnetic Fusion Energy Program of the U.S. Department of Energy. Other elements of the Materials Program are:

- *Damage Analysis and Fundamental Studies (DAFS)*
- *Plasma-Materials Interaction (PMI)*
- *Special-Purpose Materials (SPM)*

The ADIP program element is a national effort composed of contributions from a number of National Laboratories and other government laboratories, universities, and industrial laboratories. It was organized by the Materials and Radiation Effects Branch, Office of Fusion Energy, DOE, and a Task Group on *Alloy Development* for *Irradiation Performance*, which operates under the auspices of that Branch. The purpose of this series of reports is to provide a working technical record of that effort for the use of the program participants, for the fusion energy program in general, and for the Department of Energy.

This report is organized along topical lines in parallel to a Program Plan of the same title so that activities and accomplishments may be followed readily relative to that Program Plan. Thus, the work of a given laboratory may appear throughout the report. Chapters 1, 2, 7, and 8 review activities on analysis and evaluation, test methods development, status of irradiation experiments, and corrosion testing and hydrogen permeation studies, respectively. These activities relate to each of the alloy development paths. Chapters 3, 4, 5, and 6 present the ongoing work on each alloy development path. The Table of Contents is annotated for the convenience of the reader.

This report has been compiled and edited under the guidance of the Chairman of the Task Group on *Alloy Development* for *Irradiation Performance*, E. E. Bloom, Oak Ridge National Laboratory, and his efforts, those of the supporting staff of ORNL and the many persons who made technical contributions are gratefully acknowledged. T. C. Reuther, Materials and Radiation Effects Branch, is the Department of Energy Counterpart to the Task Group Chairman and has responsibility for the ADIP Program within DOE.

Klaus M. Zwilsky, Chief,
Materials and Radiation Effects Branch
Office of Fusion Energy

CONTENTS

FOREWORD.. iii

1. ANALYSIS AND EVALUATION STUDIES 1

1.1 ENGINEERING PROPERTIES FOR NEAR TERM DESIGN AND ANALYSIS 2

Interim data needs to be established for candidate first wall/blanket structural materials to permit uniformity of near term design and structural analysis. During this quarter, procedures for establishing and disseminating the needed property values were examined and work was performed toward identifying the properties requiring immediate attention.

1.2 ASSESSMENT OF CYCLIC CREEP-FATIGUE OF FIRST-WALL STRUCTURAL MATERIAL 5

Application of strain range partitioning showed that use of appropriate tensile and creep-rupture ductilities enables reasonably good estimates of the influence of hold periods and irradiation on the fully reversed fatigue life of type 316 stainless steel. Ductility values for 20%-cold-worked type 316 stainless steel irradiated in a mixed-spectrum reactor were used to estimate fusion reactor first-wall lifetimes at neutron wall loadings from 2 to 5 MW/m^2. Conjectural results indicate a lifetime of 7.5 to 8.5 $MWyr/m^2$ for loadings not exceeding 2 MW/m^2; perhaps 10 $MWyr/m^2$ is possible since the wall will be under vacuum and the data base is for tests in air.

1.3 THE SENSITIVITY OF THE FIRST WALL RADIATION DAMAGE TO FUSION REACTOR BLANKET COMPOSITION 16

The atomic displacement and hydrogen and helium gas production rates in a IO-nun-thick type 316 stainless steel first wall have been calculated as a function of blanket composition in a typical one-dimensional fusion reactor model. For a 0.5-m-thick blanket, variations in the rates of atomic displacement and hydrogen and helium gas production of factors of 2.7, 1.3, and 1.2, respectively, were obtained. The damage also showed a systematic decrease with increasing first-wall thickness.

2. TEST MATRICES AND TEST METHODS DEVELOPMENT 19

2.1 DESIGN OF MATERIALS IRRADIATION EXPERIMENTS UTILIZING SPECTRAL TAILORING 20

The helium production to displacement per atom (He/dpa) ratio expected near or at the first wall of a fusion reactor for stainless steels and nickel-base alloys can be reasonably reproduced in "real" time in fission reactors as a result of the reactions $^{58}Ni(n,\gamma)^{59}Ni(n,\alpha)^{56}Fe$. The He/dpa ratio can be reproduced by intermittent modification of the thermal-to-fast neutron flux ratio since the He production will be dominated by the thermal flux and the fast flux will determine the dpa. This report summarizes neutronic calculations and experimental design considerations to determine: (1) the needed change in the thermal-to-fast ratio as a function of time, (2) the possibility of using the EBR-II in conjunction with the ORR, and (3) the configuration of the first experimental capsule.

3. PATH A ALLOY DEVELOPMENT – AUSTENITIC STAINLESS STEELS 25

3.1 THE EFFECT OF 200 at. ppm PREINJECTED HELIUM ON 20%-COLD-WORKED TYPE 316 STAINLESS STEEL IRRADIATED AT 625°C IN EBR-II 26

Type 316 stainless steel cold-worked 20% has been preinjected with 200 at. ppm He and irradiated in EBR-II at 625°C to a neutron fluence of 1.6×10^{26} n/m^2 (>0.1 MeV). The preinjected helium results in 1.2×10^{22} cavities/m^3 that are 5 nm in diameter, while the uninjected material contains no cavities. The preinjected helium results in nearly an order of magnitude more cavities, and these cavities are slightly smaller than those produced by irradiation of the same material in HFIR. Preinjected helium appears to have no effect on the dislocation structure that develops during irradiation. However, all cavities produced by helium preinjection are attached to dislocations, as is observed after HFIR irradiation.

3.2 TENSILE PROPERTIES OF HFIR-IRRADIATED TYPES 316 AND TiM 316 STAINLESS STEEL AT 200 TO 1000 at. ppm He 32

Tensile tests were performed on type 316 stainless steel, with and without 0.23 wt % Ti added, irradiated in the HFIR to simulate fusion reactor first-wall conditions. Both annealed and 20%-cold-worked materials were examined and hardened more rapidly than similar materials irradiated in EBR-II (containing only trace amounts of helium) but had comparable ductility for the fluences attained (2×10^{26} n/m^2, <0.1 MeV).

4. PATH B ALLOY DEVELOPMENT — HIGHER STRENGTH Fe-Ni-Cr ALLOYS 51

4.1 THE SWELLING OF NIMONIC PE-16 IRRADIATED IN HFIR 52

Swelling-tensile samples of Nimonic PE-16 were irradiated in HFIR at 55 to 700°C to produce simultaneously dpa levels from 2.2 to 16.7 and helium contents from 120 to 2960 at. ppm. These conditions resulted in <2% swelling. The maximum swelling, 1.92%, was found at 500°C in solution treated and aged material. The material solution treated only resisted swelling slightly more than aged material. Neither material showed very strong temperature dependence of swelling. There was no rapid, break-away swelling above 600°C, as observed in type 316 stainless steel and alloy 600. The fluence dependence of the swelling suggests that an "incubation period" precedes significant swelling.

5. PATH C ALLOY DEVELOPMENT — REACTIVE AND REFRACTORY ALLOYS . . . 63

6. PATH D ALLOY DEVELOPMENT — INNOVATIVE MATERIAL CONCEPTS 65

7. STATUS OF IRRADIATION EXPERIMENTS 67

7.1 STATUS OF IRRADIATION EXPERIMENTS 68

The irradiation of ORR-MFE-1 was completed June 28, 1978 with an irradiation of 72,698 MWh (261.71 TJ). The experiment has been disassembled, and the specimens are being examined. Irradiation of ORR-MFE-2 began September 1, 1978, and it has accumulated an exposure of 16,212 MWh (58.363 TJ).

7.2 ETM RESEARCH MATERIALS INVENTORY 72

7.3 IRRADIATION EXPERIMENT SCHEDULE 76

8. CORROSION TESTING AND HYDROGEN PERMEATION STUDIES 83

8.1 CAPSULE TESTS OF TYPE 316 STAINLESS STEEL IN NITROGEN-CONTAMINATED LITHIUM 84

Approximately 2 wt % N in lithium significantly enhanced the degradation of type 316 stainless steel, with the corrosion rate decreasing as a function of time. At 500°C, the corrosion was uniform, while at 600 and 700°C, grain boundary attack dominated. As-rolled type 316L stainless steel had worse corrosion resistance to nitrogen-contaminated lithium than fully annealed type 316. We do not know whether the decreased resistance is attributable to differences in microstructure or alloy composition. While the corrosion of type 316 stainless steel in Li–2% N is more severe than in relatively pure lithium, such effects are expected to be transient in a closed system.

8.2 THERMAL-CONVECTION LOOP TESTS OF STAINLESS STEEL IN LITHIUM.. 92

Type 316 stainless steel thermal convection loops containing molten lithium are being used to investigate the effect of time on corrosion rates in lithium. Corrosion rates are initially time dependent, decreasing up to *2000* h, and constant after approximately *2000* h. Absolute weight losses among three loops were quite reproducible at short exposures (500 h) but diverged at longer times.

8.3 COMPATIBILITY OF BLANKET, COOLANT, AND TRITIUM-PROCESSING SALTS 99

A type 316 stainless steel thermal convection loop recently began operation with the proposed tritium-processing salt LiF-LiCl-LiBr. Two additional thermal convection loops are being used to study the corrosion properties of Li_2BeF_4 and $NaNO_2$-KNO_3-$NaNO_3$.

8.4 HYDROGEN PERMEATION CHARACTERISTICS OF PATH A, PATH B, AND PATH C ALLOYS 101

The hydrogen dissolution and permeation characteristics of the 5621S alloy of titanium have been evaluated. This alloy was found to have a permeability of approximately 3000 times greater than that of conventional 300-series stainless steels. The observation of a pressure dependence somewhat greater than half-power was construed as evidence for a permeation process that is partially limited by surface impurity effects. Roughly determined values for the solubility of hydrogen in the 5621S alloy were in the range of those reported for Ti—6% Al—4% V. The surface condition and mechanical integrity of the 5621S membrane appeared to be unaffected by approximately 2000 h of hydrogen infiltration under typical power-reactor plasma-chamber conditions with respect to temperature, gas pressure, and gas composition.

1. ANALYSIS AND EVALUATION STUDIES

The designs for power-producing fusion reactors are in a very embryonic and rapidly changing state. Requirements for materials performance are thus not well defined. However, regardless of the final designs, the environment will clearly be extremely demanding on materials in regions of high neutron flux. One cannot identify a class of alloys on which the development efforts should focus — thus the parallel paths of the Alloy Development Program. The combination of reactor designs that are evolving and the necessity for including alloys with widely different physical, chemical, and mechanical properties in the program could lead to an impossibly large number of potential problems and possible solutions. Analysis and evaluation studies are an essential part of the Alloy Development Program in order to translate fusion reactor performance goals into material property requirements and to identify crucial and generic problems on which development activities should be focused. As the Alloy Development Program proceeds and a better understanding of the behavior of materials in potential fusion reactor environments is attained, these studies will also identify problems that will necessitate design solutions.

1.1 ENGINEERING PROPERTIES FOR NEAR TERM DESIGN AND ANALYSIS -

J. W. Davis, B. A. Cramer and D. L. Kummer (McDonnell Douglas Astronautics Company - St. Louis) and R. E. Gold (Westinghouse Electric Corporation) and D. L. Smith (Argonne National Laboratory) and F. W. Wiffen (ORNL)

1.1.1 ADIP Task

Task Number l.A.l - Define Material Property Requirements and Make Structural Life Predictions.

1.1.2 Objective

Define and disseminate material properties for use in performing near term design and structural analysis of first wall/blanket components.

1.1.3 Summary

Detailed design and structural analysis of first wall/blanket components is increasing, as large test facilities having reactor like requirements, such as ETF, move closer to reality. Also several studies are addressing the design of long life or even optimized first wall/blanket components for application to a demonstration or commercial reactor. These studies and analyses require the use of material property data that most appropriately reflect the behavior of materials in the reactor environment.

There has been little effort to establish recommended material properties for use in the interim until additional testing has been performed. This has caused individual investigators to independently select property values. This has led to a wide range of conclusions regarding first wall life, failure modes, design effects on life and failure modes, and the outlook for different classes of material candidates.

Since crack growth rate was identified about two years ago as a dominate failure mode, it has received considerable attention. Available data for one of the most completely characterized candidate materials, 316 stainless steel shows crack growth rate to be a function of temperature, environment, and hold time. Interpretation of the existing data in terms of the fusion environment has resulted in greatly different property

values such that life predictions for a given design and set of operating conditions can vary from 4 to 190 years. This is one example of the need to establish recommended property values for use in interim design and analysis.

During this quarter, procedures for establishing and disseminating the needed property values were examined. In addition, work was performed toward identifying the properties requiring immediate attention.

1.1.4 Progress and Status

Discussions between various ADIP Task Group members and with R. A. Moen, Nuclear Systems Materials Handbook (NSMH), Vice Chairman, indicated that NSMH format and procedures could be used. Specifically, the practices used by the CRBRF' Materials Task Group for establishment and dissemination of INTERIM DATA pages appear appropriate to meet fusion requirements. This procedure would consist of the major steps as follows:

a) Preparation of an INTERIM DATA page in NSMH format by a fusion materials person.

b) Rapid review by ADIP Task Group.

c) Submittal directly to NSMH Committee Members.

d) NSMH Committee Members comments to R. A. Moen within a few days.

e) Resolution of differences coordinated by R. A. Moen.

f) Approved INTERIM DATA page disseminated directly to appropriate individuals by author.

g) Submittal of INTERIM DATA page NSMH individual responsible for follow-up.

h) INTERIM DATA page distributed quarterly to NSMH holders.

The next steps are to: 1) obtain ADIP approval of the proposed procedure, 2) identify and prioritize the properties to be addressed and 3) obtain commitments from individuals for INTERIM DATA page preparation.

An initial definition of property and priority is given as follows:

INITIAL PROPERTIES *AND* PRIORITIES FOR INTERIM DATA PAGES

	MATERIAL			
	SS	Ni	Ti	Nb, V
FISSION/FUSION SPECTRUM ADJUSTMENT	1	1	3	2
FLAW GROWTH RATE, K_{Ic}, AND K_C	1	1	2	3
TENSILE PROPERTIES				
UNIRRADIATED		1	1	1
IRRADIATED	1	1	2	2

NOTE: SPECIFIC ALLOYS MUST BE SELECTED

1 = FIRST PRIORITY

1.1.5 Conclusions

The NSMH format and procedures appear appropriate for establishing and disseminating INTERIM DATA pages covering fusion reactor structural materials.

1.2 ASSESSMENT OF CYCLIC CREEP-FATIGUE OF FIRST-WALL STRUCTURAL MATERIAL — K. C. Liu, C. R. Brinkman, and M. L. Grossbeck (ORNL)

1.2.1 ADIP Task

Task I.A.l, Define Material Property Requirements and Make Structural Life Predictions.

1.2.2 Objective

The objective of this subtask is to identify materials engineering problem areas and needs as well as to assess the practical implementation of existing design rules and criteria to fusion reactor systems. Specific and basic materials property requirements for MFE applications will be identified for inclusion in a materials development and engineering test plan to provide essential information in support of MFE research and development effort.

1.2.3 Summary

Application of strain range partitioning showed that use of appropriate tensile and creep-rupture ductilities enables reasonably good estimates of the influence of hold periods and irradiation on the fully reversed fatigue life of type 316 stainless steel. Ductility values for 20%-cold-worked type 316 stainless steel irradiated in a mixed-spectrum reactor were used to estimate fusion reactor first-wall lifetimes at neutron wall loadings from 2 to 5 MW/m^2. Conjectural results indicate a lifetime of 7.5 to 8.5 $MWyr/m^2$ for loadings not exceeding 2 MW/m^2; perhaps 10 $MWyr/m^2$ is possible since the wall will be under vacuum and the data base is for tests in air.

1.2.4 Progress and Status

Several methods that presently look particularly promising for estimating time-dependent fatigue life of irradiated materials include strain range partitioning,[1] frequency separation,[1] and the damage rate approach.[2] The latter two methods require considerable data in order to define material parameters. Presently, a satisfactory irradiated material data base does not exist from which to assess the applicability of the

latter two methods. In the case of the method of strain range partitioning, it has been proposed[3,4] that the influence of an environment such as irradiation be approximated by a ductility scaling or normalization process.

The objective of current efforts is to demonstrate application of the method of strain range partitioning for estimating time-dependent creep-fatigue behavior of irradiated materials and possibly use it to predict lifetime of a first wall of a fusion reactor. The first part of this objective was accomplished by using available postirradiation fatigue, tensile, and creep data, as will now be discussed.

Predictions of expected fatigue life were made using the interaction damage rule given by:

$$\frac{1}{N_{\text{pred}}} = \frac{1}{\Delta\varepsilon_{in}}\left(\frac{\Delta\varepsilon_{pp}}{N_{pp}} + \frac{\Delta\varepsilon_{pc}}{N_{pc}} + \frac{\Delta\varepsilon_{cp}}{N_{cp}} + \frac{\Delta\varepsilon_{cc}}{N_{cc}}\right) \tag{1}$$

where:

$\Delta\varepsilon_{in}$ = total inelastic strain range
$\Delta\varepsilon_{pp}$ = tensile plastic strain reversed by compressive plastic strain
$\Delta\varepsilon_{pc}$ = tensile plastic strain reversed by compressive creep strain
$\Delta\varepsilon_{cp}$ = tensile creep strain reversed by compressive plastic strain
$\Delta\varepsilon_{cc}$ = tensile creep strain reversed by compressive creep strain
N_{pred} = predicted cyclic life

N_{pp}, N_{pc}, N_{cp}, *and* N_{cc} are determined from the life relationships, which have a general form

$$N_{xy} = A_{xy}(\Delta\varepsilon_{in}/D_x)^{-B_{xy}} \quad , \tag{2}$$

in which A_{xy} and B_{xy} are material constants and D_x is the appropriate creep or tensile true ductility. Tensile and creep ductilities[5,6] for solution annealed type 316 stainless steel at 593°C are plotted in Fig. **1.2.1** as a function of minimum creep rate or tensile strain rate for material in the irradiated and unirradiated conditions. Calculated values of cycles to failure are compared with actual cycle lives in Table 1.2.1.

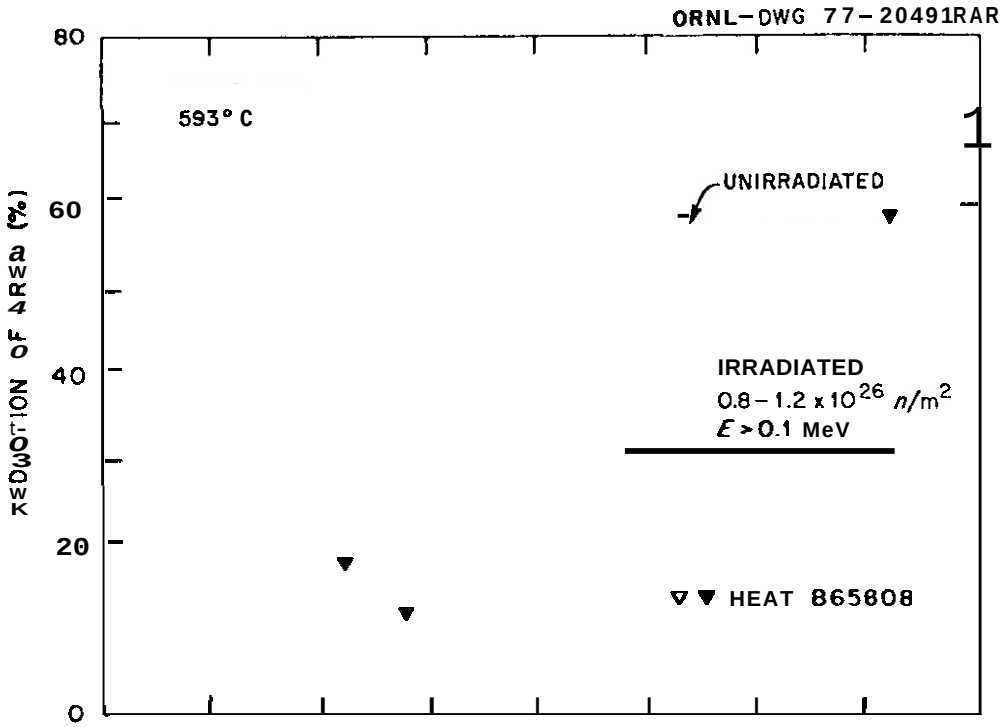

Fig. 1.2.1. Ductility as a Function of Strain Rate and Condition for Type 316 Stainless Steel (Based on refs. 5 and 6).

Comparing the actual cyclic lives in Table 1.2.1 for tests that were conducted both with and without a hold period for a given strain range shows that hold periods were very deleterious with respect to reducing fatigue life for this material in the irradiated condition. Accordingly, considering the magnitude of the reduction and the many uncertainties, comparisons between actual and calculated or estimated fatigue life generally show good agreement, as shown in Fig. 1.2.2.

Having demonstrated applicability of the method to predict post-irradiation fatigue behavior with a limited data base, the concepts were applied in estimating behavior of a first wall in a fusion reactor system.

An infinitely large thin-walled plate of 20%-cold-worked type 316 stainless steel 3 mm in wall thickness was used as a simplified first-

Table 1.2.1. Comparison of Actual and Predicted Cyclic Lives for Irradiated Type 316 Stainless Steel[a] Tested at 593°C

Total Strain Range (%)	Tensile Hold Time[b] (h)	Fluence, E > 0.1 MeV, at 580–610°C (n/m^2)	Inelastic Strain Range components, %			Lifetime Cycles	
			$\Delta\varepsilon_{in}$[c]	$\Delta\varepsilon_{pc}$[d] or $\Delta\varepsilon_{cp}$	$\Delta\varepsilon_{pp}$	Actual	Calculated from Actual $\Delta\varepsilon_{pp}$ Values
2.0	0	2.48×10^{8}	1.33	0	1.38	468	380
0.98	0	1.98	0.40	0	0.40	942	1,230
0.50	0	2.10	0.00	0	0.30	15,040	14,335
2.13	0.01 [C]	1.50	1.48	0.03	1.45	345	328
0.51	0.01	1.02	0.07	0.009	0.061	4 621	892
2.0	0.1	2.21	1.40	0.05	1.35	50	20
1.99	0.1 [C]	1.56	1.41	0.04	1.37	495	333
1.0	0.1	2.25	0.43	0.02	0.41	88	112
0.5	0.1	1.85	0.08	0.006	0.074	757	1,129
2.0	0.5	1.98	1.39	0.07	1.32	12	15
1.0	0.5	2.14	0.50	0.02	0.48	60	100
2.0	3.0	1.90	1.44	0.09	1.35	10	11
1.0	3.0	2.63	0.52	0.04	0.48	27	51

[a]Before irradiation material was solution annealed at 1075°C followed by a helium quench, and all material was from heat B6580. Data from Ref. 5.

[b][C] refers to compressive hold time.

[c]Young's Modulus, $E = 1540 \times 10^{5}$ MPa.

[d]Calculated from peak and relaxed stress values measured from hysteresis loops.

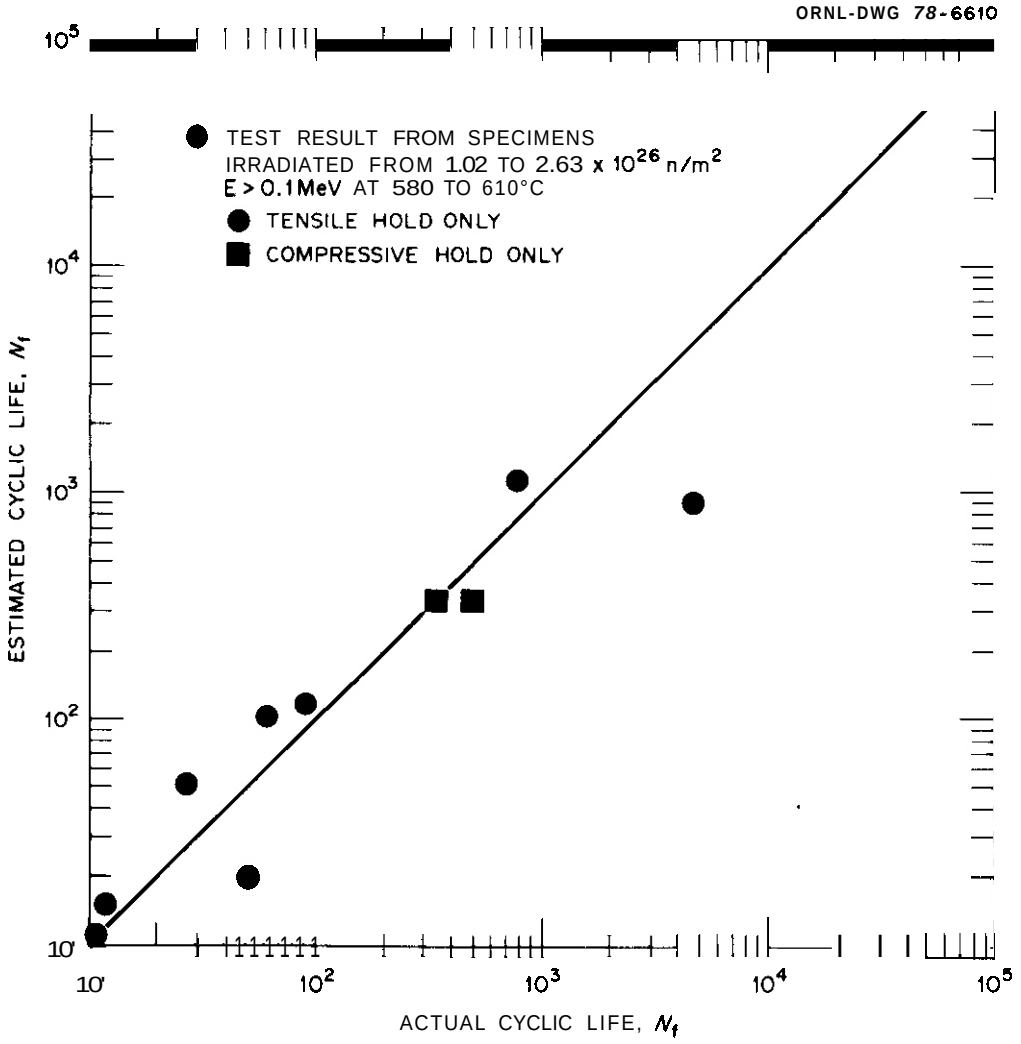

Fig. 1.2.2. Comparison of Estimated and Actual Cyclic Lives for Irradiated Stainless Steel Tested at 593°C.

wall model, as shown in Fig. 1.2.3. Alpha and neutron heating from the plasma radiation are respectively deposited on the surface and the inside of the first wall. A simplified duty cycle, also shown in Fig. 1.2.3, was assumed to calculate temperature changes at the plasma side of the first wall under various degrees of neutron wall loading and various plasma burn periods. The temperature at the cold side of the first wall was kept at 400°C and the temperature change through the wall was then calculated.

Thermal stress-strain calculations were then made, assuming equibi-axial loading, and the results are summarized in Table 1.2.2. There $\Delta\varepsilon_{pc}$

Table 12.2. Estimated Inelastic Strain Range Components and Predicted Cyclic Creep-Fatigue Lives for Fusion First Wall Using 20%-Cold-Worked Type 316 Stainless Steel

Wall Loading (MW/m^2)	Duration of Plasma Burn (min)	Temperature at Plasma Side (°C)	Total Strain Range (%)	Inelastic Strain Range Components,[a] %			Calculated Lifetime, Cycles, Based on			Calculated Lifetime ($MWyr/m^2$)	Estimated Lifetime[c] (years)
				$\Delta\varepsilon_{pp}$	$\Delta\varepsilon_{pc}$	$\Delta\varepsilon$	$\Delta\varepsilon_{pc}$ Without Radiation Effect	$\Delta\varepsilon_{pc}$ with Radiation Effect	$\Delta\varepsilon_{pp}$[b]		
2	1	480	0.457	0	0.000135	1.393	2.696×10^7	2.236×10^7	49	8.51	9.11
	3	480	0.457		0.000344		5.654×10^6	0.672×10^6		7.66	6.35
	5	480	0.457		0.000474		3.310×10^6	0.400×10^6		7.61	5.98
3	3	519	0.234	0	0.00119	1.443	6.617×10^5	2.390×10^5	46	4.09	2.33
	7	519	0.204		0.00182		3.255×10^5	1.086×10^5		4.34	2.24
	11	519	0.234		0.00229		2.218×10^5	0.712×10^5		4.47	2.24
4	5	556	0.310	nil	0.0118	1.491	1.335×10^4	1.274×10^4	4	0.48	0.20
	9	556	0.310		0.0149		0.904×10^4	0.854×10^4		0.59	0.22
	13	556	0.310		0.0173		0.705×10^4	0.661×10^4		0.65	0.25
5	7	593	0.461	nil	0.0388	1.534	1696	1690	42	0.11	0.036
	13	593	0.461		0.0465		1254	1250		0.15	0.047
	19	593	0.461		0.0519		1044	1040		0.19	0.056

[a] Effective strains based on equibiaxial strain condition.

[b] Indicates time-independent inelastic strain resulting from an accidental plasma dump.

[c] Estimated lifetime is based on 70% efficiency with downtime duration = 5 × wall loading (MW/m^2) in seconds.

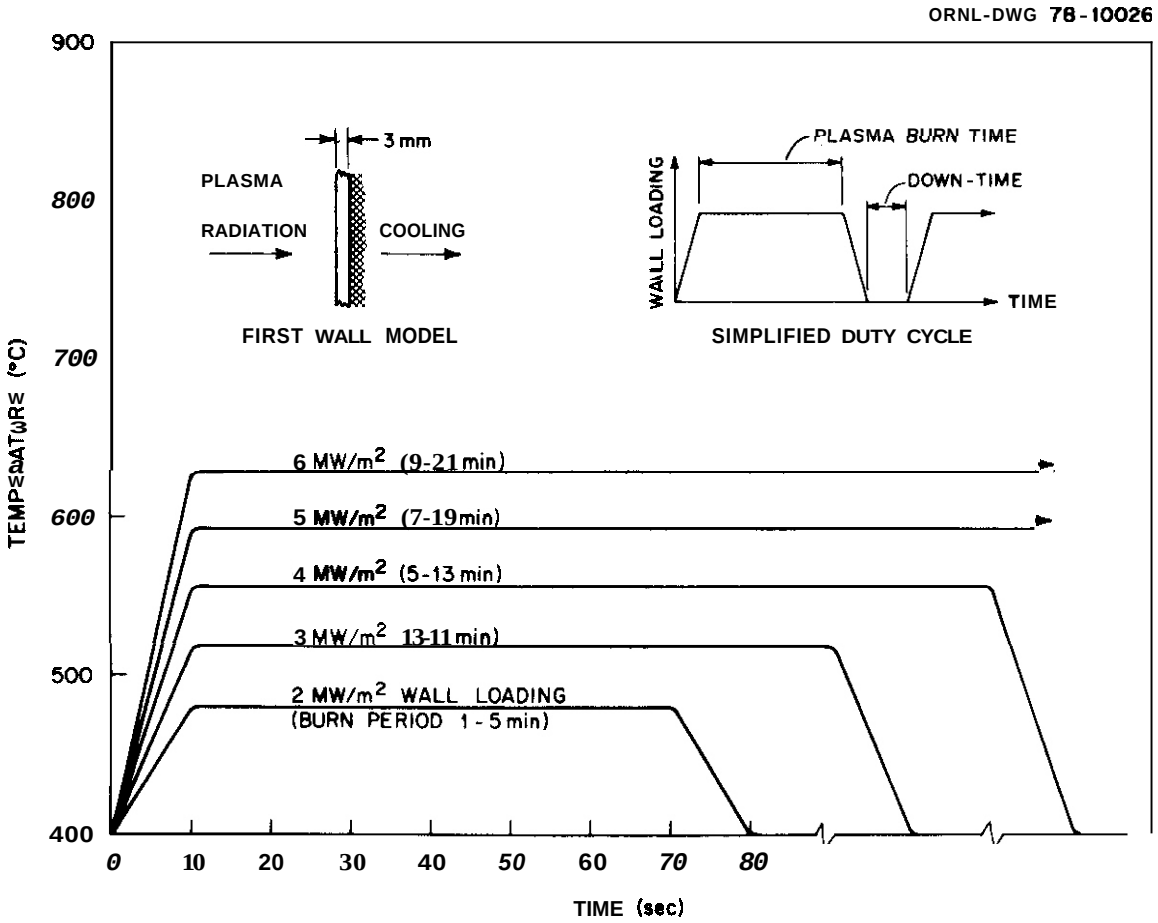

Fig. **1.2.3.** Change of Temperature at Plasma Side of the First Wall Under Various Degrees of Neutron Wall Loading During Various Plasma Burn Periods.

denotes the strain range component derived from thermal creep including the effect of irradiation-induced creep, and $\Delta\varepsilon_{pp}$ denotes the inelastic strain range component resulting from a hypothetical plasma energy dump. Equivalent strain quantities were used for the strain range components given in Table **1.2.1.**

When the interaction damage rule given in Eq. (1) is applied to fusion reactor components, it must be modified to take 'advantage of the high initial ductility and not unduly penalize design of the systems. In the absence of "cp" and "cc" components, Eq. (1) should be modified to take into account the effect of irradiation in the first wall as

$$\frac{1}{N_{\text{pred}}} = \left[\frac{\Delta\varepsilon_{pp}}{0.31\Delta\varepsilon_{in}^{-0.67}} + \frac{\Delta\varepsilon_{pc}}{0.1\Delta\varepsilon_{in}^{-0.67}}\right]\int_0^{L_f} D_p^{-1.67}\,\frac{dL}{L_f} \qquad (3)$$

where L_f is the total wall exposure in MWyr/m^2.

Independent evaluations of cyclic lifetimes are based on the calculated strain range components given in Table 1.2.2. The following equations were used to approximate the engineering tensile ductility of 20%-cold-worked type 316 stainless steel:[7,8]

350°C

$$\varepsilon_t = 13.0 - 5.79L \quad (L < 1.2) \qquad (4)$$

$$\varepsilon_t = 8.89 - 2.29L \quad (L > 1.2) \qquad (5)$$

450°C

$$\varepsilon_t = 17.0 - 3.7L \quad (L < 3.2) \qquad (6)$$

$$\varepsilon_t = \varepsilon_t\ (575°C) \quad (L > 3.2) \qquad (7)$$

575°C

$$\varepsilon_t = 14.6 - 1.51L \quad (L < 2.3) \qquad (8)$$

$$\varepsilon_t = 27.2 - 6.91L \quad (2.3 < L < 3.2) \qquad (9)$$

$$\varepsilon_t = 8.14 - 0.81L \quad (3.2 < L < 8.6) \qquad (10)$$

$$\varepsilon_t = 2.52 - 0.16L \quad (L > 8.6)\ , \qquad (11)$$

where ε_t is the percent total elongation and L is the wall exposure in MWyr/m^2.

The paucity of experimental data concerning the cyclic fatigue behavior of 20%-cold-worked type 316 stainless steel applicable to fusion first-wall conditions presently is a serious hindrance to making a realistic evaluation of the results given in Table 1.2.2. However, it appears that calculated cyclic lifetimes for neutron wall loading from 2

to 4 MW/m^2 are within an order of magnitude of what has been reported [9,10] for similar studies performed elsewhere. Direct comparison cannot be made since different methods of analysis for lifetime estimates were used. Cyclic lifetimes for higher wall loadings (5 MW/m^2) are considerably lower than the lifetimes at 2 to 4 MW/m^2. However, these figures do not seem to be unrealistic when compared with experimental results of laboratory tests of irradiated material under comparably similar strain ranges and temperatures, such as those for low strain ranges given in Table 1.2.1. The calculations also show that a high level of plasma energy accidentally deposited on the first wall is detrimental to the wall life. Frequent accidental thermal loading will considerably shorten the wall lifetime.

A limited number of tests have shown that cyclic fatigue and creep-fatigue damage are sensitive to test environment as well as to changes incurred by radiation. Higher cyclic fatigue lives by a factor of 3 to 10 are not uncommon for tests in vacuum when compared with those in air. Accordingly, additional conservatism could well have been introduced by failure to consider the expected fusion reactor environment in this analysis.

The interactions of cyclic loading with the developing irradiation microstructure, including neutronically produced helium, are still other uncertainties in the present analysis. Ideally, specimens should be cyclically stressed during irradiation. Experiments of this type are difficult and costly, but it is expected that they will be planned.

1.2.5 Conclusions

1. Actual cyclic failure lives were compared with lives predicted by the method of strain range partitioning for a number of uniaxial strain controlled fatigue test results involving either tensile or compressive hold times. The specimens had been irradiated in EBR-II to a fluence of 1 to 2.63 $\times 10^{26}$ n/m^2 (>0.1 MeV). Good estimates of the strain controlled time-dependent fatigue life were made for the irradiated material.

2. Lifetime estimates of a fusion first wall were made for neutron wall loading ranging from 2 to 5 MW/m^2 in an air environment using the

strain range partitioning technique. Irradiation effects were included through the use of postirradiation tensile and creep ductilities.

3. Results, although conjectural because of the many assumptions, tended to show that 20%-cold-worked type 316 stainless steel can be used as a first-wall material with an excess of 10 MW-years/m^2 lifetime for a vacuum environment, provided the neutron wall loading does not exceed 2 MW/m^2. It is expected that ongoing alloy development efforts aimed at improving ductility while not sacrificing strength will further increase projected lifetimes.

1.2.6 References

1. L. F. Coffin et al., *The-Dependent Fatigue of Structural Alloys — A General Assessment (1975)*, ORNL-5073 (January 1977).
2. S. Majumder and P. S. Maiya, "A Damage Equation for Creep-Fatigue Interaction," pp. 323–44 in *1976 ASME-MPC Synposium on Creep-Fatigue Interaction*, ed. by R. M. Curran, MPC-3, The American Society of Mechanical Engineers, New York, 1976.
3. G. R. Halford, J. F. Saltsman, and M. H. Hirschberg, *Ductility Normalized Strainrange Partitioning Life Relations for Creep-Fatigue Life Predictions*, NASA-TM-73737 (October 1977).
4. S. S. Manson and R. Zab, "A Framework for Estimation of Environmental Effect in High Temperature Fatigue," pp. 757–70 in *Environmental Degradation of Engineering Materials*, ed. by M. R. Louthan and R. P. McNitt, Virginia Polytechnic Institute, Blacksburg, Va., 1977.
5. C. R. Brinkman and G. E. Korth, "Low Cycle Fatigue and Hold Time Comparisons of Irradiated and Unirradiated Type 316 Stainless Steel," *Metall. Trans.* 5(3): 792–94 (March 1974).
6. Personal communication, A. Ward, Westinghouse-Hanford, November 1977.
7. E. E. Bloom and F. W. Wiffen, "The Effects of Large Concentrations of Helium on the Mechanical Properties of Neutron-Irradiated Stainless Steel," *J. Nucl. Mater. 58:* 171–84 (1975).
8. M. L. Grossbeck and P. J. Maziasz, unpublished data, May 1978.
9. E. S. Bettis, J. M. Barnes, T. J. Huxford, K. C. Liu, R. T. Santoro, and H. L. Watts, "A Practical Blanket Design For a Toroidal Fusion

Reactor," pp. 1453–58, in *Proc. 7th Symp. Engineering Problems of Fusion Reactors,* Vol. II, ed. by M. S. Lubell and C. Whitmire, IEEE Publ. 77CH1267-4-NDS, The Institute of Electrical and Electronics Engineers, New York, 1977.

10. M. Abdou et al., *The Establishment of Alloy Development Goals Important to the Commercialization of Tokamak-Based Fusion Reactors,* ANL/FPP/TM-99 (MDCE-1743) (November 1977).

1.3 THE SENSITIVITY OF THE FIRST WALL RADIATION DAMAGE TO FUSION REACTOR BLANKET COMPOSITION — J. M. Barnes, R. T. Santoro, and T. A. Gabriel (ORNL)

1.3.1 ADIP Task

ADIP Task I.A.l, define material property requirements and make structural life predictions.

1.3.2 Objective

The purpose of this study was to assess the sensitivity of radiation damage parameters in the first structural wall of a fusion reactor to the composition of the blanket. The first-wall composition was taken to be type 316 stainless steel. Some of the materials considered for use in the blanket may not be of practical application in an actual reactor design, but the results obtained are of interest in defining the sensitivity of the damage parameters.

1.3.3 Summary

The atomic displacement and hydrogen and helium gas production rates in a 10-mm-thick type 316 stainless steel first wall have been calculated as a function of blanket composition in a typical one-dimensional fusion reactor model. For a 0.5-m-thick blanket, variations in the rates of atomic displacement and hydrogen and helium gas production of factors of 2.7, 1.3, and 1.2, respectively, were obtained. The damage responses also showed a systematic decrease with increasing first-wall thickness.

1.3.4 Progress and Status

The atomic displacement and gas production rates in the 10-nun-thick stainless steel first wall are compared as a function of blanket composition in Table 1.3.1. Also given in the table are the ratios of the hydrogen and helium gas production to the atomic displacement production. All the values are normalized to a neutron wall loading of 1 MW/m^2.

The atomic displacement rates range from a low value of 8.4 dpa/year for an empty blanket to a high value of 22.6 dpa/year for a lead-filled blanket. The hydrogen gas production rates vary from 423 to 536 at. ppm/year

Table 1.3.1. Atomic Displacement and Gas Production Rates in the Type 316 Stainless Steel First Structural Wall as a Function of Blanket Composition[a]

Blanket Composition	Atomic Displacement Rate[b] (dpa/year)	Hydrogen Production Rate		Helium Production Rate	
		at. ppm / year	Ratio to dpa	at. ppm / year	Ratio to dpa
Void	8.4	423	50.4	134	16.0
Lithium	12.6	532	42.2	159	12.6
Carbon	13.1	536	40.9	159	12.2
Sodium	11.9	481	40.4	147	12.4
Aluminum	12.9	474	36.8	149	11.5
Potassium	10.7	472	44.1	147	13.8
Iron	14.9	484	45.2	148	10.0
Copper	14.6	468	32.1	145	9.9
Lead	22.6	488	21.6	148	6.6
Water	9.8	463	47.3	143	14.6
316 SS	14.5	489	33.7	149	10.3
SS + H_2O	11.2	484	43.2	148	13.2
K + SS	14.2	487	34.3	149	10.5
NaOH	10.6	478	45.1	146	13.8
EBTR[c]	14.2	621	43.7	188	13.2

[a]Normalized to a neutron wall loading = 1 MW/m^2.

[b]Based on an effective displacement energy for type 316 stainless steel of 40 eV.

[c]To have a basis for comparison with a realistic reactor model, the radiation damage responses in the 1.4-mm-thick first wall of the ELMO Bumpy Torus Reactor are also included in the table.

and the helium gas production rates vary from 134 to 159 at. ppm/year for the empty and carbon-filled blankets, respectively. The case where the blanket zone is treated as a void is included for reference, since in this case the radiation damage in the stainless steel wall is not sensitive to the neutrons that are backscattered by the blanket material. However, the inclusion of a shield or toroidal field coils would influence the results for this case.

Analyses[1] based on somewhat arbitrary assumptions suggest that the lifetime of a stainless steel wall in a fusion neutron environment will be of the order of 100 dpa. Based on this criterion, the lifetime of the first wall would vary from 4.4 to 11.9 years, depending on the blanket composition. However, it is reasonable to assume that several of the blanket materials considered in this study have no practical application in a fusion reactor blanket (e.g., void, sodium, potassium, iron, lead, potassium plus stainless steel, and NaOH). When these materials are eliminated, the life span range of the first wall changes to from 6.8 to 10.2 years for the remaining materials.

This investigation has been concluded.

1.3.5 Conclusions

It has been demonstrated that the induced damage (displacement and gas production) in the first wall of a fusion reactor is sensitive to the blanket composition and to the thickness of the first wall, primarily because of self-shielding characteristics. Variations in the damage of about 10 to 20% are possible, so, depending upon the reactor configuration, the operating lifetime of the first wall could be reduced.

1.3.6 Reference

1. E. E. Bloom, F. W. Wiffen, P. J. Maziasz, and J. O. Stiegler, "Temperature and Fluence Limits for a Type 316 Stainless-Steel Controlled Thermonuclear Reactor First Wall," *Nucl. Technol.* 31: 115–20 (1976).

2. TEST MATRICES AND TEST METHODS DEVELOPMENT

An important part of the alloy development effort is the definition of test matrices and development of test methods. The alloy development strategy will proceed through stages requiring tests of generally increasing difficulty and complexity.

1. Scoping tests will be used to make relative judgments between materials and metallurgical conditions and to identify critical properties. Such tests, which will be used where large numbers of variables are involved, must be rapid, simple, and decisive.

2. Developmental tests will be used for optimization of the Prime Candidate Alloys. They will be broader and more extensive than the scoping tests, In-reactor testing will be an important part of this work.

3. Engineering property tests will be devised to provide the broad data base needed for reactor design.

2.1 DESIGN OF MATERIALS IRRADIATION EXPERIMENTS UTILIZING SPECTRAL TAILORING — T. A. Gabriel, W. E. Thomas, A. F. Zulliger, J. W. Woods, and E. E. Bloom (ORNL)

2.1.1 ADIP TASK

ADIP Task I.A.2, Define Test Matrices and Test Procedures.

2.1.2 Objective

To reproduce in real time in fission reactors the helium to displacement per atom (He/dpa) ratio expected near or at the first wall in fusion reactors for stainless steel and nickel-base alloys, the thermal-to-fast neutron flux ratio within the experimental locations must be varied since the helium production will be dominated by the thermal flux and the fast flux will determine the dpa. The objective of this work is to determine the amount of variation necessary and to design experimental capsules that will produce the needed changes.

2.1.3 Summary

The helium production to displacement per atom (He/dpa) ratio expected near or at the first wall of a fusion reactor for stainless steels and nickei-base alloys can be reasonably reproduced in "real" time in fission reactors such as ORR because the helium production characteristics of nickel ($^{58}Ni + n_{th} \rightarrow {}^{59}Ni$; $^{59}Ni + n_{th} \rightarrow {}^{56}Fe + \alpha$). The He/dpa ratio can be reproduced by intermittent modification of the thermal-to-fast neutron flux ratio since the He production will be dominated by the thermal flux and the fast flux will determine the dpa. This report summarizes some of the neutronic calculations as well as experimental design considerations that are being carried out to determine: (1) the amount of change as a function of time necessary in the thermal-to-fast ratio, (2) the possibility of using the EBR-II in conjunction with the ORR, and (3) the possible configuration of the first experimental capsule.

2.1.4 Progress and Status

The previous report[1] presented calculations in which the ORR was used to obtain in real time the same He/dpa ratio for one melt of

stainless steel. However, these calculations presented data only up to 14 dpa (or ∿1.4 $MWyr/m^2$). These calculations have now been extended up to 80 dpa (or ∿8.0 $MWyr/m^2$). The present results are shown in Figs. 2.1.1 and 2.1.2. The straight lines in both figures are for the first-wall damage in a fusion reactor. The results shown in Fig. 2.1.1 are for when only the ORR is used. An ORR reactor time of 5.6 years can produce a level of damage that would correspond to about 5 years in a fusion reactor with a 1 MW/m^2 wall loading. Figure 2.1.2 gives the results when a combination of reactors is employed (ORR and EBR-II). Since the EBR-II has essentially no thermal flux, helium production proceeds almost entirely by direct nuclear interaction. Therefore, the rate at which the helium concentration increases is considerably slowed. For the combination, the time required to obtain equivalent damage between fusion and fission reactors can be accelerated. For example, 5.5 years of ORR and EBR-II time corresponds to about 7.5 years of fusion reactor time, again assuming a 1 MW/m^2 wall loading.

The calculated data obtained by use of the 3-D neutron-diffusion code VENTURE,[2] which was given in the previous progress report and deals with methods for increasing the thermal flux during the initial phase of the experiment, are now being used to design an experimental capsule. These data along with experience gained in designing previous experimental capsules for magnetic fusion energy application should lead to a designed capsule that will accomplish the intended task.

Detailed calculations using VENTURE[2] are currently under way to determine the best means of reducing the thermal flux while maintaining or increasing the fast flux. It is hoped that the results of these calculations will be available shortly.

2.1.5 Conclusion

It appears very promising that the ORR fission reactor or a combination of the ORR and EBR-II can be used to duplicate in real time the He/dpa ratio in stainless steel and nickel-bearing alloys expected near or at the first wall of a fusion reactor. So far, the interpretation of calculated results as well as information based on previous experience indicate that the experiment is possible.

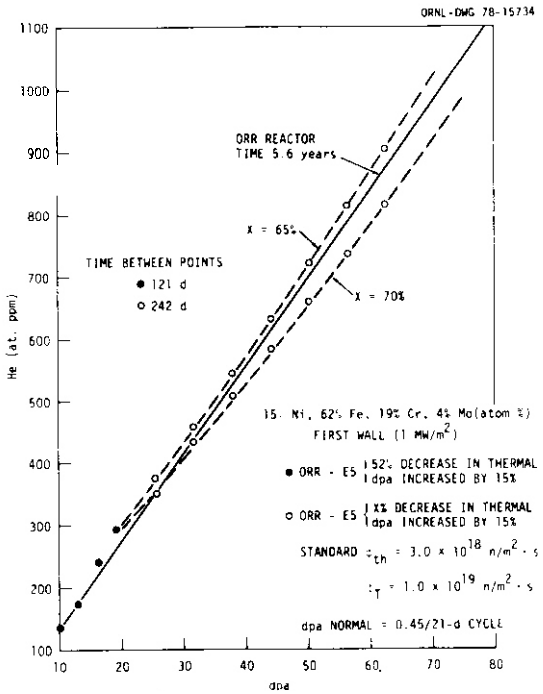

Fig. 2.1.1. Helium Production vs Displacements as Expected on the First Wall of a Fusion Reactor and What Can Be Obtained in the ORR.

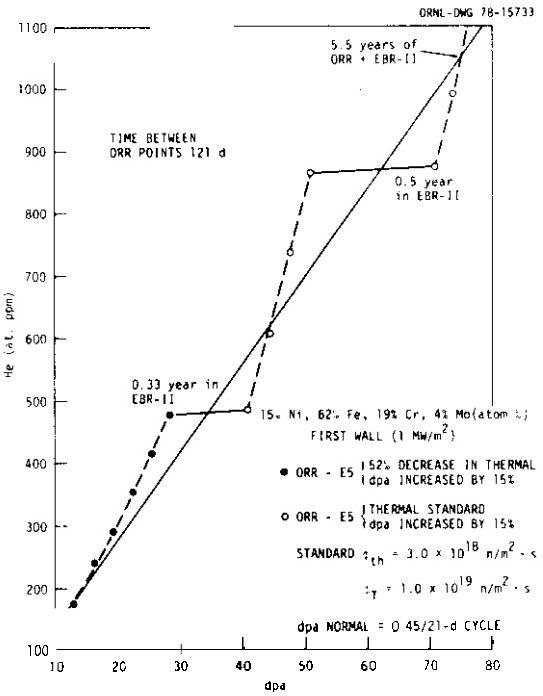

Fig. 2.1.2. Helium Production vs Displacements as Expected on the First Wall of a Fusion Reactor and What Can Be Obtained in a Combination of the ORR and EBR-II.

2.1.6 References

1. T. A. Gabriel, E. J. Allen, A. F. Zulliger, J. W. Woods, and E. E. Bloom, "Design of Materials Irradiation Experiments for Specimen Tailoring" *ADIP Development for Irradiation Performance Quart. Prog. Rep. April–June 1978*, DOE/ET-0058/2, pp. 14–19.
2. D. R. Vondy, T. B. Fowler, and G. W. Cunningham, *VENTURE, A Code Block for Solving Multigroup Neutrons Problems Applying the Finite-Diffusion-Theory Approximations to Neutron Transport*, ORNL-5062 (October 1975).

3. PATH A ALLOY DEVELOPMENT – AUSTENITIC STAINLESS STEELS

Path A Alloys are those alloys generally known as austenitic stainless steels. The most common U.S. designations are AISI types 304, 316, 321, and 347. Primary considerations for selecting this class of alloys for further development are:

1. state-of-the-art production and fabrication technology;
2. extensive data on the effects of neutron irradiation on properties, which show the potential of these alloys for MFR applications;
3. compatibility with proposed coolants and breeding fluids;
4. evidence that for MFR conditions (He, dpa, temperatures) the properties are sensitive to composition and microstructure — thus showing potential for further development.

The strategy for development of these alloys has two related objectives:

1. to determine for a reference alloy the effects of irradiation on those properties most important to fusion reactor design;
2. to develop a path A alloy that is optimized for fusion reactor applications.

The first objective will provide a data base for near-term reactor design and, most important, guidance as to which properties limit performance of this type alloy. Work on the reference alloy will provide direction for the actual alloy development efforts of the second objective. Type 316 stainless steel in the 20%-cold-worked condition appears to be the best choice as a reference alloy. It is the present reference cladding and duct alloy in the breeder reactor programs, and there are extensive data on the unirradiated mechanical properties, effects of heat treatment on properties, structure, and phase stability, and the effects of fast neutron irradiation on properties. The present technology of austenitic stainless steels, including understanding of the physical and mechanical properties and irradiation response, is such that alloy development efforts can move to optimization for use in fusion reactor applications. A Prime Candidate Alloy (PCA) (Fe—16% Ni–14% Cr—2% Mo—2% Mn—0.5% Si—0.2% Ti—0.05% C) has been selected by the ADIP task group. Efforts will now focus on optimizing the composition and microstructure of the PCA leading toward the selection of OPT-A1 (Program Plan designation of first optimized path A alloy).

3.1 THE EFFECT OF 200 at. ppm PREINJECTED HELIUM ON 20%-COLD-WORKED TYPE 316 STAINLESS STEEL IRRADIATED AT 625°C IN EBR-II — P. J. Maziasz (ORNL)

3.1.1 ADIP Task

ADIP Task I.C.2, Microstructures and Swelling in Austenitic Alloys.

3.1.2 Objective

The objective is to determine the effect of helium preinjection followed by irradiation to produce only displacement damage on the microstructure of 20%-cold-worked type 316 stainless steel and compare the results with irradiation producing simultaneous helium and displacement damage to similar levels.

3.1.3 Summary

Type 316 stainless steel cold-worked 20% has been preinjected with 200 at. ppm He and irradiated in EBR-II at 625°C to a neutron fluence of 1.6×10^{26} n/m^2 (>0.1 MeV). The preinjected helium results in 1.2×10^{22} cavities/m^3 that are 5 nm in diameter, while the uninjected material contains no cavities. The preinjected helium results in nearly an order of magnitude more cavities, and these cavities are slightly smaller than those produced by irradiation of the same material in HFIR. Preinjected helium appears to have no effect on the dislocation structure that develops during irradiation. However, all cavities produced by helium preinjection are attached to dislocations, as is observed after HFIR irradiation.

3.1.4 Progress

Details of specimen preparation have been reported previously.[1,2] Small sheets of type 316 stainless steel were annealed for 1 h at 1050°C and rolled to a 20% reduction in thickness. The specimens were irradiated with 60-MeV alpha particles at 20°C in the Oak Ridge Isochronous Cyclotron (ORIC) to preinject the helium. The alpha beam passed through a degrader to spread the incident energy of the beam, resulting in a spatially uniform distribution of helium in the specimens. The specimens were irradiated in EBR-II, row 8, in subassembly X-264. The specimens examined here were

irradiated at about 625°C by locating the specimens near a heat pipe at approximately that temperature. These specimens were exposed to a neutron fluence of about 1.6×10^{26} n/m^2 (>0.1 MeV), producing about 9 dpa.

The composition of the steel used is given in Table 3.1.1. The specimens were electropolished to thin foils and examined by transmission electron microscopy (TEM). Comparison is made with the same material, cold swaged to a 20% redurtion in area, irradiated in HFIR at 580°C to a neutron fluence of 4.7×10^{25} n/m^2 00.1 MeV) to produce 85 at. ppm He and 3.3 dpa. Table 3.1.2 shows the microstructural statistics for the various samples considered. Bear in mind, however, that the cold-worked states are not exactly equivalent for the EBR-II and the HFIR-irradiated material since the cold-working was accomplished by rolling and swaging, respectively.

Table 3.1.1. Composition of Type 316 Stainless Steel

Content, wt %										
Cr	Ni	Mo	Mn	C	Ti	Si	P	S	N	B
18.0	13.0	2.6	1.9	0.05	0.05	0.80	0.013	0.016	0.05	0.0005

Table 3.1.2. Microstructural Statistics for Cold-Worked Type 316 Stainless Steel Irradiated in EBR-II or in HFIR

Sample	Irradiation Temperature (°C)	Neutron Fluence >0.1 MeV (n/m^2)	Helium Content (at. ppm)	Cavity Concentration (m^{-3})	Cavity Diameter (nm)	Swelling (%)	Total Dislocation Density (m^{-3})
EBR-II, no helium	625	1.6×10^{26}	0				$\sim 2 \times 10^{14}$
EBR-II, preinjected helium	625	1.6×10^{26}	200	1.2×10^{22}	5.0	0.084	$\sim 3 \times 10^{14}$
HFIR	580	4.1×10^{25}	86	2.5×10^{21}	7.0	0.060	$\sim 9 \times 10^{13}$

The data in Table 3.1.2 indicate that no voids are observable after irradiation in EBR-II at 625°C to a fluence of 1.6×10^{26} n/m^2, with no preinjected helium. For a similar heat of type 316 stainless steel reduced 20% in area by cold swaging Brager[3] and Brager and Garner[4] both present data that indicate that void formation begins at $1.5-2.0 \times 10^{26}$ n/m^2 for EBR-II irradiation at about 625°C. Brager reports a combination of voids and bubbles at 650°C for a neutron fluence of 2.4×10^{26} n/m^2, and indicates that the average diameter is about 19 nm and the average density is about 1.3×10^{19} cavities/m^3. Bloom and Stiegler,[5] however, report no voids for the same heat of sheet examined in this work, swaged to a 20% reduction in area and irradiated in EBR-II under similar conditions. Therefore the observations here are consistent with previous work on the same heat of steel, but may reflect differences due to pretreatment or minor alloying element content[6] when compared with other heats of type 316 irradiated in EBR-II. Table 3.1.2 clearly indicates that 200 at. ppm of preinjected helium results in formation of cavities. Since no voids form in the control or uninjected material, statistics are difficult to compare. Using Brager's[3] data as representative of cavity formation in type 316 stainless steel once swelling ensues, preinjection of helium results in a three-order-of-magnitude higher concentration of much smaller cavities than would be expected in uninjected material. Clearly, nucleation is enhanced since no cavities have nucleated yet in the uninjected material.

Comparison of the dislocation density in the uninjected and preinjerted material indicates that preinjected helium has little or no efect on the total dislocation density (see Table 3.1.2). This is consistent with recent ion-irradiation measurements made by Packan[7] on the effect of helium preinjection. There is, however, a strong interaction between the ravity and dislocation portions of the microstructure. All cavities observed are attached to dislocations and do not appear alone in the matrix, and all dislocations observed have cavities attached to them. Greenwood et al.[8] predicted theoretically that bubbles of inert gas should prefer to nucleate at dislocations. Barnes and Mazey[9] noted the same association between helium bubbles and dislocations in helium-preinjected copper. Vela and Russell[10] observed preferential association of bubbles and dislocations

in neutron-irradiated copper-boron alloys. Maziasz et al.[11] have noted the preferential attachment of bubbles to dislocations in both annealed and 20%-cold-worked type 316 stainless steel of the same heat examined in this work, after irradiation in HFIR to high fluences at 350 to 680°C. The association of cavities and dislocations found in this work is consistent with the literature and is expected. Consistent also is the fact that calculations of the amount of gas contained in the cavities as compared with the amount of gas originally introduced into the sample indicate that these are very nearly equilibrium bubbles, to the uncertainty with which surface energies are known.

Table 3.1.2 also compares helium-preinjected cold-worked type 316 stainless steel with the same heat of material irradiated to a low fluence in HFIR. There is nearly an order-of-magnitude higher number density and a slight reduction in size in the EBR-II irradiated material as compared with the HFIR irradiated material. The HFIR irradiation corresponds to about one-third the fluence and contains about one-half the helium of the EBR-II irradiated material. A helium preinjected sample containing 80 at. ppm He has been irradiated in EBR-II for comparison, and work on it is in progress now.

3.1.5 Conclusions

1. Type 316 stainless steel cold-worked 20%, irradiated in EBR-II at 625°C with no preinjected helium, contains no voids or cavities after exposure to a neutron fluence producing about 9 dpa.

2. The same material containing 200 at. ppm preinjected helium and irradiated under the same conditions has 1.2×10^{22} cavities/m^3 with an average diameter of 5 nm.

3. The dislocation structure consists of $2\text{–}3 \times 10^{14}$ m/m^3 dislocation tangles, with no faulted or unfaulted loops observed. The dislocation structure shows little or no effect of preinjected helium.

4. All cavities observed after helium preinjection are associated exclusively with dislocations. This is consistent with the cavity behavior observed in HFIR-irradiated material.

5. The cavity density is greater by nearly an order-of-magnitude and the size slightly smaller for helium preinjected material irradiated in EBR-II than for material subjected to HFIR irradiation, which produces simultaneous helium.

Work is under way to examine the dependence of the microstructure on the amount of helium preinjected and on irradiation temperature. The samples can then be used to evaluate the potential of helium preinjection as a simulation tool and give us knowledge about the general behavior of helium in influencing this development of the irradiation-produced microstructure.

3.1.6 References

1. J. A. Horak, "Helium Implantation in Potential CTR Structural Materials,'' *Controlled Thermonuclear Materials Technology Program Annu. Prog. Rep. June 30, 1975,* ORNL-5082, pp. 40–42.
2. P. J. Maziasz and J. A. Horak, "Status of Helium-Preinjected Annealed and 20%-Cold-Worked Type 316 Stainless Steel Irradiated in EBR-II at 500 and 625°C," *ADIP Quart. Prog. Rep. April–June 1978,* DOE/ET-0058/2, pp. 42-46.
3. H. R. Brager, "The Effects of Cold Working and Pre-Irradiation Heat Treatment on Void Formation in Neutron-Irradiated Type 316 Stainless Steel," J. *Nucl. Mater.* 57: 103–18 (1975).
4. H. R. Brager and F. A. Garner, "Swelling as a Consequence of Gamma Prime (γ') and $M_{23}(C,Si)_6$ Formation in Neutron Irradiated 316 Stainless Steel," *J. Nucl. Mater.* **73**: 9–19 (1978).
5. E. E. Bloom and J. O. Stiegler, "Effect of Irradiation on the Microstructure and Creep-Rupture Properties of Type 316 Stainless Steel," pp. 360–80 in *Effects of Radiation on Substructures and Mechanical Properties of Metals and Alloys, Am. Soc. Test. Mater. Spec. Tech. Publ.* 529, American Society for Testing and Materials, Philadelphia, September 1973.
6. J. M. Leitnaker, E. E. Bloom, and J. O. Stiegler, "The Effect of Minor Constituents on Swelling in Stainless Steel," J. *Nucl. Mater.* 49: 57-66 (1973174).

7. N. H. Packan, Oak Ridge National Laboratory, private communication.

8. G. W. Greenwood, A.J.E. Foreman, and D. E. Rimmer, "The Role of Vacancies and Dislocations in the Nucleation and Growth of Gas Bubbles in Irradiated Fissile Material," *J. Nucl. Muter.* 4: 305–24 (1959).

9. R. s. Barnes and D. J. Mazey, "The Migration and Coalescence of Inert Gas Bubbles in Metals," Proc. *R. Soc. London Ser. A* 275: 47–57 (1963).

10. P. Vela and B. Russell, "The Behavior of Helium Gas in Irradiated Copper-Boron Alloys," *J. Nucl. Muter.* 19: 312–26 (1966).

11. P. J. Maziasz, F. W. Wiffen, and E. E. Bloom, "Swelling and Microstructural Changes in Type 316 Stainless Steel Irradiated Under Simulated CTR Conditions, pp. 259–86 in *Radiation Effects and Tritium Technology for Fusion Reactors,* CONF-750989, Vol. I (March 1976).

3.2 TENSILE PROPERTIES OF HFIR-IRRADIATED TYPES 316 AND TiM 316 STAINLESS STEEL AT 200 TO 1000 at. ppm He — M. L. Grossbeck and P. J. Maziasz (ORNL)

3.2.1 ADIP Task

ADIP Task I.B.13, Tensile Properties of Austenitic Alloys (Path A).

3.2.2 Objective

This series of experiments has been done to evaluate the strength and ductility of types 316 and TiM (titanium-modified) 316 stainless steel irradiated in the High Flux Isotopes Reactor (HFIR) to medium fluence and helium levels.

3.2.3 Summary

Miniature tensile specimens of types 316 and 316 with 0.23 wt % Ti (TiM 316) stainless steel in the annealed and 20%-cold-worked conditions were irradiated in HFIR to displacement damage levels of 5–17 dpa and helium levels of approximately 200–1000 at. ppm He. The specimens were tested near the irradiation temperatures and the results compared with similar materials irradiated in EBR-II for cases where such data were available.

For irradiation and test temperatures of 350°C, the yield strength of annealed (1 h at 1050°C) types 316 and TiM 316 and 20%-cold-worked type 316 stainless steel increases very rapidly compared with EBR-11-irradiated material. The yield strength of 20%-cold-worked type TiM 316 remains essentially constant over the fluence range investigated. At 450 and 575°C the yield strength of 20%-cold-worked material decreases monotonically with an indication of saturation above approximately 1.6 x 10^{26} n/m^2 (>0.1 MeV). As opposed to the lower temperature, where types 316 and TiM 316 had nearly the same yield strength, at the higher temperatures the titanium-modified alloy exhibited 40–50% greater strength, depending upon fluence and temperature. In the annealed condition, the two alloys behaved similarly with increasing fluence.

The ductility of both alloys in the cold-worked condition decreased monotonically, tending to approach saturation, except at 350 and 450°C,

where 20%-cold-worked TiM 316 appeared to have an essentially constant elongation of about 8% *to* a fluence of 2×10^{26} n/m^2 (>0.1 MeV), the highest fluence attained. .This behavior differs from EBR-11-irradiated 20%-cold-worked type 316 stainless steel, which displays a ductility maximum at low fluence. In the annealed conditions the total elongation of both alloys decreases rapidly but then levels off at a value always above 6% after about 1×10^{26} n/m^2. The properties of all materials examined at these temperatures and fluences appear adequate for fusion reactor first-wall application.

3.2.4 Progress and Status

3.2.4.1 Introduction

In a fusion reactor the first wall will be subject to intense neutron radiation, resulting in displacement damage as well as formation of helium and hydrogen from transmutation reactions. Since type 316 stainless steel is a candidate first-wall material, the strength and ductility of this alloy and a titanium-modified variation were investigated. Irradiations were conducted in the High Flux Isotope Reactor (HFIR), which has an appropriate spectrum *to* produce both displacement damage and helium through a two-step thermal neutron reaction with nickel contained in the stainless steel.

3.2.4.2 Experimental Description

Miniature tensile specimens of dimensions shown in Fig. 3.2.1 were fabricated from types 316 and 316 + 0.23 wt % Ti (TiM 316) stainless steel of the compositions shown in Table 3.2.1. The specimens were irradiated in HFIR in a peripheral target position, where the peak thermal flux is 2.5×10^{19} n/m^2 s and the peak fast flux is 1.3×10^{19} n/m^2 s (>0.1 MeV). The specimen holder geometry is illustrated in Fig. 3.2.2. A gas gap was provided around each specimen to restrict radial heat transfer so as to obtain the desired elevated temperatures. The specimen holder geometry was modified from that used in earlier work to achieve a more uniform temperature profile across the specimen gage and shoulders.

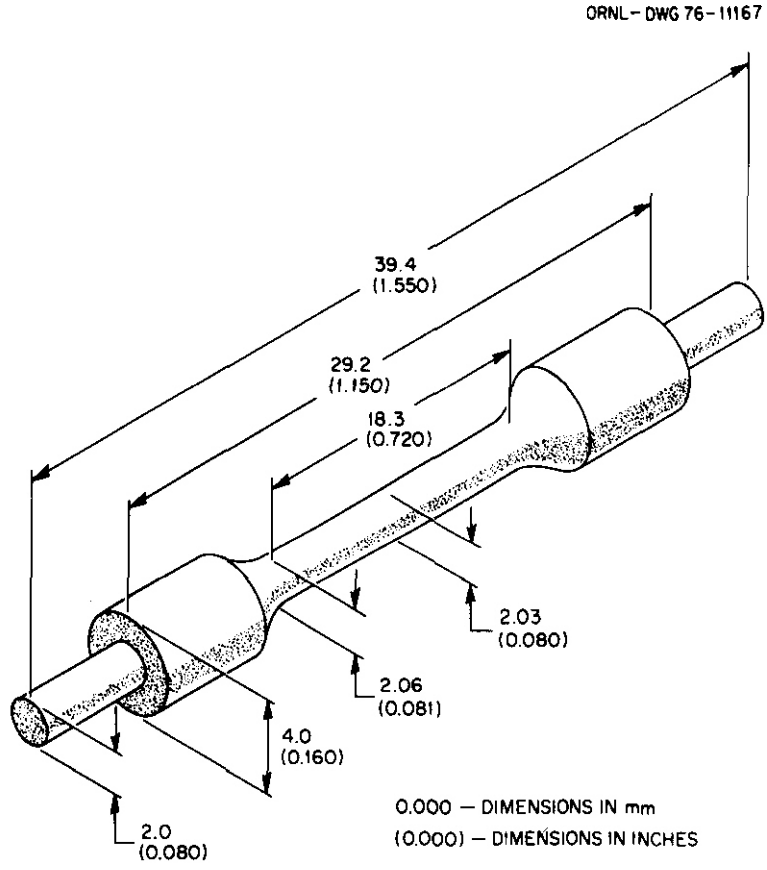

Fig. 3.2.1. Tensile Specimen for **HFIR** Irradiation.

Table **3.2.1.** Composition of Stainless Steel Used for Investigation

Alloy	Content,[a] wt %										
	Cr	Ni	Mo	Mn	Ti	si	C	P	S	N	B
316	18.0	13.0	2.58	1.9	0.05	0.8	0.05	0.013	0.016	0.05	0.0005
TIM	17.0	12.0	2.50	0.5	0.23	*0.40*	0.06	0.01	0.013	0.0055	0.0007

[a]Balance Fe.

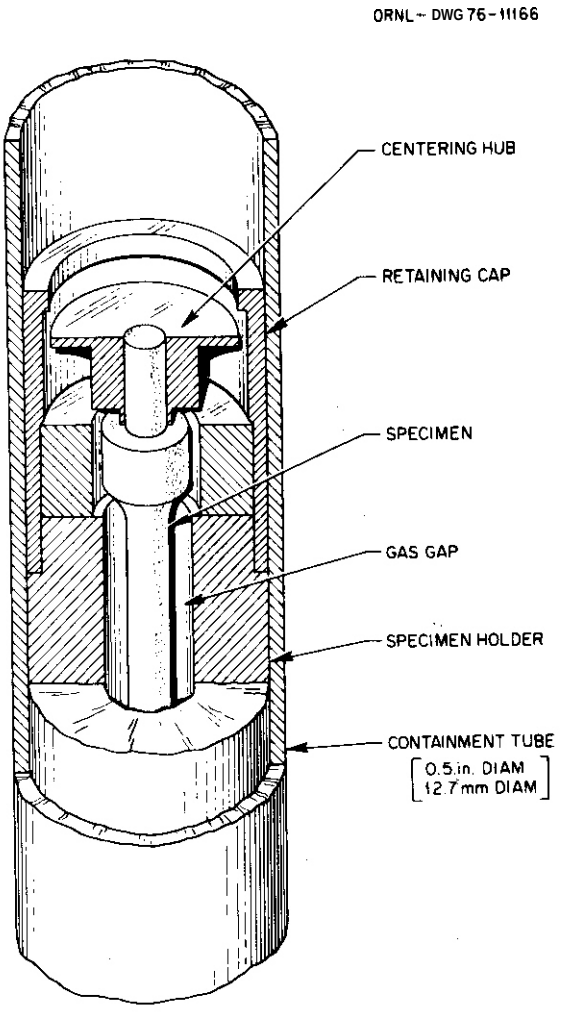

Fig. 3.2.2. Holder for Irradiating Tensile Specimen in HFIR Peripheral Target Position.

All specimen material was initially annealed 1 h at 1150°C. The standard type 316 stainless steel was then swaged to a 50% reduction in area and annealed for 1 h at 1050°C. The cold-worked samples were swaged to a 20% reduction in area, and then tensile specimens were machined. The annealed samples were machined from the material annealed for 1 h at 1050°C and then annealed an additional 15 min at 1050°C to relieve any surface cold work. The type TiM 316 stainless steel was initially annealed for 1 h at 1150°C. The cold-worked material was swaged to a 28% reduction in area, annealed for 1 h at 1050°C, swaged to a 20% reduction in area, and machined into tensile specimens. The annealed material was swaged to a 42.2% reduction in area. Tensile specimens were machined, and these were annealed for 1 h at 1050°C.

No instrumentation was installed in the capsule; however, extensive dosimetry has been done in the past and temperature monitors from more recent irradiations are now being analyzed. Helium levels were calculated from an empirical relation determined by Wiffen et al.[1] and based on fusion mass spectrographic analysis of HFIR-irradiated specimens. The calculations are believed to have an accuracy of ±25%.

Tensile tests were conducted on a hot-cell-installed Instron machine using a crosshead speed of 0.85 μm/s, resulting in a nominal strain rate of 4.6×10^{-5}/s. Tests were performed in air in a resistance furnace with a 150-mm hot zone to provide temperature uniformity over the center region of 50 mm.

Following immersion density measurements to determine swelling, as previously reported,[2] postirradiation tensile tests were performed on specimens irradiated at temperatures in the range from 300 to 600°C. Test temperatures were chosen as 350, 450, and 575°C, and specimens were selected with irradiation temperatures as close to these values as possible. Fluences ranged from 0.63×10^{26} to 2.1×10^{26} n/m^2 (>0.1 MeV) and damage levels from 5 to 17 dpa. Helium contents ranged from 200 to 1000 at. ppm.

3.2.4.3 Results

Results of the tensile tests are tabulated in Table 3.2.2. Elongations were measured from the machine modulus line at the appropriate load on tensile load-elongation curves. The yield stresses as functions of fast-neutron fluence for all samples at the test temperatures of 350, 450, and 575°C are plotted in Figs. 3.2.3, 3.2.4, and 3.2.5, respectively.

Figure 3.2.3 indicates that at 350°C the yield strength of annealed material increases very rapidly initially. Type 316 stainless steel in the 20%-cold-worked condition exhibits a similar trend, but 20%-cold-worked TiM material exhibits a nearly constant yield strength with increasing fluence. At this temperature, there is no significant difference in strength between the TiM and standard materials in the annealed condition; however, data are sparse, and as a result, straight

Table 3.2.2. Mechanical Properties of HFIR–Irradiated Types 316 and TiM 316 Stainless Steel

Temperature, °C		Neutron Fluence[b] >0.1 MeV (n/m²)	Helium Content[c] (at. ppm)	Strength, MPa		Elongation, %	
Test	Irradiation[a]			Yield	Ultimate	Uniform	Total
			Annealed Type 316				
350[d]		0 × 10²⁶		165	620	14	41
350		0		176	558	12	37
350	375	1.7	740	786	869	4.6	6.9
450		0		156	565	32	39
450	465	1.4	600	399	591	8.4	9.1
450	475	2.1	980	345	586	12	14
575[d]		0		118	524	12	18
575	565	1.2	440	248	468	6.4	7.7
575	565	1.9	880	236	467	6.1	6.3
			Annealed Type 316 with 0.23 wt % Ti				
350[e]		0		172	503	15	41
150	110	1.0	390	758	186	1.6	6.9
350	375	1.1	740	676	745	2.4	6.1
450		0		161	542	31	36
450	465	1.4	600	446	613	11	14
450	415	2.1	980	352	586	11	17
575[e]		0		165	414	30	45
575	565	1.2	440	217	454	11	12
575	565	1.9	880	236	468	11	12
			20%-Cold-Worked Type 316				
100	325	1.0	390	998	998	0.22	5.1
150		0		527	633	12	17
350		0		585	676	7.8	13
350	370	0.63	180	780	848	4.5	8.5
350	370	1.0	390	855	917	4.2	8.7
350	175	1.1	380	611	752	3.3	6.8
350	375	1.7	740	594	731	3.3	6.4
350	315	1.7	740	688	800	4.6	8.3
450		0		496	641	12	18
450		0		572	663	8.3	14
450		0		542	645	10	16
450	465	0.9	290	481	641	11	14
450	475	1.3	500	405	584	8.3	11
450	465	1.4	600	459	619	10	12
450	475	2.1	1020	395	613	11	13
550	560	1.9	880	310	490	4.4	4.6
575		0		480	516	10	17
575		0		638	158	8.2	15
575		0		512	589	8.3	15
575	560	0.9	290	296	503	11	17
575	565	1.2	440	332	510	4.4	4.6
575	560	1.4	600	341	538	9.5	12
575	620	2.1	1020	290	448	4.8	4.9
			20%-Cold-Worked Type 316 with 0.21 wt % Ti				
350		0		159	119	0.56	5.7
350		0		786	814	0.87	5.9
350	170	0.61	180	152	786	3.1	8.5
350	375	1.1	380	786	848	2.6	7.0
350	375	1.7	740	112	855	4.2	8.4
350	375	1.7	740	758	834	4.1	9.0
450		0		710	165	2.1	6.9
450	465	0.9	290	643	717	3.7	7.6
450	475	1.1	500	603	696	3.7	7.2
450	415	2.1	980	588	687	4.7	8.3
575		0		643	687	1.3	5.8
575		0		678	711	2.0	6.8
575	560	0.9	290	490	581	4.5	7.2
575	565	1.2	440	462	570	4.1	4.6
575	560	1.4	600	519	600	1.9	4.4
575	565	1.9	880	537	625	2.1	2.6
515	565	1.9	880	400	497	1.1	3.5

[a]Irradiation temperatures calculated from assumed values of nuclear heating.
[b]Calculated from dosimetry of previous experiments.
[c]Calculated from empirical equation.
[d]From D. Fahr. ORNL/TM-4292 (November 1973).
[e]From E. E. Bloom et al., ORNL/TM-4105, p. 3.14.

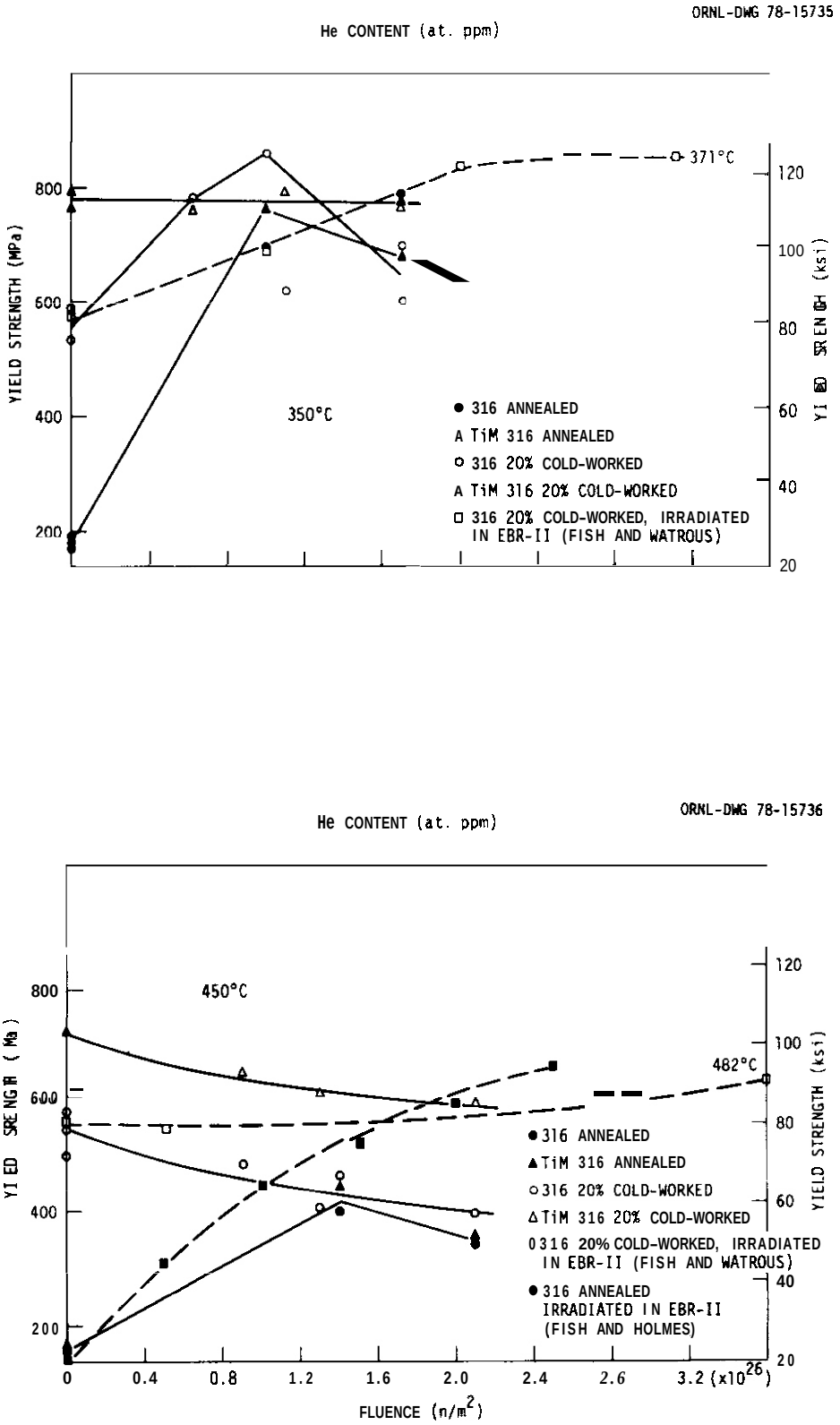

Fig. 3.2.4. Yield Strength as a Function of Fluence for Annealed and 20%-Cold-Worked Types 316 and TiM 316 Stainless Steel Tested at 450°c. Data on EBR-11-irradiated material from refs. 3 and 4.

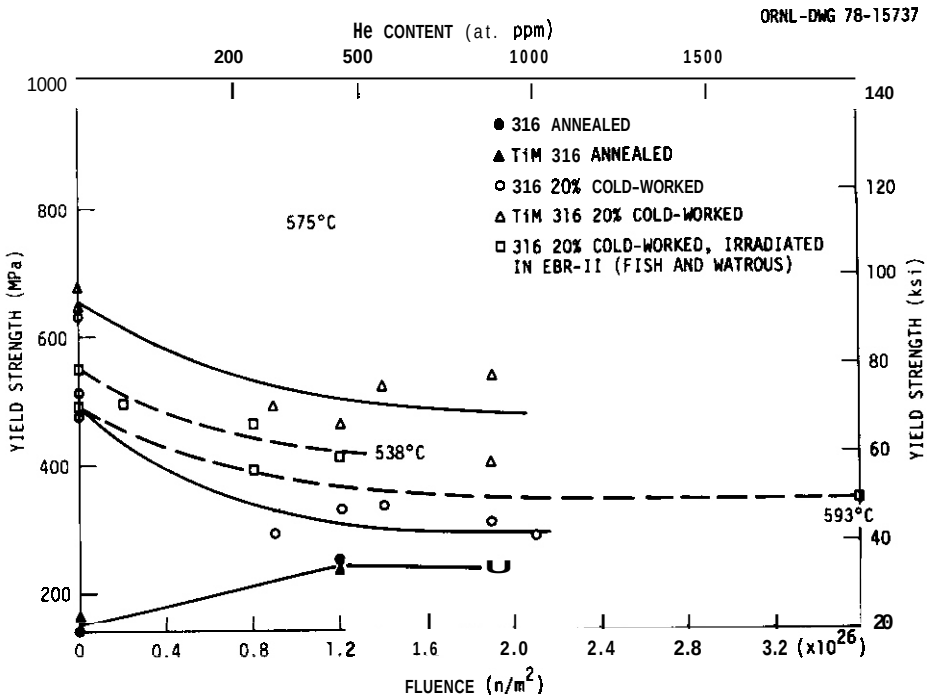

Fig. 3.2.5. Yield Strength as a Function of Fluence for Annealed and 20%-Cold-Worked Types 316 and TiM 316 Stainless Steel Tested at 575°C. Data on EBR-11-irradiated material from ref. 3.

line segments are drawn between data points. With the exception of 20%-cold-worked TiM material, the HFIX-irradiated material appears to harden about twice as fast as EBR-11-irradiated material.

Figure 3.2.4 shows similar data taken at 450°C. At this temperature, yield strength of 20%-cold-worked material decreases with increasing fluence, with an indication of tending to approach a constant value. It is also apparent that at 450°C, titanium-modified material in the 20%-cold-worked condition is significantly stronger than standard type 316 stainless steel. The EBR-11-irradiated material shows a slight increase in strength as fluence increases.[3] The annealed materials exhibit behavior similar to those tested at 350°C. Data from annealed type 316 stainless steel irradiated in EBR-II were available for comparison.[4]

At 575°C (Fig. 3.2.5) both HFIR and EBR-II 20%-cold-worked materials decrease in yield strength with increasing fluence. The higher strength of the titanium-modified material is also apparent at

this temperature. The annealed materials exhibit strengthening followed by apparent saturation. Again, data are insufficient to draw a firm conclusion. For comparison, data show that 20%-cold-worked type 316 stainless steel irradiated in EBR-II and tested at 538 and 593°C behaves similarly to the cold-worked material irradiated in HFIR.

The yield strength at a given fluence tends to decrease with increasing test temperature for all four materials. The annealed material of both types of steel shows the largest sensitivity to temperature, and the 20%-cold-worked TiM 316 shows the least sensitivity to test temperature.

Differences in behavior between HFIR- and EBR-11-irradiated materials are more apparent from ductility measurements. Total elongation of HFIR-irradiated material tested at 350°C decreases monotonically, tending to saturate near 6% at a fluence of about 1×10^{26} n/m^2 (Fig. 3.2.6). Data from similar 20%-cold-worked material containing only trace amounts of helium (irradiated in EBR-II) display a maximum of 13% ductility at a fluence of nearly 1×10^{26} n/m^2. It, too, tends to saturate with increasing fluence. The decrease in total elongation is much more marked in annealed material than in 20%-cold-worked material.

At a test temperature of 450°C, there is a greater difference between the ductility of the various steels, as shown in Fig. 3.2.7. Behavior of 20%-cold-worked type 316 stainless steel is similar to that at 350°C except that ductility decreases more slowly with some indication of saturation near 12% at a fluence of about 2×10^{26} n/m^2. The 20%-cold-worked TiM material exhibits a nearly constant ductility of about 7% up to a fluence of 2.1×10^{26} n/m^2. The EBR-II data show a trend similar to that from the lower temperature tests. Annealed material for both temperatures shows a very rapid decline in total elongation with increasing fluence up to about 1×10^{26} n/m^2, followed by an apparent leveling off that is above 6%.

Data from tests at 575°C (Fig. 3.2.8) show behavior more closely resembling the ductility behavior of EBR-11-irradiated material. There is even an indication of a possible peak in total elongation of the

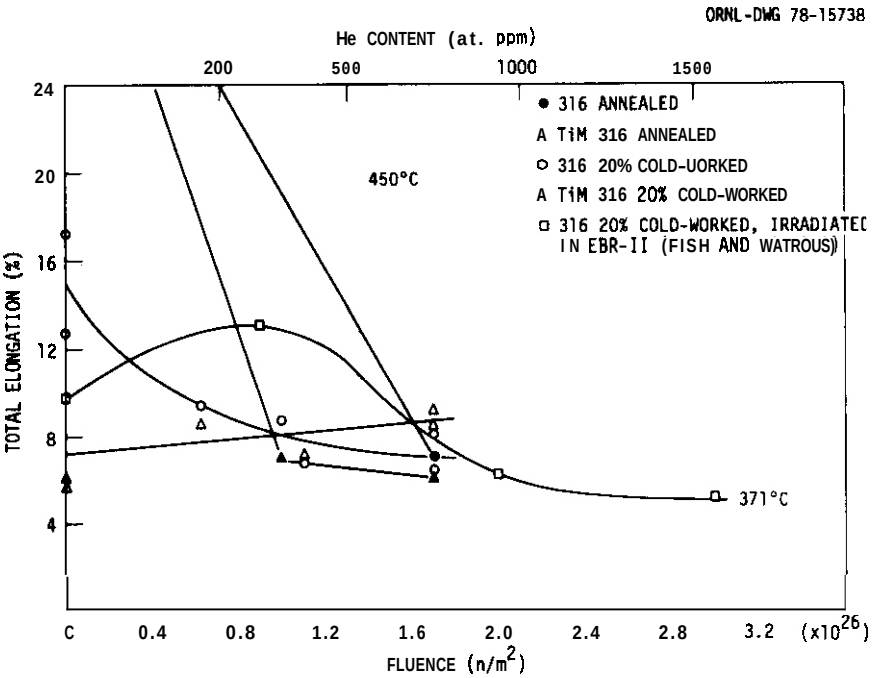

Fig. 3.2.6. Total Elongation as a Function of Fluence for Annealed and 20%–Cold–Worked Types 316 and TiM 316 Stainless Steel Tested at 350°C. Data on EBR–11–irradiated material from ref. 3.

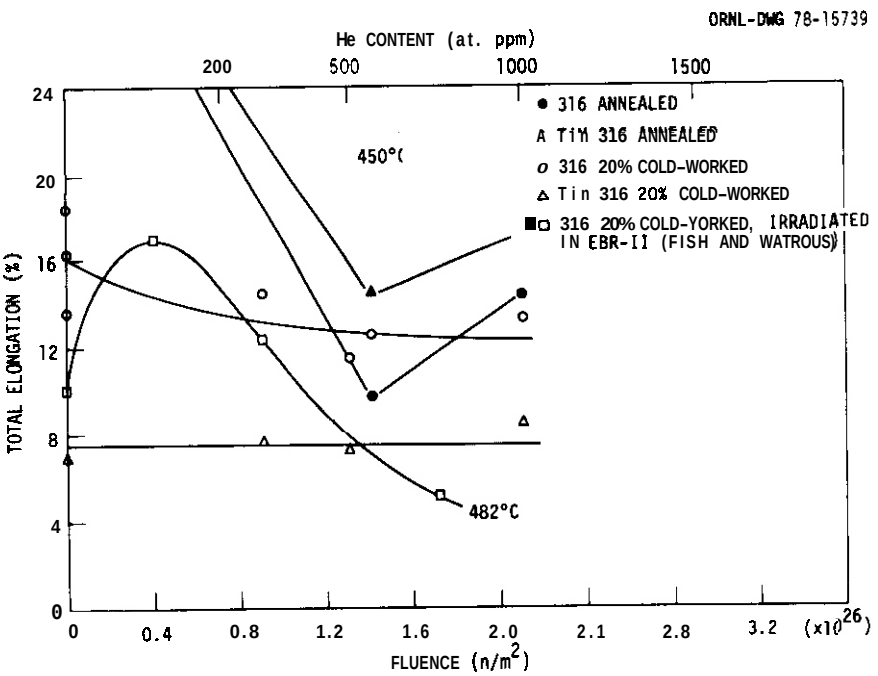

Fig. 3.2.7. Total Elongation as a Function of Fluence for Annealed and 20%-Cold-Worked Types 316 and TiM 316 Stainless Steel Tested at 450°C. Data on EBR–11–irradiated material from ref. 3.

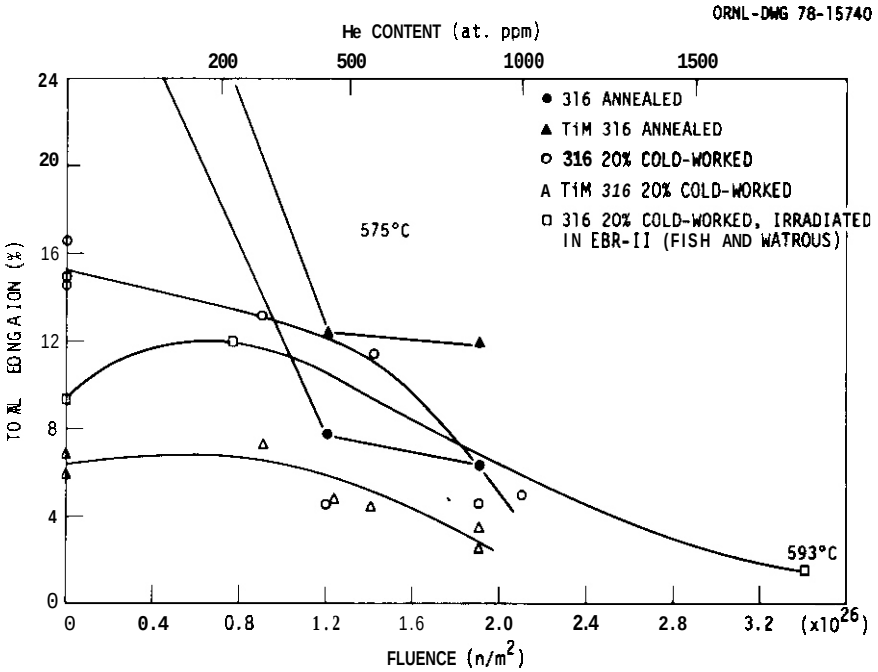

Fig. 3.2.8. Total Elongation as a Function of Fluence for Annealed and 20%-Cold-Worked Types 316 and TiM 316 Stainless Steel Tested at 575°C. Data on EBR-11-irradiated material from ref. 3.

TiM 316 material similar to that of the EBR-II-irradiated material. However, the standard type 316 stainless steel in the 20%-cold-worked condition still does not show a maximum in ductility. The ductility of the annealed material decreases monotonically. Although the rate of decrease declines at the high end of the fluence range examined for annealed material, there is not yet a clear indication of saturation for any of the four materials examined. (However, previous high-fluence experiments indicate the possibility of an eventual saturation in tensile ductility.[5]) The elongation of 20%-cold-worked type 316 stainless steel is approximately twice that of the TiM 316 at low fluences, but they tend to approach similar values at fluences near 2×10^{26} n/m^2. In the annealed materials, the TiM 316 exhibits higher ductility throughout the fluence range investigated, similar to its behavior at 450°C.

3.2.4.4 Discussion

Before considering the data, a few comments about irradiation temperature are appropriate. Work is now in progress to determine more

accurately irradiation temperature using melt wire devices and silicon carbide temperature monitors. Although the evaluation is incomplete, the actual irradiation temperatures were apparently above the design temperature, although the correction applies equally to all specimens and all temperatures. The difference in temperature must be considered as a possible explanation when interpreting results. However, the data show trends that are definitely attributable to helium or preirradiation microstructure and appear to be outside the possible differences due to irradiation temperature. Comparisons between alloys irradiated in HFIR at similar conditions can still be drawn.

Several very striking differences become evident when HFIR irradiation, which produces high levels of helium and displacement damage simultaneously, is compared with EBR-II irradiation, which produces displacement damage at nearly the same rate as HFIR but very little helium. Consider first the yield strength behavior of annealed and 20%-cold-worked type 316 stainless steel as a function of fluence. Irradiation in HFIR of annealed material results in irradiation hardening at all test temperatures, whereas irradiation of 20%-cold-worked material results in hardening at 350°C and softening at 450 and 575°C. The trend is the same as in EBR-11-irradiated material, but at 350°C both alloys in the 20%-cold-workedcondition harden approximately twice as fast up to a fluence of 0.6×10^{26} n/m^2 (>0.1 MeV), and at 450 and 575°C they soften. The higher rate of hardening may be attributable to helium and its effect of increasing cavity nucleation. Greenwood et al.[6] predicted theoretically that bubbles should prefer to nucleate at dislocations, Barnes and Mazey[7] noted almost complete association between helium bubbles and dislocations in helium-preinjected copper, and Vela and Russell[8] observed preferential association of bubbles with dislocations in neutron-irradiated copper-boron alloys. Vela and Russell also noted that the yield stress increased linearly with decreased bubble spacing. In HFIR-irradiated type 316 stainless steel helium bubbles have always been seen attached to dislocations or precipitate interfaces.[9,11] The presence of helium bubbles could also account for the greater strengthening of 20%-cold-worked material observed after

HFIR irradiation than after EBR-II irradiation since the latter results in much lower cavity densities at the fluences examined. Thus, there is evidence to support the hardening effect of helium. The bubble density should decrease as the irradiation temperature increases, and this effect has been observed;[9] the temperature dependence of yield strength could be attributed to this phenomenon. The bubble density should initially increase as a function of fluence but saturate at some level, with coalescence coarsening the distribution. Coarsening of bubbles in addition to precipitation should also produce softening. However, the major mechanism of softening at higher temperatures in cold-worked material is probably simple recovery of the dislocation structure. The effects observed at 450 and 575°C are not as straightforward and await microstructural analysis by transmission electron microscopy.

At 450°C the yield strength of the 20%-cold-worked material decreases while similar material irradiated in EBR-II at 482°C demonstrates a slight increase in yield strength. The yield strength of EBR-11-irradiated material decreases with fluence at 575°C and higher temperatures. Since helium hardens the matrix, this decrease in strength with increasing fluence similar to that associated with higher irradiation temperatures cannot be due to helium but rather is evidence to support the theory that the irradiation temperatures are higher than calculated. This does not alter the conclusion that the more rapid hardening in the HFIR-irradiated material is likely to be primarily the result of helium. Since higher temperatures would lead to decreased hardening, any hardening observed in type 316 stainless steel is probably attributable to helium and not to an error in irradiation temperature.

Now compare the behavior of the ductility response to irradiation in HFIR and in EBR-II. Here, because of the limited data, the comparison is restricted primarily to 20%-cold-workedmaterial. At test temperatures from 350 to 575°C, the ductility of EBR-11-irradiated material increases, passes through a maximum and then decreases with increasing fluence, asymptotically approaching a constant value. The value of the ductility maximum, the fluence at which it occurs, and the

asymptotic limit all vary with temperature. In contrast, HFIR-irradiated material monotonically decreases in ductility with increasing fluence for temperatures in the same range. Apparently only a few hundred atomic parts per million helium was sufficient to eliminate the peak in elongation, attributed to "irradiation-assisted annealing" by Fish and Watrous.[3] The fluence achieved was too low to observe saturation. A decrease in ductility at 350°C (Fig. 3.2.6) in HFIR-irradiated 20%-cold-worked type 316 is consistent with the observed increase in strength (Fig. 3.2.3) as a function of fluence. But the decreases in ductility at 450 and 575°C (Figs. 3.2.7, 3.2.8) accompanying the decrease in yield strength at those temperatures (Figs. 3.2.4, 3.2.5) do not normally follow. This effect may also be attributable to helium. If helium bubbles are interfering with dislocation motion in the matrix and if numerous cavities of sufficiently large size are forming at grain boundaries and thereby reducing the cross-sectional area, yielding in the vicinity of the grain boundary area occurs at a seemingly lower stress. Furthermore, this localized yielding in the vicinity of potentially deleterious defects such as grain boundary cavities may cause early fracture — that is, failure at lower values of total elongation. Microstructural examination is needed on these samples, but the assumption of grain boundary cavities at this fluence is consistent with the observation9 of grain boundary cavities from 375 to 680°C in 20%-cold-worked type 316 stainless steel irradiated to high fluences in HFIR.

At 450 and at 575°C (Figs. 3.2.4, 3.2.5, 3.2.7, 3.2.8) we note that the yield strength and ductility decrease gradually or remain constant with increasing fluence for 20%-cold-worked types 316 and TiM 316 stainless steel. However, the 20%-cold-worked type TiM 316 stainless steel maintains significantly higher strength and lower ductility than 20%-cold-worked unmodified alloy at all fluences examined. This behavior is consistent with strengthening due to TiC precipitation in the titanium-modified alloy. Van Aswegen and Honeycombe[12] first observed stacking fault precipitation of MC-type carbides, and Silcock and Tumstall[13] studied the mechanism of formation. Harding and Honeycombe[14]

studied the effect of MC-type precipitation on the mechanical properties of austenitic steels and found that TiC could lock dislocations and thereby increase the yield strength and decrease the ductility. But this was for aging after very short times at 700°C. Shepherd[15] noted that irradiation in a thermal reactor considerably enhanced precipitation of MC-type particles with a corresponding increase in yield strength and decrease in ductility. Therefore, HFIR irradiation, including a possible temperature shift, could have enhanced the precipitation of TiC. This could explain the differences in strength and ductility observed between the standard and TiM 20%-cold-worked material. However, the increased strength in the type TiM 316 stainless steel before irradiation might be due to titanium in solid solution lowering the stacking fault energy.[16]

Similar arguments can explain the results observed in the annealed materials. The sharp decreases in ductility with increasing fluence (Figs. 3.2.6, 3.2.7, and 3.2.8) of both materials are consistent with the rapid increases in yield strength observed with increasing fluence (Figs. 3.2.3, 3.2.4, and 3.2.5) as explained above. The relative behavior of the ductility for the annealed standard and TiM material at 450 and 575°C is opposite that observed for the 20%-cold-worked materials, in that the ductility of the TiM material is considerably higher than that of standard type 316 stainless steel. This may be expected, however, if we consider the behavior of the annealed material irradiated in HFIR at higher fluences.[10,17] Precipitation of TiC in type TiM 316 stainless steel has been shown to have a pronounced effect on trapping helium,[10] and this has been shown to reduce the embrittling effects of helium and increase the total elongation.[17] If helium bubbles are causing embrittlement by forming at the grain boundaries of 20%-cold-worked material, then grain boundary precipitation precluding grain boundary bubble formation may be responsible for the ductility response of annealed material at 450 and 575°C. Grain boundary precipitation of $M_{23}C_6$ has been observed[9,10] in annealed types 316 and TiM 316 after HFIR irradiation below 600°C and has been observed[17,18] to be responsible in both alloys for ductility greater than that observed for

microstructures having large cavities rather than precipitate at the grain boundaries. Grain boundary precipitation of $M_{23}C_6$ is expected for these temperatures and fluences, and the observed ductility response of HFIR-irradiated annealed material at 450 and 575°C is consistent with the effect of grain boundary precipitation. However, confirming microstructural analysis needs to be done to support this.

3.2.5 Conclusions

1. At 350°C 20%-cold-worked type 316 stainless steel irradiated in HFIR hardens at nearly twice the rate of similar material irradiated in EBR-II. Both tend to soften with increasing fluence at 575°C.

2. The yield strengths of all HFIR-irradiated materials behave similarly at 350°C, but the yield strength of 20%-cold-worked type 316 with 0.23 wt % Ti is significantly higher at 450 and 575°C.

3. The total elongation of all materials irradiated in HFIR tends generally to decrease with increasing fluence, with 20%-cold-worked material showing a more gradual decrease and annealed material showing a much sharper decline at all temperatures observed.

4. The total elongation of all materials remains above 6% at 350°C, 7% at 450°C, and 2.5% at 575°C in the fluence range investigated (up to 2.1×10^{26} n/m^2). Consistent with its higher strength, type 316 with 0.23 wt % Ti has the lowest ductility at 450 and 575°C.

5. The strength and ductility of all materials examined appear adequate for early life as structural materials for a fusion reactor.

3.2.6 References

1. F. W. Wiffen, E. J. Allen, E. E. Bloom, H. Farrar, T. A. Gabriel, A. T. Kerr, and F. G. Perey, "The Rate of Helium Generation in HFIR Irradiation of Nickel," *Magnetic Fusion Energy Materials Technology Program Annu. Prog. Rep. June 30, 1977,* ORNL-5323, pp. 42-43.
2. M. L. Grossbeck and P. J. Maziasz, "The Swelling of 20%-Cold-Worked Type 316 Stainless Steel Irradiated in HFIR to Helium Levels of 200-3700 at. ppm," *ADIP Quart. Prog. Rep. Jan.-March 1978,* DOE/ET-0058/1, pp. 82-85.

3. R. L. Fish and J. D. Watrous, "Effect of Test Reactor Irradiation on the Tensile Properties of 20%-Cold-Worked Type 316 Stainless Steel,'' pp. 91—100 in *Irradiation Effects on the Microstructure and Properties of Metals, ASTM Spec. Tech. Publ.* 611, American Society for Testing and Materials, Philadelphia, 1976.

4. R. L. Fish and J. J. Holmes, "Tensile Properties of Annealed Type 316 Stainless Steel After EBR-II Irradiation," *J. Nucl. Mater.* 46: 113—20 (1973).

5. F. W. Wiffen, *The Effects* of *CTR Irradiation on the Mechanical Properties of Structural Materials,* ORNL/TM-5624 (November 1976).

6. G. W. Greenwood, A.J.E. Foreman, and D. E. Rimmer, "The Role of Vacancies and Dislocations in the Nucleation and Growth of Gas Bubbles in Fissile Material," *J. Nucl. Mater.* 4: 305—24 (1959).

7. R. S. Barnes and D. J. Mazey, "The Migration and Coalescence of Inert Gas Bubbles in Metals," *Proc. R. Soc. London, Ser. A,* 275: 47—57 (1963).

8. P. Vela and B. Russell, "The Behavior of Helium Gas in Irradiated Copper-Boron Alloys," *J. Nucl. Mater.* 19: 312—26 '(1966).

9. P. J. Maziasz, F. W. Wiffen, and E. E. Bloom, "Swelling and Microstructural Changes in Type 316 Stainless Steel Irradiated Under Simulated CTR Conditions," pp. 259—86 in *Radiation Effects and Tritium Technology for Fusion Reactors,* CONF-750989, Vol. I (March 1976).

10. P. J. Maziasz and E. E. Bloom, "Comparison of Titanium-Modified and Standard Type 316 Stainless Steel Irradiated in HFIR — Swelling and Microstructure," ADIP *Quart. Prog. Rep. January—March, 1978,* DOE/ET-0058/1, pp. 40—53.

11. P. J. Maziasz, "Precipitation Response of Annealed Type 316 Stainless Steel in HFIR Irradiations at 550 to 680°C," *ADIP Quart. Prog. Rep. January—March, 1978,* DOE/ET-0058/1, pp. 63—81.

12. J.S.T. Van Aswegen and R.W.K. Honeycombe, "Segregation and Precipitation in Stacking Faults," *Acta Metall.* 10: 262—64 (1962).

13. J. M. Silcock and W. J. Tumstall, "Partial Dislocations Associated with NbC Precipitation in Austenitic Stainless Steels," *Philos. Mag.* 10: 316–89 (1964).

14. H. J. Harding and R.W.K. Honeycombe, "Effect of Stacking Fault Precipitation on the Mechanical Properties of Austenitic Steels," *J. Iron Steel Inst. London* 204: 259–67 (March 1966).

15. J. P. Shepherd, "Irradiation–Induced Precipitation in a Niobium-Stabilized Stainless Steel," *Met. Sci. J.* 3: 229–34 (1969).

16. D. Fahr, "Microstructural Studies of Unirradiated Standard and Titanium–Modified Type 316 Stainless Steel and Consequential Considerations," *Fuels and Materials Development Program Quart. Prog. Rep. Dec. 31, 1971*, ORNL/TM-3300, pp. 112–20.

17. P. J. Maziasz and E. E. Bloom, "Mechanical Properties of Type 316 and Titanium–Modified Type 316 Stainless Steel Irradiated in HFIR, *ADIP Quart. Prog. Rep. January–March, 1978*, DOE/ET-0058/1, pp. 54-62.

18. E. E. Bloom and F. W. Wiffen, "The Effects of Large Concentrations of Helium on the Mechanical Properties of Neutron–Irradiated Stainless Steel," *J. Nucl. Mater.* 58: 171–84 (1975).

4. PATH B ALLOY DEVELOPMENT – HIGHER STRENGTH Fe-Ni-Cr ALLOYS

Path B alloys are the Fe-Ni-Cr "superalloys" in which tensile, creep-rupture, and fatigue strength levels higher than attainable in the austenitic stainless steels are achieved by precipitation of one or more phases. Many alloys in this class exhibit low swelling in fast-reactor irradiations. The technology for use of path B alloys in neutron radiation environments is not as advanced as for path A alloys. A basis to select a specific alloy type for further development is lacking. Accordingly, the ADIP task group has selected five base research alloys that are representative of the basic systems of path B alloys and deserve consideration for fusion reactor applications. The systems under investigation include γ' strengthened-molybdenum modified, γ' strengthened-niobium-modified, $\gamma'\gamma''$ strengthened, and a high-nickel precipitation-strengthened alloy (~75% Ni).

Near-term activities are focused on evaluating the effects of a fusion reactor neutron spectrum on key mechanical and physical properties. Damage created by the fusion reactor neutron spectrum is approximated by fission reactor irradiation. Data are presently being obtained on a limited number of commercial alloys on which scoping studies were initiated two to three years ago. The emphasis will shift to base research alloys as they become available. For those properties that are either inadequate or degraded to an unacceptable level, the influence of composition and microstructure on the response will be examined. The research program will be oriented toward determination of mechanisms responsible for the observed property changes and the effects of metallurgical variables on the response. The objective is to develop a basis for selection of the path B prime candidate alloy(s).

4.1 THE SWELLING OF NIMONIC PE-16 IRRADIATED IN HFIR — F. W. Wiffen (ORNL)

4.1.1 ADIP Task

ADIP Task I.C.3, Microstructures and Swelling in Higher Strength Fe-Ni-Cr Alloys.

4.1.2 Objectives

Nimonic PE-16 was chosen as a representative precipitation-strengthened Path B alloy for investigation of the effect of HFIR irradiation on physical and mechanical properties. The swelling resistance of this alloy under neutron irradiation and ion bombardment has been demonstrated in a number of experiments where high displacement levels but low helium contents were produced. The HFIR experiments were initiated to investigate the response to irradiation producing helium levels more representative of fusion reactor service simultaneously with production of displacement damage. Specimens irradiated at temperatures between 55 and 700°C are being examined to determine swelling, microstructural changes, tensile properties, and fracture mode. Experiments in this series have been irradiated to neutron fluences producing 2 to 28 dpa and helium contents of 120 to 5400 at. ppm.

4.1.3 Summary

Swelling-tensile samples of Nimonic PE-16 were irradiated in HFIR at 55 to 700°C to produce simultaneously dpa levels from 2.2 to 16.7 and helium contents from 120 to 2960 at. ppm. These conditions resulted in <2% swelling. The maximum swelling, 1.92%, was found at 500°C in solution treated and aged material. The material solution treated only resisted swelling slightly more than aged material. Neither material showed very strong temperature dependence of swelling. There was no rapid, breakaway swelling above 600°C, as observed in type 316 stainless steel and alloy 600. The fluence dependence of the swelling suggests that an "incubation period" precedes significant swelling.

4.1.4 Progress and Status

4.1.4.1 Experiments

The composition of PE-16 (heat NNW-2282) used in this investigation is:

Element:	Ni	Cr	Fe	Mo	Al	Ti	Si	C	Mn
wt %:	43.1	16.5	bal	3.2	1.24	1.18	0.21	0.05	0.04

This composition produces an austenitic alloy that can be hardened by the precipitation of γ' phase, $Ni_3(Al,Ti)$. Rod specimens of this alloy were machined with a gage section 2 mm in diameter and 18 mm long. Machined samples were solution annealed in argon, either 2 h at 1120°C or 4 h at 1080°C, and then furnace cooled. Samples to be irradiated with a solution annealed and aged microstructure were treated 16 h at 700°C.

Samples to be irradiated at about 55°C were in direct contact with the reactor cooling water. Details of this experiment, HFIR-CTR-16, were reported previously.[1] Samples for elevated-temperature irradiation were contained in sealed irradiation capsules. In these experiments temperatures were controlled by the width of a helium-filled gap between the specimen and the specimen holder. Nuclear hearing of the sample then established the temperature gradient across this gap and thus the irradiation temperature. More experimental details and a schematic illustration of the experiment were included in a previous report.[2]

Tensile-swelling specimens of Nimonic PE-16 have been irradiated in eight HFIR irradiation capsules. All were exposed in the PTP (peripheral target position) location of the reactor. Table 4.1.1 identifies these experiments and summarizes the temperature range and irradiation parameters achieved. Helium contents were calculated from the equation developed3 to correlate experimentally measured values of helium production from the reaction sequence

$$^{58}Ni + n \rightarrow {}^{59}Ni + \gamma$$

$$^{59}Ni + n \rightarrow {}^{56}Fe + \alpha \, .$$

Table 4.1.1. Summary of HFIR Experiments Containing Nimonic PE-16 Swelling and Tensile Specimens

Experiment	Irradiation Temperature (°C)	Range of Displacement Level (dpa)	Range of Helium Produced[a] (at. ppm)
HFIR-CTR-3	300—700	4.2—8.1	367–1040
HFIR-CTR-4	300–700	2.2—4.3	119—365
HFIR-CTR-5	300—700	4.2—8.0	360—1020
HFIR-CTR-6	300—700	4.2—8.0	360—1020
HFIR-CTR-7	300—700	8.7–16.7	1210—2960
HFIR-CTR-8	300—700	8.7–16.7	1210—2960
HFIR-CTR-16	-55	3.9—9.9	355—1400
HFIR-CTR-18	300–700	17.5—27.6	3260—5350

[a]Helium calculated as discussed in text.

These values were further normalized to the single available measurement for PE-16, at 1030 ± 10 at. ppm He.

The length of samples measured before and after irradiation yielded an approximate measure of swelling, useful as an indication of trends. The swelling values reported here were determined by immersion density measurements. Densities were measured in either water or ethyl phthalate, with the temperature controlled to ±0.05°C. The liquid density was calibrated against a quartz standard.

4.1.4.2 Relationship to Fusion Reactor Conditions

Irradiation in HFIR-PTP experiments produces displacement damage at a rate equivalent to that in a fusion reactor operating at about 3 MW/m^2. The relationship between helium production rates in the two facilities is more complicated. In a fusion reactor, helium is produced by single-step (n,α) reactions between the higher energy neutrons and all the alloy constituents. For a first wall of PE-16 in a lithium blanket tokamak the helium is produced at a rate of 240 at. ppm per $MWyr/m^2$. In HFIR the helium is produced in a two-step reaction between

^{58}Ni and thermal energy neutrons, and thus the production rate is not linear with time. Irradiation in the center of the PTP location for one year will produce greater than 6000 at. ppm He in PE-16. This amount of helium would be produced in PE-16 in a fusion reactor first wall after 25 $MWyr/m^2$ of operation.

The relationship between the irradiation parameters achieved in these experiments and fusion reactor operation is given in Table 4.1.2. The equivalence is given for fusion service time to produce the displacement level and time to produce the helium level for several of the HFIR irradiation conditions.

Table 4.1.2. The Correspondence Between HFIR Irradiation Parameters and Fusion Reactor Service for Nimonic PE-16

Parameters of HFIR Experiments			Fusion Reactor Service to Achieve Same Parameters, $MWyr/m^2$	
Displacement Level (dpa)	Helium Content (at. ppm)	Ratio,[a] (at. ppm He/dpa)	dpa Level	Helium Level
2.2	120	54.5	0.19	0.5
8.0	1020	128	0.68	4.3
16.7	2960	177	1.4	12.3
27.6	5350	194	2.4	22.3

[a]This ratio is 20.5 for a Tokamak fusion reactor with a lithium blanket and a first wall of PE-16.

4.1.4.3 Results

The results of swelling measurements (density decrease) on all the Nimonic PE-16 swelling-tensile specimens irradiated and examined to date are given in Table 4.1.3. The fast-neutron fluence, displacement level, and calculated helium content for each datum are also given. The swelling data for three irradiation temperatures — 300, 500, and 700°C – are plotted as a function of helium content produced during the irradiation in Fig. 4.1.1. Since helium production from ^{58}Ni during HFIR irradiation

Table 4.1.3. **Swelling** in Nimonic PE-16 Irradiated in HFIR

Irradiation Conditions				Solution Annealed Microstructure		Solution Annealed and Aged Microstructure	
Temperature (°C)	Fluence >0.1 MeV (n/m^2)	Displacement Level (dpa)	Helium (at. ppm)	Heat Treatment[a]	Density Decrease (%)	Heat Treatment[a]	Density Decrease (%)
-55	5.4×10^{25}	3.9	355			(1)	0.26
-55	9.7	7.2	820			(1)	0.45
-55	13.2	9.9	1400			(1)	0.58
300	2.9	2.2	119			(1)	-0.19
300	5.2	3.9	305			(1)	-0.15
300	5.4	4.2	367	(2)	-0.21		
300	9.6	7.3	866	(2)	-0.15	(3)	-0.31
300	11.1	8.7	1210	(4)	0.10	(1)	0.07
300	20.0	15.2	2580	(4)	0.71	(1)	0.69
400	3.0	2.3	123			(1)	-0.19
400	4.6	3.5	245			(1)	-0.26
400	5.7	4.3	376	(2)	0.32		
400	8.5	6.5	707	(2)	-0.16	(3)	-0.20
400	11.7	8.8	1230	(4)	0.32	(1)	0.19
400	17.6	13.5	2170	(4)	0.93	(1)	0.96
500	3.8	3.0	184			(1)	-0.20
500	5.6	4.2	349			(1)	-0.21
500	7.1	5.6	551	(2)	-0.17		
500	10.4	7.9	978	(2)	-0.26	(3)	-0.12
500	14.6	11.5	1720	(4)	0.42	(1)	1.22
500	21.6	16.4	2860	(4)	0.86	(1)	1.92
600	4.0	3.0	183			(1)	-0.17
600	5.3	3.9	307			(1)	-0.24
600	7.6	5.6	549	(2)	0.18		
600	9.8	7.3	872	(2)	0.00	(3)	0.12
600	15.5	11.5	1720	(4)	0.45	(1)	0.64
600	20.5	15.2	2590	(4)	0.84	(1)	1.10
650	5.7	4.3	365			(1)	0.08
650	10.4	8.0	1020	(2)	0.51	(3)	0.23
650	21.9	16.7	2960	(4)	1.33	(1)	0.96
700	4.7	3.5	250			(1)	-0.03
700	5.6	4.2	35b			(1)	-0.05
700	8.8	6.6	735	(2)	0.15		
700	10.4	7.9	981	(2)	0.56	(3)	0.35
700	18.3	13.7	2210	(4)	0.43	(1)	1.31
700	21.6	16.4	2860	(4)	0.91	(1)	1.35

[a]Heat treatments are as follows:
(1) 4 h at 1080°C plus 16 h at 700°C
(2) 2 h at 1120°C
(3) 2 h at 1120°C plus 16 h at 700°C
(4) 4 h at 1080°C.

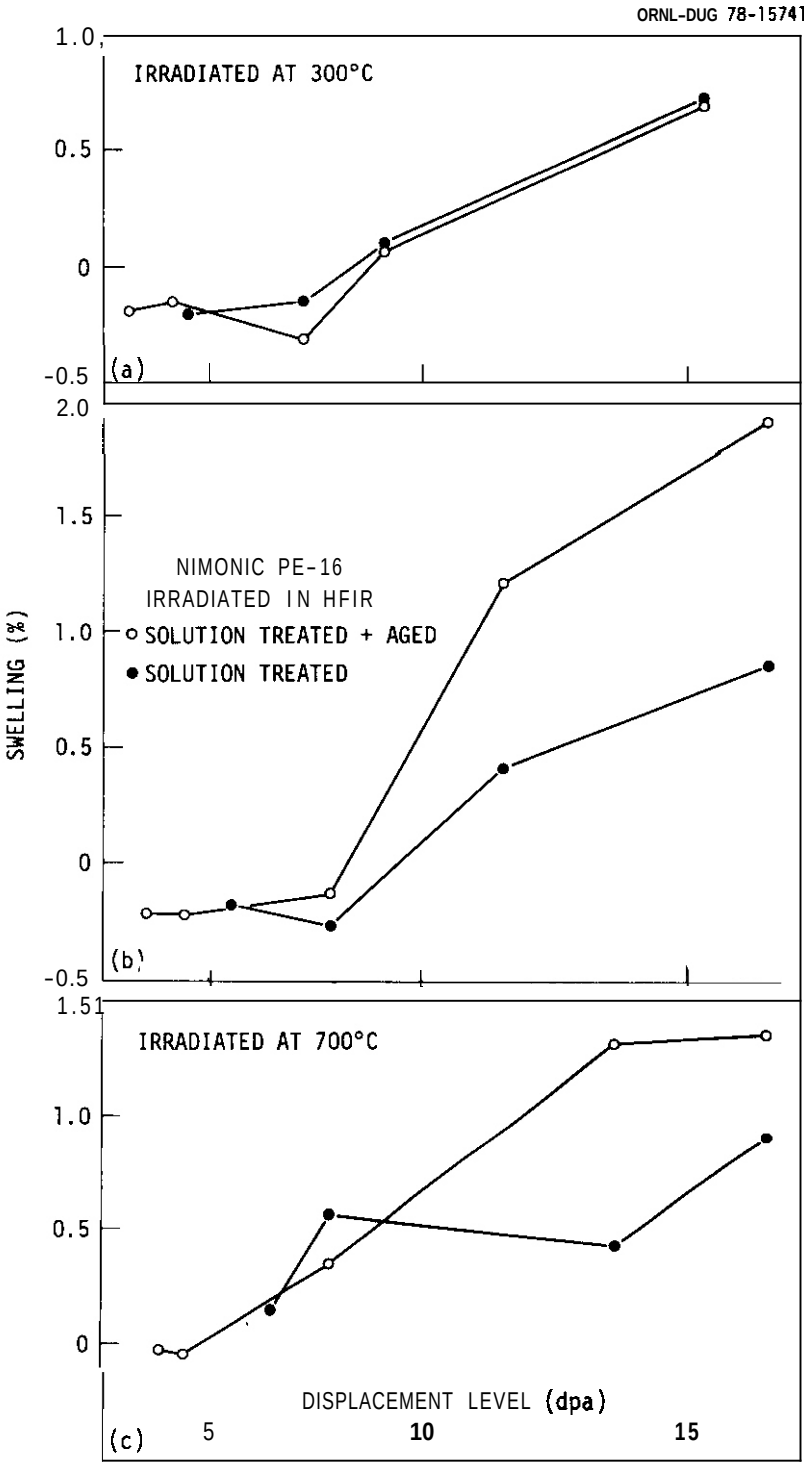

Fig. *4.1.1.* The Dependence of Swelling of Nimonic PE-16 on Irradiation Parameters for HFIR Irradiation. The swelling data are plotted vs a linear scale of helium content, thus neutron fluence or dpa is not linear on the abscissa. (a) Irradiated at 300°C. (b) 500°C. (c) 700°C.

is not a linear function, fluence and dpa level do not correspond linearly to the abscissa on Fig. 4.1.1. However, approximate dpa scales are given on these figures.

Qualitatively similar behavior was found for all irradiation temperatures. Low-fluence irradiation produced some densification, but as fluence increased swelling resulted. Material either solution treated only or solution treated and aged behaved qualitatively similarly.

Too few data are available to establish the analytical dependence of swelling on helium produced or on dpa level. The data do suggest an "incubation range" before a true swelling rate is established. However, whether the swelling rate is controlled by dpa level, by helium, or by a function of both of these will require more analysis and likely also more experimental data.

The greatest amount of swelling measured in these experiments was 1.92%. This occurred at the highest fluence irradiation at 500°C in the solution treated and aged material. A specimen of solution treated only material swelled less than half as much under identical irradiation conditions.

Swelling is plotted against temperature in Figs. 4.1.2 and 4.1.3 for solution treated only and solution treated plus aged material, respectively. In both figures swelling data are plotted at two helium levels, 1000 and 2400 at. ppm. Swelling at these helium levels was obtained by linear interpolation between the two closest data points for the appropriate temperature, on graphs similar to those of Fig. 4.1.1.

For irradiation producing approximately 1000 at. ppm He the swelling of Nimonic PE-16 is near zero for most temperatures, and in any case not over 0.5%, for both preirradiation microstructures. Since inspection of Fig. 4.1.1 shows that the "swelling threshold" is likely near 1000 at. ppm He, the lack of a well-defined temperature dependence of swelling at this fluence is not surprising. At a fluence producing 2400 at. ppm He, swelling of the solution treated only PE-16 varies between 0.5 and 1.1% over the temperature range 300 to 700°C, Fig. 4.1.2. Local swelling maxima are indicated at 400 and 650°C, but data more closely spaced across this temperature span would be required to confirm these maxima. It is

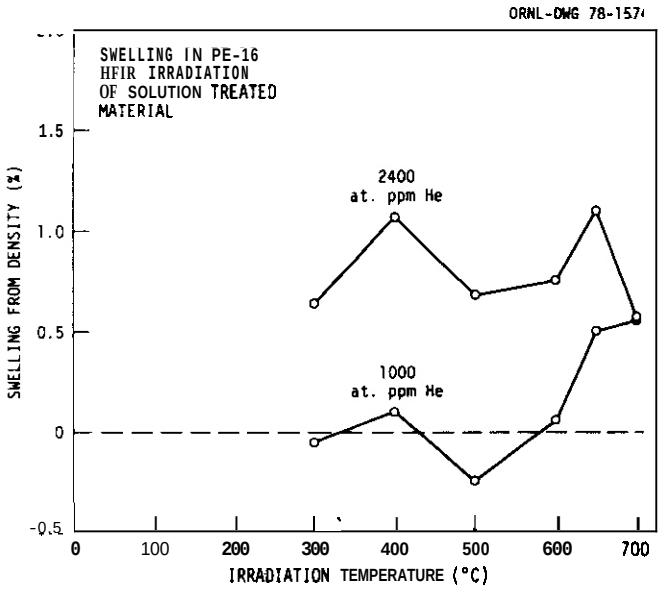

Fig. 4.1.2. The Temperature Dependence of Swelling for Solution Annealed Nimonic PE-16 Irradiated in HFIR. The data plotted at constant helium levels were obtained by linear interpolation between the two closest data on graphs similar to Fig. 4.1.1.

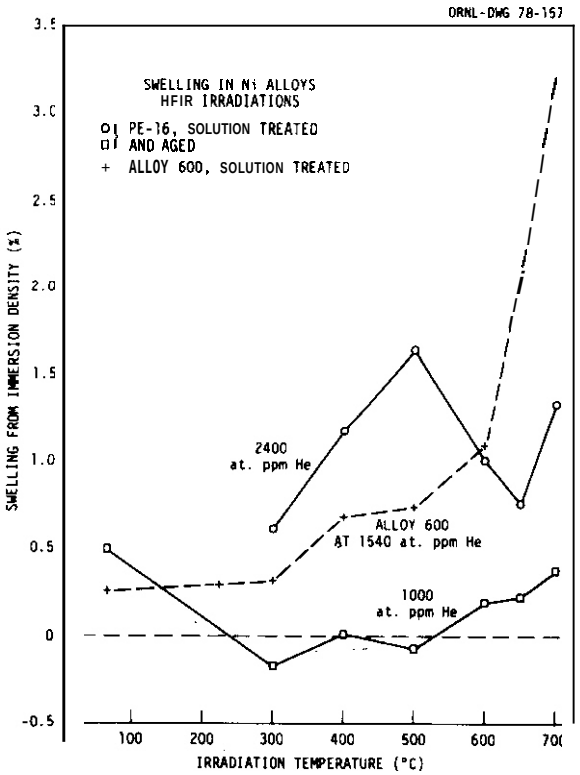

Fig. 4.1.3. The Temperature Dependence of Swelling in Nimonic PE-16 Irradiated in HFIR. These specimens were solution treated, then aged 16 hr at 700°C before irradiation. Constant helium content data were obtained by linear interpolation on graphs similar to Fig. 4.1.1. The swelling of solution annealed alloy 600, shown for comparison, is from ref. 2.

significant that the 700°C swelling is not a local maximum. At 2400 at. ppm He in the solution annealed and aged material (Fig. 4.1.3) the peak swelling occurs at 500°C, and the data suggest there may be a second peak at 700°C or higher.

4.1.4.4 Comparison of PE-16 with Other Alloys

For irradiation temperatures of 600°C or lower, the swelling of PE-16 is slightly higher than that of 20%-cold-worked type 316 stainless steel[4] and comparable to solution annealed alloy 600,[2] when comparisons are made at comparable helium contents. However, these alloys differ significantly for higher irradiation temperatures. In the PE-16, swelling shows little temperature dependence for irradiation temperatures up to 700°C. In contrast, swelling in alloy 600 (Fig. 4.1.3) and type 316 stainless steel[5] increased rapidly with increasing temperature above 600°C. Identification of the mechanisms providing this extra swelling resistance of PE-16 will require microstructural examination of the samples. Only preliminary results are available now.[6]

4.1.5 Conclusions and Future Work

Irradiation of Nimonic PE-16 in HFIR, producing up to 17 dpa and 2900 at. ppm He, has been completed for the temperature range 300 to 700°C. On the basis of equivalent fusion reactor service time, the highest dpa level would be produced by 1.4 $MWyr/m^2$ of fusion reactor operation, and the highest helium content by 12 $MWyr/m^2$ of operation. The maximum amount of swelling measured was 1.92% for the highest fluence irradiation at 500°C. The solution treated only material was slightly more resistant to swelling than material in the solution treated plus aged condition. The fluence dependence of the swelling suggests an "incubation period" before significant swelling occurs. Beyond this incubation fluence the tem-perature dependence of swelling is still not very strong. In particular, the swelling rate did not rapidly increase with increasing temperature above 600°C, as was the case in type 316 stainless steel and alloy 600.

The sample set treated in this report will be tensile tested at temperatures near the irradiation temperature. Future reports will include tensile results, fractography, and microstructural characterization.

4.1.6 References

1. F. W. Wiffen, "The Effects of Irradiation at About 55°C on Type 316 Stainless Steel," *ADIP Quart. Prog. Rep. January–March, 1978*, DOE/ET-0058/1, pp. 89–93.
2. F. W. Wiffen, "The Response of Inconel 600 to Simulated Fusion Reactor Irradiation," *ADIP Quart. Prog. Rep. April–June, 1978*, DOE/ET-0058/2, pp. 62–81.
3. F. W. Wiffen, E. J. Allen, H. Farrar, E. E. Bloom, T. A. Gabriel, H. T. Kerr, and F. G. Perey, "The Production Rate of Helium During Irradiation of Nickel in Thermal Spectrum Fission Reactors," paper in preparation for First Topical Meeting on Fusion Reactor Materials, Miami Beach, Fla., January 1979.
4. M. L. Grossbeck and P. J. Maziasz, "The Swelling of 20%-Cold-Worked Type 316 Stainless Steel Irradiated in HFIR to Helium Levels of 200–3700 at. ppm," *ADIP Quart. Prog. Rep. January–March, 1978*, DOE/ET-0058/1, pp. 82–85.
5. F. W. Wiffen and E. E. Bloom, "Effect of High Helium Content on Stainless-Steel Swelling," *Nucl. Technol.* 25: 113–23 (1975).
6. D. N. Braski and F. W. Wiffen, "The Microstructure of Nimonic PE-16 Irradiated to Produce High Helium Contents," *ADIP Quart. Prog. Rep. January–March, 1978*, DOE/ET-0058/1, pp. 96–105.

5. PATH C ALLOY DEVELOPMENT – REACTIVE AND REFRACTORY ALLOYS

Two distinct and separate subgroups fall under the broad classification of path C alloys. These subgroups are conveniently classified as "reactive metal alloys" and "refractory metal alloys." Analyses of the properties required for performance of materials in high-flux regions of fusion reactors and assessments of the known and extrapolated properties have identified titanium alloys of the reactive metal alloys and vanadium and niobium alloys of the refractory metal alloys as having the most promise for fusion reactor applications. For both the reactive and refractory alloys, there is an extreme lack of data that are relevant and necessary for selection of specific alloy types for development (i.e., solid solution, precipitation strengthened, single or multiphase). In the case of titanium alloys, the most critical deficiency is the lack of data on the response of these alloys to high-fluence neutron radiation. For vanadium and niobium alloys, while the effects of radiation on mechanical behavior are not adequately known, perhaps the most alarming deficiency is the near total lack of base-line information on the effects of cyclic (fatigue) loading on mechanical performance. Precisely because of these deficiencies in the data base and overall metallurgical experience, these alloys are still in a "scoping study" phase of their evaluation as candidates for fusion reactor first-wall materials.

The ADIP task group has selected four titanium alloys, three vanadium alloys, and two niobium alloys for the scoping phase of the development program. Titanium alloys are generally classified according to the relative amounts of α (hcp) and β (bcc) phases that they contain. The titanium alloys selected represent the three alloys (types α plus β, α rich, and β rich). Vanadium and niobium alloys are not in commercial use as are the other alloy systems in the program. Selection of the scoping alloys was based primarily on results of previous programs on vanadium cladding development for LMFBRs and high-temperature alloys for space power systems. The three vanadium alloys are V–20% Ti, V–15% Cr–5% Ti, and Vanstar 7. The binary has relatively good fabricability, and appears to be swelling resistant in fast-reactor irradiations but

is rather weak. The ternary V–15% Cr–5% Ti and precipitation-strengthened Vanstar 7 alloys are significantly stronger. The Nb–1% Zr binary alloy is included as a reference material, since a significant amount of data exists for this alloy irradiated in fast reactors. The alloy Nb–5% Mo–1% Zr is much stronger than the binary and can be developed for applications near 800°C.

Near-term activities on path C alloys will focus on obtaining data on the unirradiated mechanical properties, corrosion, and compatibility, and the effects of irradiation on physical and mechanical properties. Fission reactor irradiation with and without helium preinjection, high-energy neutron sources, and charged-particle irradiations will be used in the development of techniques to approximate the effects of the fusion reactor neutron spectrum (He/dpa production). The objective is to develop sufficient understanding of the behavior of path C alloy systems (Ti, V, and Nb alloys) to allow selection of path C base research alloys. The effects of composition and microstructure on alloy performance will then be investigated in the base research alloys.

6. PATH D ALLOY DEVELOPMENT — INNOVATIVE MATERIAL CONCEPTS

Innovative material concepts are included as a path in the alloy development program because the fusion reactor environment is extremely demanding on materials in the high-flux region and the more conventional materials and metallurgical concepts may not be adequate. Novel approaches to alloy design, nonconventional material processing to tailor properties, or alternate materials such as structural ceramics and fiber composites will be considered.

7. STATUS OF IRRADIATION EXPERIMENTS

Irradiation experiments are presently being conducted in the ORR and HFIR, which are mixed-spectrum fission reactors, and in the EBR-II, which is fast-spectrum reactor. Experiments are generally cooperative between several program participants. Experiment plans, test matrices, etc., are reviewed by the Alloy Development for Irradiation Performance Task Group.

7.1 STATUS OF IRRADIATION EXPERIMENTS — J. W. Woods, E. E. Bloom, and A. F. Zulliger (ORNL)

7.1.1 ADIP Task

These experiments support those tasks of the ADIP Program Plan that require neutron irradiations to accomplish their objectives. The experiments contain alloys from each alloy development path.

7.1.2 Objective

ORR-MFE-1 and ORR-MFE-2 irradiation experiments are vehicles for irradiation of samples for postirradiation testing and examination (e.g., tensile, creep-rupture, and fatigue testing; measurement of irradiation creep; and microstructural examination). The objectives of these experiments from the viewpoint of alloy development are to examine:

1. effects of composition on the tensile properties of stainless steels with nominal compositions near that of type 316 stainless steel;
2. effects of preirradiation heat treatment on the tensile properties of type 316 stainless steel;
3. effects of irradiation on the tensile properties of type 316 and 16-8-2 stainless steel welds;
4. effects of irradiation on the tensile properties of representative path B alloys;
5. effects of irradiation on the tensile, creep-rupture, and fatigue properties and on the microstructures of representative titanium alloys, vanadium alloys, and niobium alloys;
6. irradiation creep of type 316 stainless steel and Nimonic PE-16, path A and B alloys, respectively;
7. postirradiation fatigue properties of type 316 stainless steel, Nimonic PE-16, and high-nickel alloys X-750 and Inconel 600;
8. effects of irradiation on tensile and creep-rupture properties of alloys with long-range order (path D).

7.1.3 Summary

The irradiation of ORR-MFE-1 was completed June 28, 1978 with an irradiation of 72,698 MWh (261.71 TJ). The experiment has been disassembled,

and the specimens are being examined. Irradiation of ORR-MFE-2 began August 31, 1978, and it has accumulated an exposure of 16,212 MWh.

7.1.4 Progress and Status

7.1.4.1 Status of ORR-MFE-1

The first experiment, ORR-MFE-1, in support of fusion reactor materials development conducted in the ORR was placed in position C-7 February 13, 1978, with fuel elements on all four sides. Temperatures in the experiment exceeded the desired control temperatures at many positions within the capsule. To remedy the situation, the core configuration was changed, and several control temperatures were reevaluated and raised for operation of the experiment. The experiment was terminated June 28, 1978 after having accumulated an irradiation of 72,698 MWh. The temperature history of each position in the experiment is summarized in Table 7.1.1. The experiment has been disassembled in the hot cell, and specimen examination is in progress.

7.1.4.2 Status of ORR-MFE-2

The results of ORR-MFE-1 showed that the desired lower irradiation temperatures for ORR-MFE-2 could not he obtained with the present design unless the number of samples was drastically reduced. It was, therefore, decided to redesign ORR-MFE-2 to obtain more efficient heat removal to enable testing the required number of specimens. A detailed description of the redesigned experiment was presented in the previous report.[1] Figure 7.1.1 shows the completed experiment before being placed inside the experiment container.

The experiment was inserted in the E-7 position of the ORR on August 31, 1978 and to date has accumulated an exposure of 16,212 MWh.

The reactor has been operated at a power level of 25 MW during the residence of ORR-MFE-2. This constraint was imposed by a previously installed experiment unrelated to the MFE program, which is to be removed

Table 7.1.1. Temperature Summary of ORR-MFE-1

Position	Temperature, °C			Duration of max Temperature (h)
	max[a]	av	range[a]	
1	450	370	349-436	1.55
2	453	450	448-453	72
3	553	511	343-553	192
4	653	651	647-563	24
5	457	370	349-416	1.55
6	467	450	448-452	1.55
7	560	552	548-559	24
8	659	652	650-659	24
9	557	457	448-483	1.55
10	522	438	399-467	1.55
11	654	552	549-558	1.55
12	779	650	647-653	1.55
13	779	610	598-642	1.55
14	752	615	575-637	1.55
15	760	649	623-703	1.55
16	752	652	646-557	1.55
17	683	516	500-537	1.55
18	662	513	500-532	1.55
19	665	860	550-578	1.55
20	686	602	598-603	1.55
21	799	527	524-562	1.55
22	662	577	575-582	1.58
23	684	577	573-578	1.55
24	712	652	649-653	1.55
25	649	521	513-539	1.55
26	638	478	471-493	1.55
27	708	577	574-593	1.55
28	662	654	547-662	24
29	622	502	500-504	1.55
30	600	452	450-478	1.55
31	641	552	549-554	1.55
32	635	602	599-604	1.55

[a]The maximum is for the entire irradiation, and in most cases it occurred during the early period of operation above intended temperatures. The range is for the period after core configuration adjustment and control readjustment and thus may not include the maximum.

Y-156182

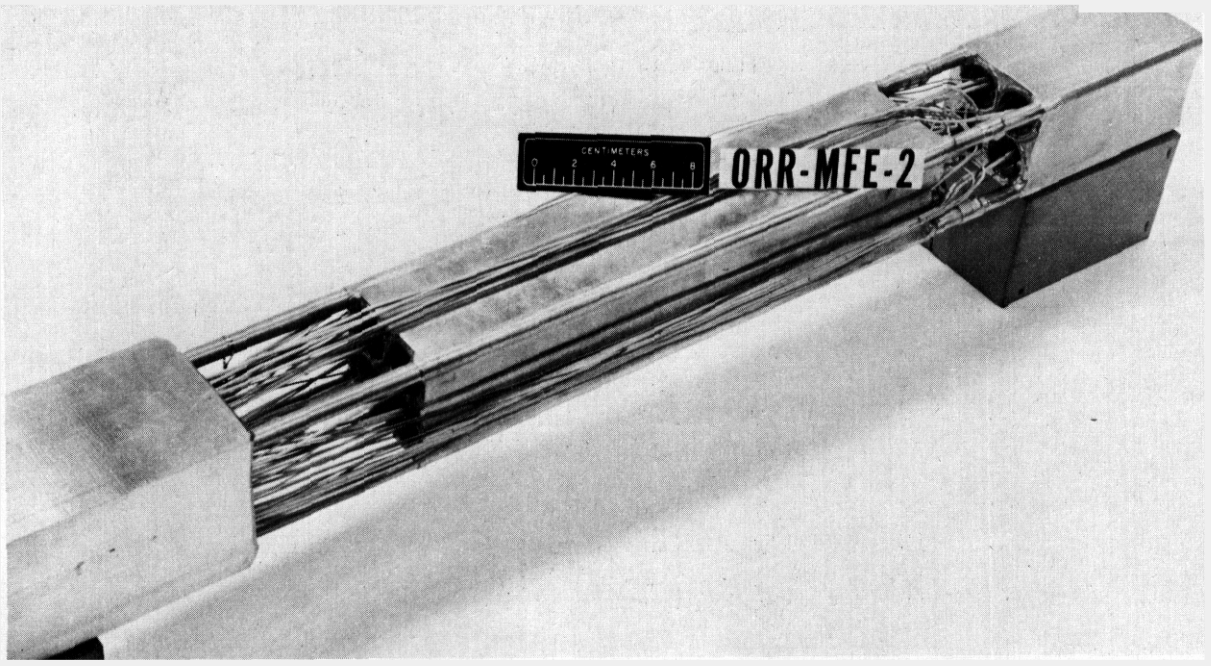

Fig. 7.1.1. Experiment ORR-MFE-2 Before Insertion in Experiment Container.

October 15, 1978. Because of this 25-MW operation, the MFE-2 experiment could not reach planned control temperatures with helium cooling. The gas system was modified to provide for a helium-neon mixture rather than pure helium. By use of the gas mixture, the thermal conductivity of the gas was adjusted to permit reaching desired control temperatures.

7.1.5 Conclusion

Irradiation of ORR-MFE-1 has been concluded, and the experiment has been disassembled. Exposure time was 72,698 MWh (261.71 TJ). Fabrication of ORR-MFE-2 was completed, the experiment was installed in the E-7 position of the ORR, and it has now accumulated an exposure of 16,212 MWh (58.363 TJ) at the desired control temperatures.

7.1.6 Reference

1. J. W. Woods, E. E. Bloom, A. F. Zulliger, and L. R. Greenwood, "Status of ORR-MFE-2," *ADIP Quart. Prog. Rep. April-June, 1978,* DOE/ET-0058/2, pp. 132-40.

7.2 ETM RESEARCH MATERIALS INVENTORY — F. W. Wiffen, T. K. Roche, E. E. Bloom (ORNL), and J. W. Davis (McDonnell Douglas)

7.2.1 ADIP Task

ADIP Task I.D.l, Materials Stockpile for MFE Programs.

7.2.2 Purpose and Scope

The Office of Fusion Energy (ETM) of the Department of Energy has assigned program responsibility to ORNL for the establishment and operation of a central source or inventory of research materials to be used in the Fusion Reactor Materials research and development programs of the DOE. The primary objective is to provide a common supply of materials for use in the nationally coordinated Fusion Reactor Materials Programs. This will minimize unintended materials variables, and provide for economy in procurement and for centralized recordkeeping. Initially this inventory is to focus on materials related to first wall and structural applications and related research, but various special-purpose materials may be added in the future. It is recognized that materials supplementary to this inventory will be introduced to the ETM programs from time to time, and records of those materials shall be made available to ORNL and incorporated in the records of the ETM Research Materials Inventory.

The use of materials from this inventory for research that is coordinated with or otherwise related technically to the Fusion Reactor Materials Program of DOE but which is not an integral or directly funded part of it is encouraged, with the understanding that the results of such research be made available to the Fusion Reactor Materials Program.

7.2.3 Materials Requests and Release

Materials requests from DOE contractors shall specify the requested amount of material and the preferred product form. The request must provide a statement of the programmatic end use and agreement and that any characterization information developed by the user shall be supplied to the inventory records. Requests for materials shall be directed to ETM Research Materials Inventory at ORNL (Attention: F. W. Wiffen).

Materials will be released directly if:

(a) The material is to be used for programs funded by ETM, with goals consistent with the approved Materials Program Plans of the Materials and Radiation Effects Branch.

(b) The requested amount of material is available, without compromising other intended uses.

Materials requests that do not satisfy both (a) and (b) will be discussed with the staff of the Materials and Radiation Effects Branch, Office of Fusion Energy, for agreement on action.

7.2.4 Records

Chemistry and materials preparation records will be maintained for all inventory material. Additional characterization of materials will be recorded when it becomes available.

All materials supplied to program users will be accompanied by summary characterization information, as well as a list of other information that is available on request.

All materials transfers will be reported to the Materials and Radiation Effects Branch, Office of Fusion Energy. Periodic reporting will be quarterly until such time as the amount of material handled warrants more frequent reporting.

7.2.5 Summary of Current Inventory (September 1978)

7.2.5.1 Path A Alloys

1. Reference alloy — 20%-cold-worked type 316 stainless steel.
   Sheet and rod are at ORNL now.
   Tubing is scheduled for October 1978 delivery.
   Rework will be scheduled as required.
2. Prime Candidate Alloy (PCA) (Fe–16 Ni–14 Cr–2 Mo–Mn, Ti, Si, C).
   An order has been placed for 450 kg (1000 lb) product.
   Delivery of sheet, rod, and ingot is scheduled for October 1978.
3. PCA tube production and remelt for composition variation is planned for FY 1979.

7.2.5.2 Path B Alloys

4. A reference heat of PE-16 is in stock at ORNL.
   Sheet and rod are available.
   Tubing is scheduled for October 1978 delivery.
   Rework will be scheduled as required.

5. Base Research Alloys

Alloy	Ni	Cr	Mo	Nb	Ti	Al	Si
B-1	25	10	1		3	1.5	0.3
B-2	40	12	3		1.5	1.5	0.3
B-3	30	12		2	2	0.5	0.3
B-4	40	12		3	1.8	0.3	0.3
B-6	75	15		1	2.5	1.5	0.3

An order has been placed for two 140-kg (300-lb) heats of each alloy in 0.1 by 0.1-m (4 by 4-in.) bars. These are due at ORNL in September 1978. The breakdown to product form will be delayed until FY 1979, and remelt for compositional variation will be delayed until FY 1979 or later.

7.2.5.3 Path C Alloys (Refractory Alloys)

6. Small amounts of several niobium- and vanadium-base alloys are currently available at ORNL. Quantity and product forms are limited.

7. An order has been placed for the purchase of approximately 6 kg each of five alloys. Only sheet and rod will be produced.

   Alloys: Nb–1% Zr
   Nb–5% Mo–1% Zr
   V–20% Ti
   V–15% Cr–5% Ti
   V–9% Cr–3.3% Fe–1.3% Zr–0.05% C (Vanstar 7)

   Delivery of material is scheduled for April 1979.

7.2.5.4 Path C Alloys (Reactive Alloys)

8. The titanium-base scoping alloys have the following compositions, wt %:

Alloy	Al	V	Mo	Zr	Sn	Cr	Si
Ti-64	6	4					
Ti-6242s	6		2	4	2		0.09
Ti-5621s	5		1	2	6		0.25
Ti-38644	3	8	4	4		6	

At least 0.75 m^2 (1200 $in.^2$) of each of these alloys is currently available in 0.76-mm (0.030-in.) thickness. This sheet is from the same heat as material currently in reactor experiments. Larger section sheet of alloy Ti-56215 is also available.

Orders are now being developed to purchase new stocks of each of these alloys, to provide all needed product forms from a single heat. Delivery dates have not yet been determined.

The titanium-base alloys are stored at McDonnell Douglas. However, inventory control and materials release are handled by ORNL. Material requests should be addressed to ORNL.

7.3 IRRADIATION EXPERIMENT SCHEDULE

The following charts show the irradiation experiment schedule, including experiments completed, in progress, and planned. Experiments are presently under way in the ORR and HFIR, which are mixed-spectrum reactors, and the EBR-II, a fast reactor. There has been considerable revision in the experiments planned for irradiation in HFIR in 1979 and early 1980. Both materials and schedule of HFIR-CTR-26 through HFIR-CTR-33 have been revised because of alloy availability and recommendations developed by the ADIP Subtask groups on swelling and microstructure and on mechanical. behavior. It is recognized that HFIR provides the only effective means of examining behavisr of those alloys containing nickel (Path A and B alloys) at the very high helium contents representative of our goal fusion reactor exposures or lifetimes. Briefly, the strategy is to examine the effects of high helium content (up to several thousand parts per million) on the key properties of a reference alloy (20%-cold-worked type 316 stainless steel). Displacement damage effects will also be present, but the He/dpa ratio will not be that of a fusion spectrum. Once trends are established for the variation of a given property with helium content, it will be possible to select a more limited matrix (irradiation temperature and helium contents as variables) for use in alloy development. The influence of helium-to-displacement ratio will be examined through a comparison of changes in key properties determined in the ORR spectral tailoring experiments (i.e., He/dpa ratio approximately matches that of a fusion spectrum) with property changes determined in EBR-II (He/dpa $\ll$ fusion spectrum) and HFIR (He/dpa $\gg$ fusion spectrum).

Experiment Designation	Major Objective
A. Oak Ridge Research Reactor	
ORR-MFE-1 / ORR-MFE-2	Experiments to scope the effects of composition and microstructure on the tensile, fatigue, and irradiation creep of representative path A, B, and C alloys.
ORR-MFE-3	Effects of irradiation on postirradiation fatigue crack growth in representative path A, B, and C alloys.
ORR-MFE-4	Effect of irradiation on tensile, fatigue, and irradiation creep of path A PCA (Prime Candidate Alloy) and path B base research alloys. Spectral tailoring to maintain correct He/dpa ratio. Irradiation on continuing basis.

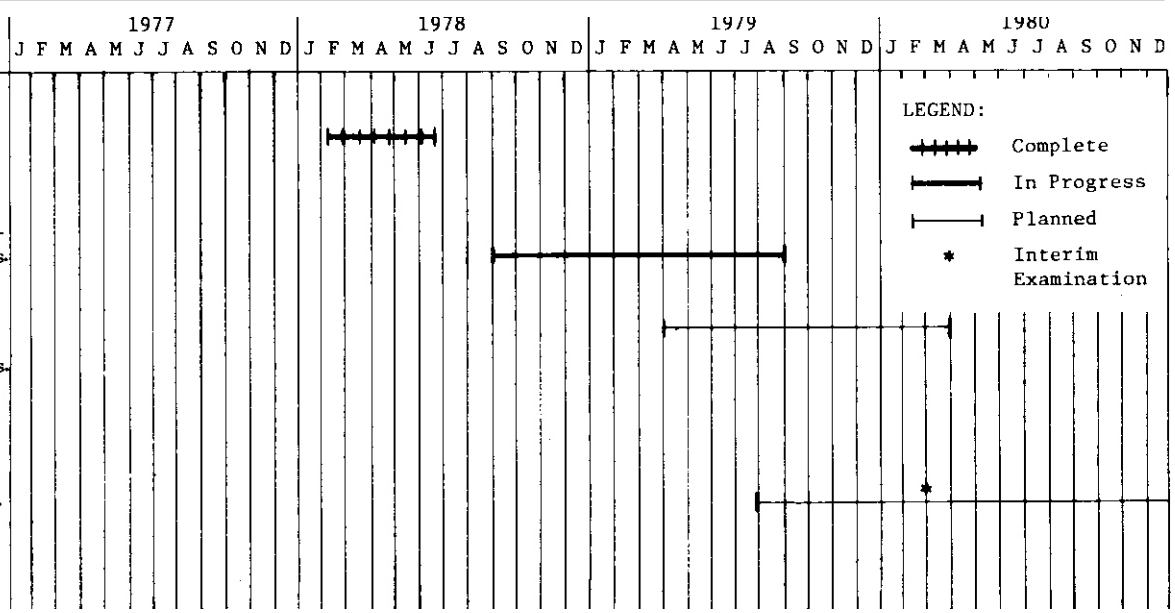

Experiment Designation	Major Objective
ORR-MFE-5	In-reactor fatigue crack growth experiment
B. Experimental Breeder Reactor II	
Subassembly X 264	Effect of preinjected helium (2–200 at. ppm) on microstructure and tensile properties of 316 SS, PE-16, V and Nb alloys. Fluence $\leq 2.3 \times 10^{26}$ n/m^2, 500–825°C.
Subassembly X 287	Effect of preinjected helium (2–200 at. ppm He) on microstructure and tensile properties of 316 SS, PE-16, V and Nb alloys. Fluence $\leq 4 \times 10^{26}$ n/m^2, 400–700°C.
Subassembly X 217D	Stress relaxation Ti Alloys
See footnotes [1] [2] and [3]	Effect of irradiation on swelling, tensile, fatigue, and crack growth properties of Ti scoping alloys. 370, 450, and 550°C, position in reactor not finalized, therefore no fluence estimate.

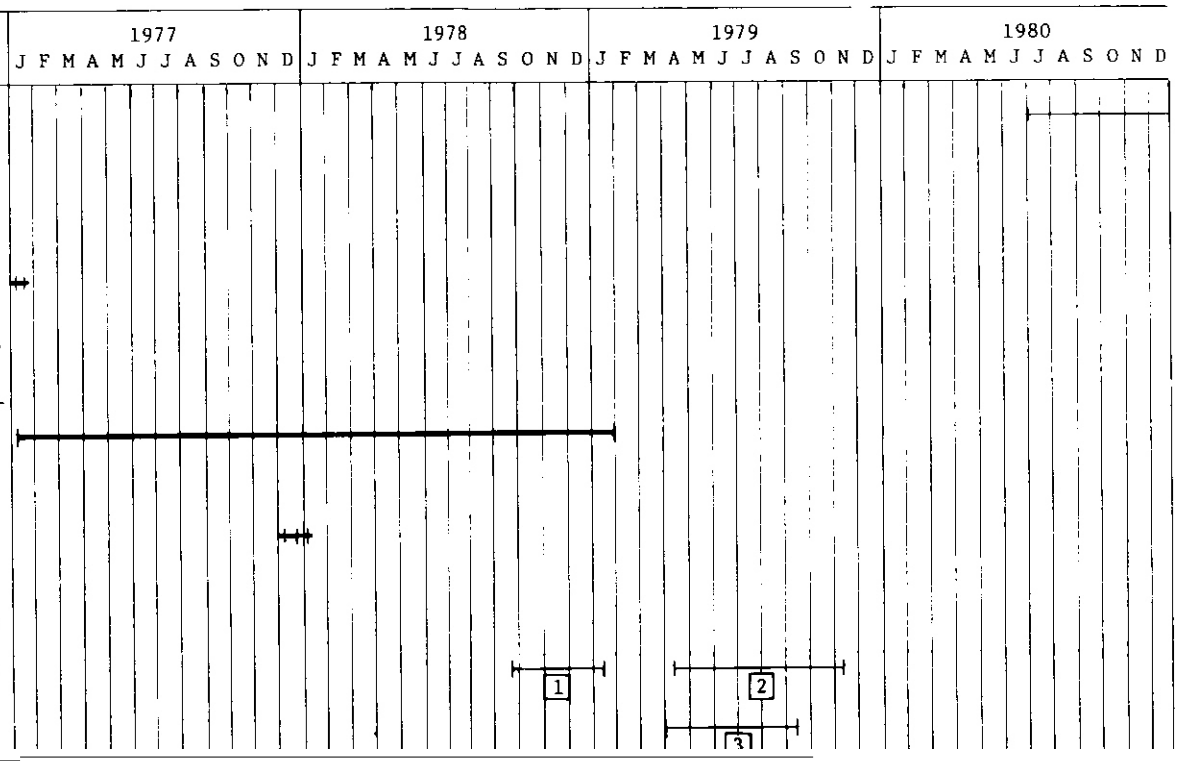

[1] EBR-II, row 2, pins 284, 285, and 286.

[2] EBR-II, row 2, pins 285 and 286.

[3] EBR-II, row 4, pin 284 reconstituted and irradiation continued in row 4.

Experiment Designation	Major Objective
Experiment plan depends on alloy availability. EBR-II space not yet identified.	Effect of Irradiation on swelling, tensile, fatigue, and crack growth properties of V and Nb scoping alloys. 370, 450, 550, and 650°C. Position in reactor not finalized, therefore no fluence estimate.
C. High Flux Isotope Reactor (HFIR)	
HFIR-CTR-4	PE-16 for swelling and tensile properties, 300–700°C 2.2–4.5 dpa, 100–350 at. ppm He
HFIR-CTR-7	PE-16 for swelling and tensile properties, 300–700°C 9–18 dpa, 1250–3000 at. ppm He
HFIR-CTR-8	duplicate of -7
HFIR-CTR-9	316 and 316 + Ti for swelling and tensile properties, 280–680°C, 9–18 dpa, 400–1000 at. ppm He

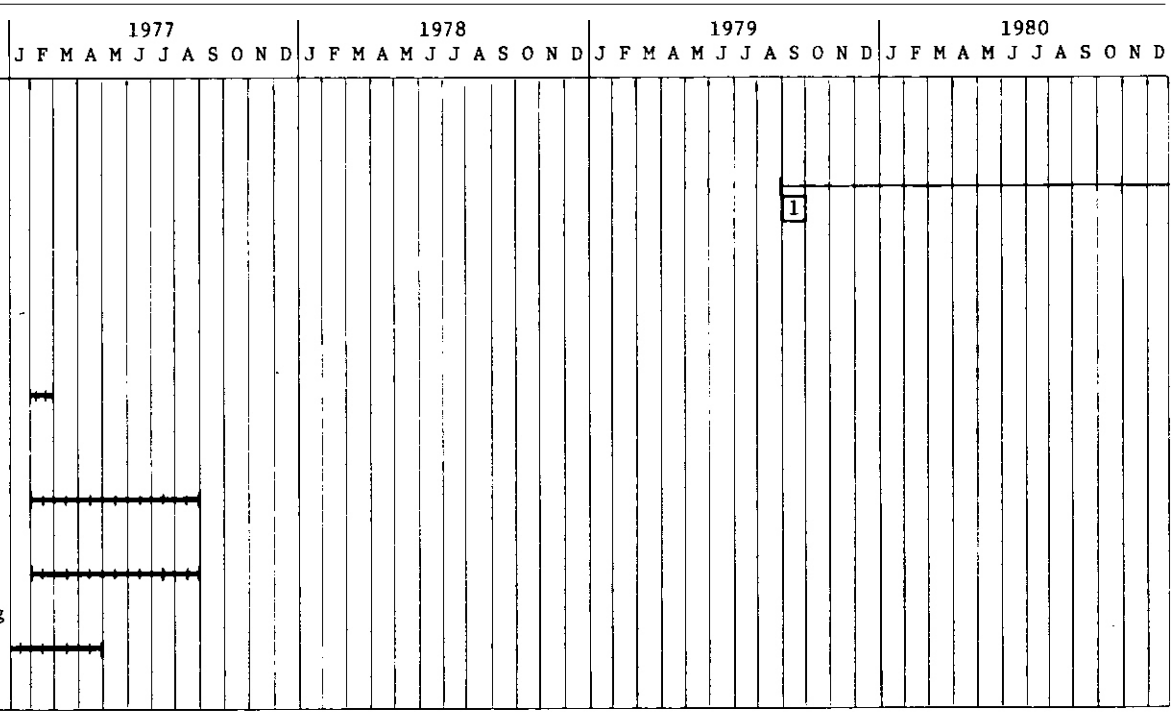

[1] Earliest date irradiations can begin on present alloy development schedule.

Experiment Designation	Major Objective
HFIR-CTR-10	duplicate of -9
HFIR-CTR-11	duplicate of -9
HFIR-CTR-12	316 and 316 + Ti for swelling and tensile properties, 280–680°C, 5.5–11 dpa, 200–500 at. ppm He
HFIR-CTR-13	duplicate of -12
HFIR-CTR-14	20%-CW 316 for fatigue testing 300°C. 9–18 dpa, 400–1000 at. ppm He
HFIR-CTR-15	20%-CW 316 for fatigue testing 500°C, 5.5–11 dpa, 200–500 at. ppm He
HFIR-CTR-16	316, welds, PE-16, and Inconel 600 for swelling and tensile properties, ~55°C, 5.5–11 dpa, 150–2700 at. ppm He (depending on alloy)
HFIR-CTR-17	Type 316 welded with 16-8-2 filler metal for tensile properties and failure analysis, 280–620°C, 6.7–13 dpa, 180–460 at. ppm He in weld metal

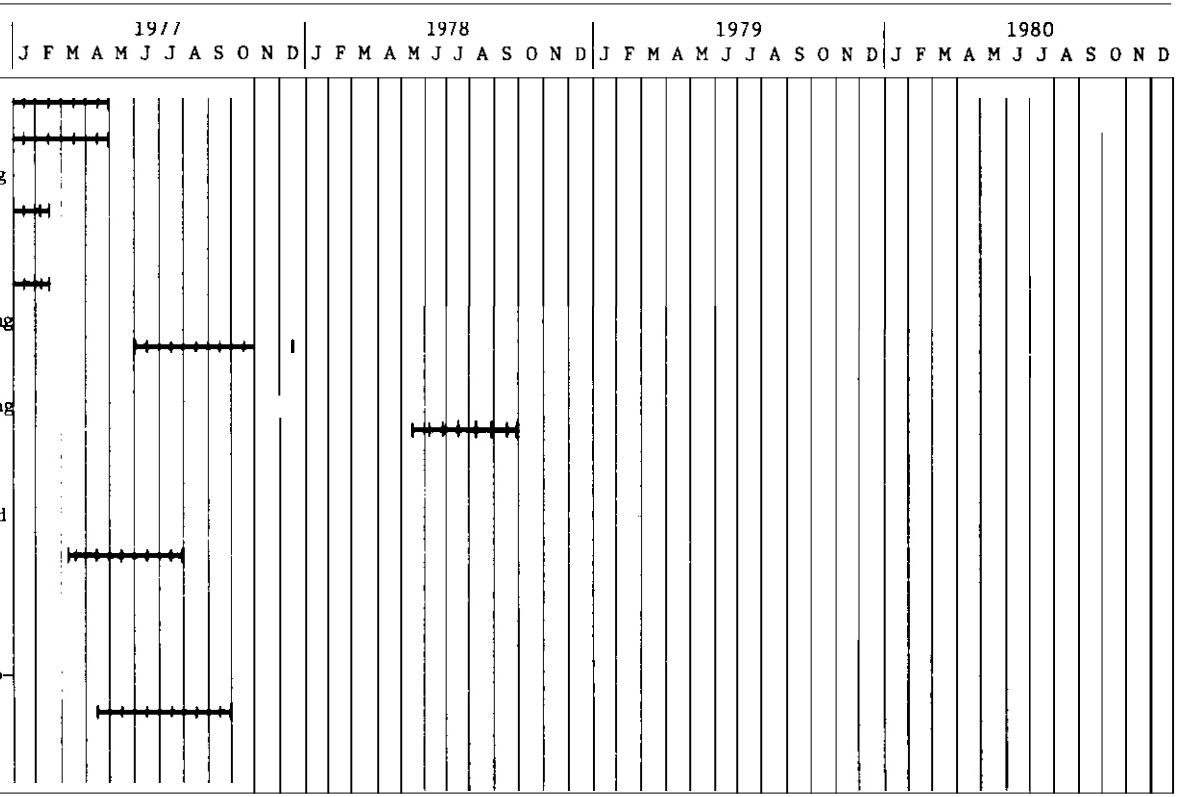

Experiment Designation	Major Objective
HFIR-CTR-18	PE-16 and 20%-CW type 316 for swelling and tensile properties, 280–700°C, PE-16: 17–27 dpa, 3400–5600 at. ppm He 316: 27–34 dpa, 1600–2100 at. ppm He
HFIR-CTR-19	316 welded with 316 filler metal for tensile properties, 280–620°C, 5.5–11 dpa, 200–500 at. ppm He
HFIR-CTR-20	20%-CW 316 for fatigue testing, 300°C, 5.5–11 dpa 200–500 at. ppm He
HFIR-CTR-21	20%-CW 316 for fatigue testing, 500°C, 9–18 dpa, 400–1000 at. ppm He
HFIR-CTR-22	duplicate of -20
HFIR-CTR-23	PE-16 for fatigue testing 300°C, 4.4–9 dpa, 370–1000 at. ppm He

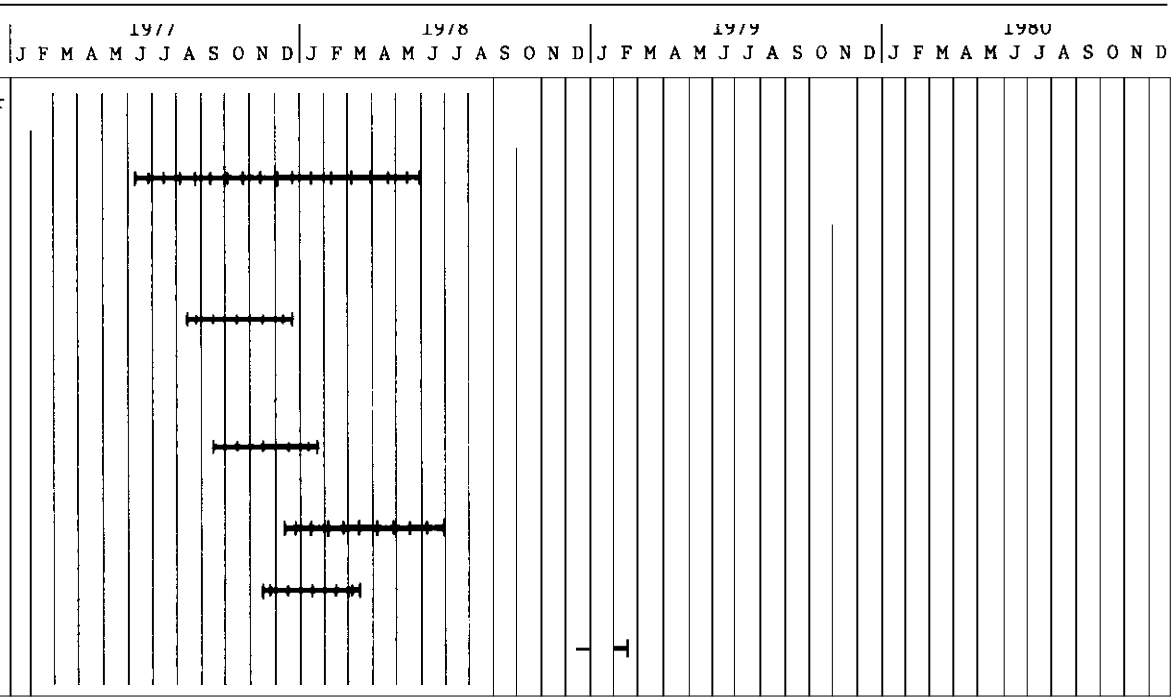

Experiment Designation	Major Objective
HFIR CTR-24	Temperature calibration, tensile properties of MFE Ref. 316, 2.25 dpa, 30 at. ppm He
HFIR CTR-25	Temperature calibration, tensile properties of MFE Ref. 316, 2.25 dpa, 30 at. ppm He
HFIR CTR-26	Swelling and tensile properties of MFE Ref. 316, 32 dpa, 1900 at. ppm He
HFIR CTR-27	Swelling and tensile properties of MFE Ref. 316, 56 dpa, 3450 at. ppm He
HFIR CTR-28	Swelling and tensile properties of MFE Ref. 316, 32 dpa, 1900 at. ppm He
HFIR CTR-29	Swelling and tensile properties of MFE Ref. 316, 56 dpa, 3450 at. ppm He
HFIR CTR-30[a]	Swelling and tensile properties, Path A PCA microstructural variations, 40 dpa, 2500 at. ppm He
HFIR CTR-31[b]	Swelling and tensile properties, Path B PCA microstructural variations

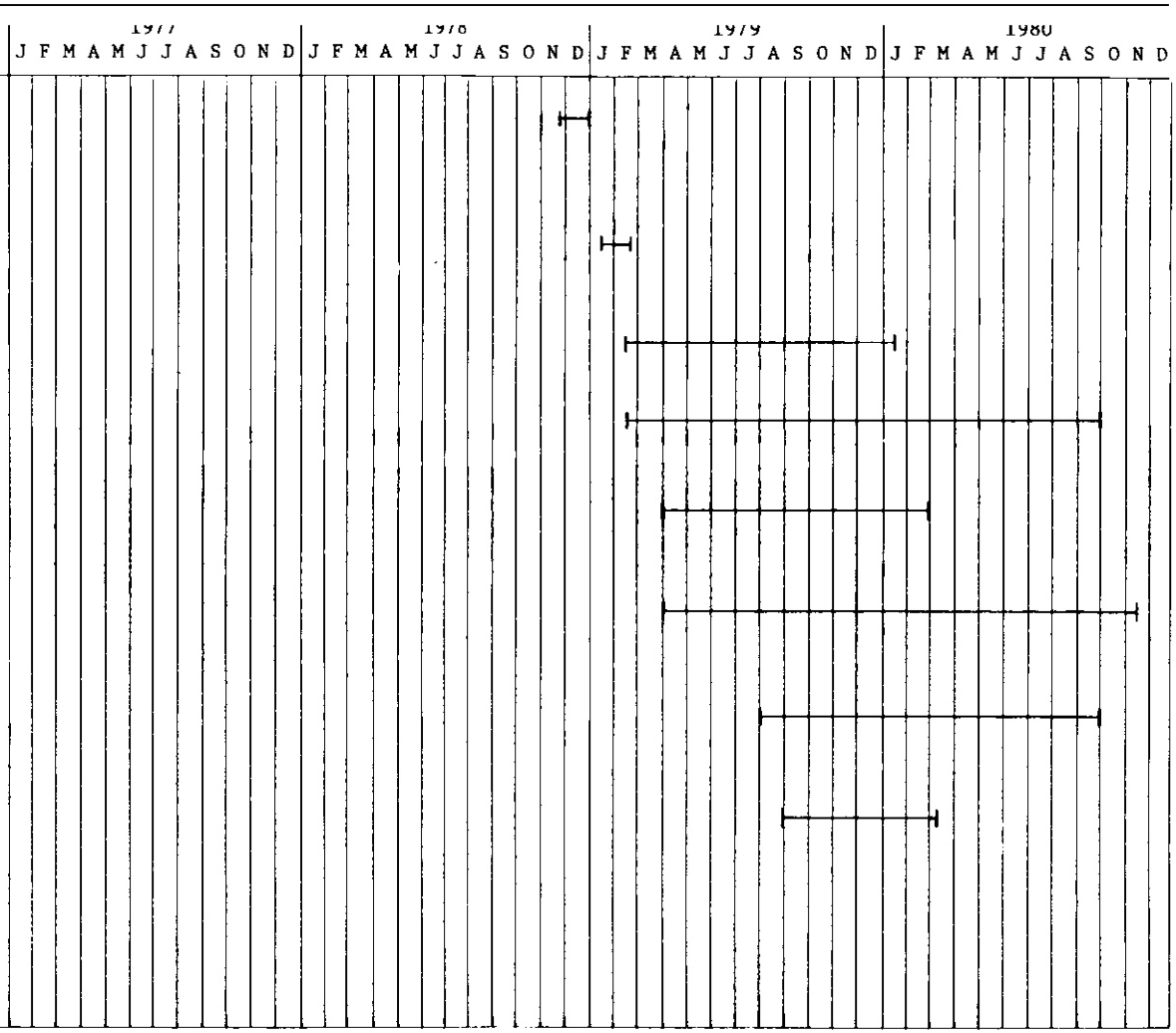

[a]Assumed 18 cycles for planning.

[b]Assumed 8 cycles for planning.

8. CORROSION TESTING AND HYDROGEN PERMEATION STUDIES

Corrosion, erosion, and mass transfer are processes that may degrade mechanical properties, alter heat transfer characteristics of heat transport systems, and present maintenance problems when radioactive nuclides are involved. The importance of hydrogen permeation and the behavior of hydrogen in the alloy systems under development is clear from consideration of tritium inventory, containment, etc. In the early stages of the development program, base-line information is required to define compatible or noncompatible alloy systems and coolants. As optimized alloys are developed, more detailed data on effects of adjustments in alloy composition or structure may be required. Extensive engineering compatibility data will be required on the final optimized alloys.

8.1 CAPSULE TESTS OF TYPE 316 STAINLESS STEEL IN NITROGEN-CONTAMINATED LITHIUM — P. F. Tortorelli and J. H. DeVan (ORNL)

8.1.1 ADIP Task

ADIP Task I.A.3, Perform Chemical and Metallurgical Compatibility Analyses.

8.1.2 Objective

The purpose of this program is to determine the chemical compatibility of iron-base alloys with metallic lithium. Structural steel specimens are exposed to static lithium containing selected solute additions to identify the kinetics and mechanisms that govern the corrosion of steels by lithium. Specific program objectives are (1) to determine the effects of N, C, H, and O on apparent solubilities of stainless steel components in lithium; (2) to determine the C and N partitioning coefficients between stainless steels and lithium; (3) to determine the effects of soluble (Ca, Al) and solid (Y, Zr, Ti) active metal additions on corrosion of stainless steels by lithium; and (4) to determine the tendencies for dissimilar-metal mass transfer between stainless steel and V, Nb, and Mo.

8.1.3 Summary

Approximately 2 wt % N in lithium significantly enhanced the degradation of type 316 stainless steel, with the corrosion rate decreasing as a function of time. At 500°C, the corrosion was uniform, while at 600 and 700°C, grain boundary attack dominated. As-rolled type 316L stainless steel had worse corrosion resistance to nitrogen-contaminated lithium than fully annealed type 316. We do not know whether the decreased resistance is attributable to differences in microstructure or alloy composition. While the corrosion of type 316 stainless steel in Li–2% N is more severe than in relatively pure lithium, such effects are expected to be transient in a closed system.

8.1.4 Progress and Status

An earlier report[1] presented initial results from static capsules containing nitrogen-contaminated lithium. The capsules were tested for 1000 and 2000 h at 500, 600, and 700°C. Approximately 2 wt % N was added to the

lithium in the form of Li_3N, and the solution was sealed inside a type 316 stainless steel capsule with a type 316 coupon. The results from these experiments showed that the presence of nitrogen in lithium significantly increased the corrosion. To study this corrosion behavior in more detail, additional capsule tests were conducted between 50 and 1500 h at 500, 600, and 700°C. The weight change data from these tests are listed in Table 8.1.1 together with earlier data from the 1000- and 2000-h exposures. We attribute the scatter in the results to inadequate mixing of the Li_3N in the lithium, leading to nonuniform corrosion in certain cases. Depsite the scatter, it is apparent from these data that the corrosion is much more severe at all exposure times than for base-line tests conducted with relatively pure lithium.

Table 8.1.1. Weight Changes Due to Exposure of Type 316 Stainless Steel to Li—2 wt % N

Time (h)	Temperature (°C)	Weight Change (g/m^2)
	Type 316 Stainless Steel	
50	500	−17.3
50	600	−13.4
50	700	−17.1
100	500	−20.3, −2.7, −39.0
100	600	−14.7, +0.7, −44.5
100	700	−18.9, −28.8, −6.2, −35.6
243	600	−16.2
243	700	−20.0
1000	500	−51.5
1000	600	−39.0
1000	700	−51.0
1500	500	−58.6
1500	600	−62.9
1500	700	−57.4
2000	500	−49.8
2000	600	−43.0
2000	700	−44.8
	Type 316L Stainless Steel	
100	500	−37.0
100	600	−43.8
100	700	−52.3

The metallographic examinations of type 316 stainless steel coupons exposed to Li—2% N provided a more consistent index of corrosion than the weight change measurements. At 500°C, the specimens exhibited a uniform corrosion product film, as shown in Fig. 8.1.1(a). At 600 and 700°C, the attack was predominantly intergranular [for example, see Fig. 8.1.1(b) and (c)]. The depth of attack, x_u, defined as the thickness of the product layer at 500°C [as illustrated in Fig. 8.1.1(a)], is plotted as a function of exposure time in Fig. 8.1.2(a). Note that the rate of attack decreases with time. Similarly, a grain boundary penetration distance can be measured from the optical micrographs of samples exposed at 600 and 700°C. This depth is denoted x_g and is the average perpendicular distance from the surface to the point where the grain boundary attack stopped [see Fig. 8.1.1(b) and (c)]. Plots of x_g versus exposure time at 600 and 700°C are shown in Fig. 8.1.2(b) and (c), respectively. As at the lower temperature, the rates of attack decrease with time.

One set of type 316L stainless steel coupons was exposed to the Li—2%N solution for 100 h at 500, 600, and 700°C, and the resulting weight changes are listed in Table 8.1.1. These samples were inadvertently left in the as-rolled condition so that metallographic examinations of these specimens revealed microstructures that differed from those of the type 316 coupons. It is therefore difficult to compare the results from the two materials. The 700°C type 316L coupon exhibited grain boundary attack to a depth of 69 μm (see Fig. 8.1.3). At 500 and 600°C, the type 316L samples exhibited uniform corrosion attack to depths of 17 and 20—44 μm, respectively, after 100 h.

Olson et al.[2,3] studied corrosion of type 304L stainless steel in nitrogen-contaminated lithium and found that both the weight loss and grain boundary penetration were proportional to the square root of the exposure time. The penetration, x, could thus be expressed as

$$x = (kt)^{1/2} , \qquad (1)$$

where k is a function of temperature and the concentration of nitrogen in the lithium.[2,3] The present penetration data show a lower order power time dependence for exposures up to 2000 h:

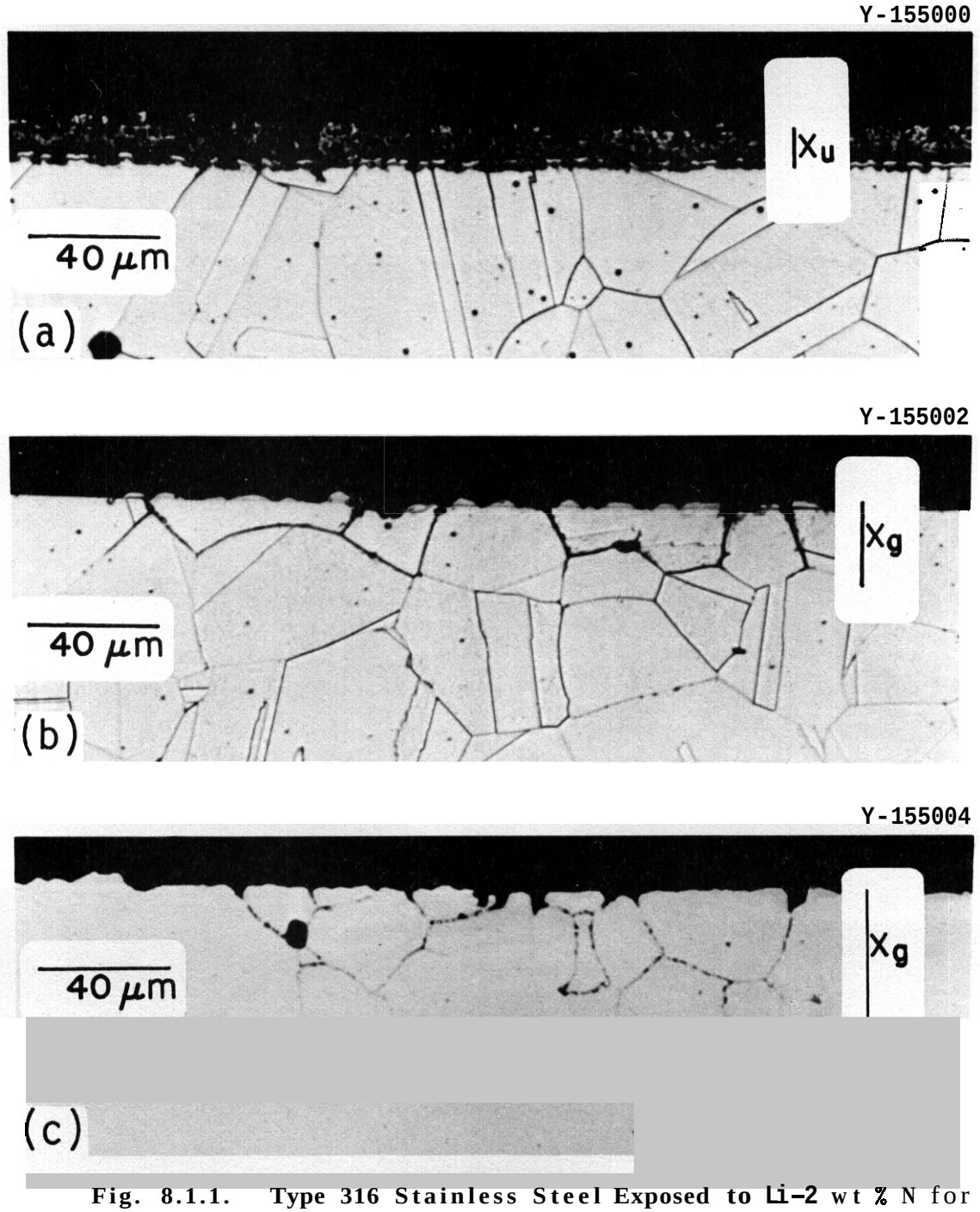

Fig. 8.1.1. Type 316 Stainless Steel Exposed to Li–2 wt % N for 100 h. (a) 500°C. (b) 600°C. (c) 700°C.

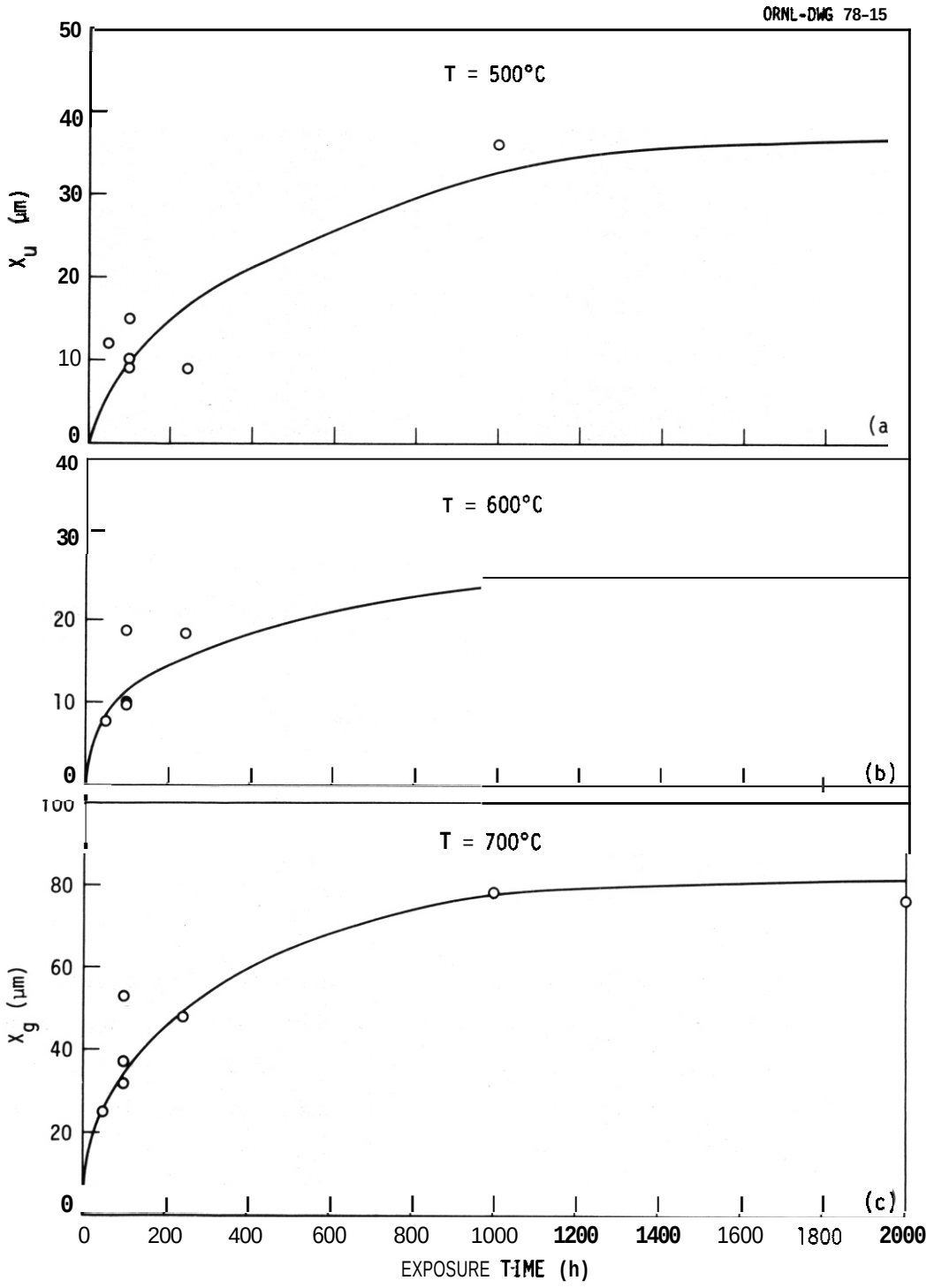

Fig. 8.1.2. Corrosion Depths as a Function of Exposure Time.

Y-156354

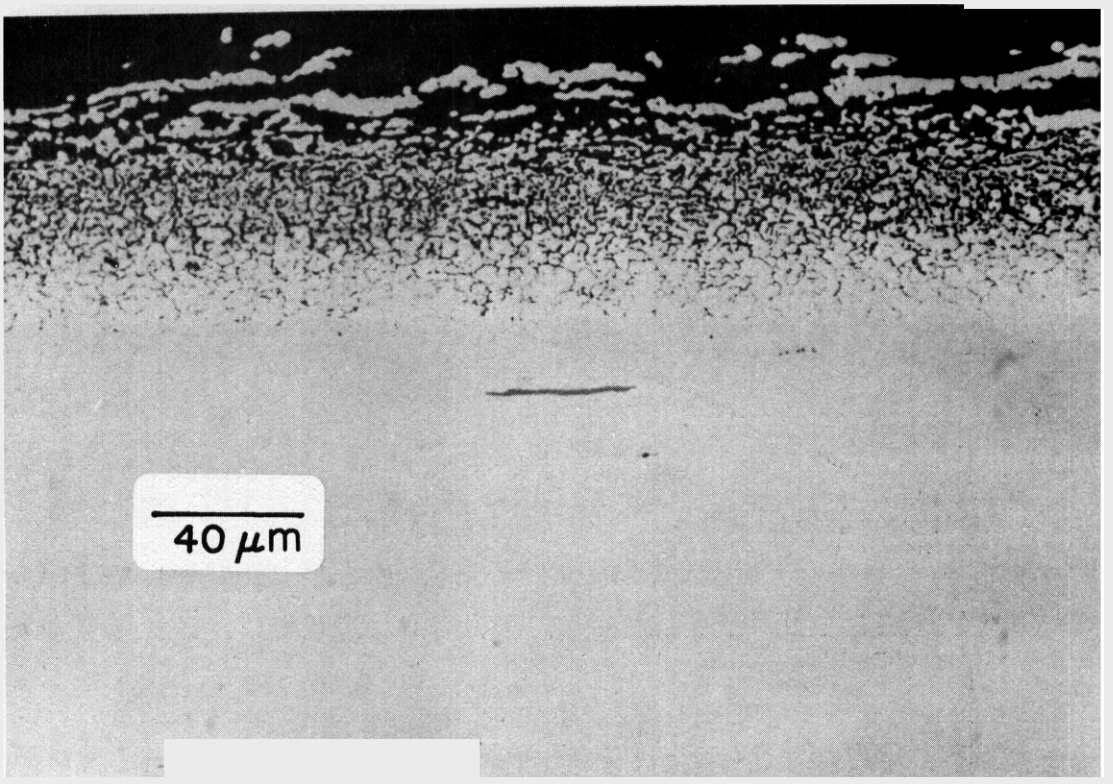

Fig. 8.1.3. As-Rolled Type 316L Stainless Steel Exposed to Li–2 wt % I for 100 h at 700°C.

$$x_u = 1.8 \quad (500°C) , \tag{2}$$

$$x_g = 3.1\ t^{0.29} \quad (600°C) , \tag{3}$$

$$x_g = 10.1\ t^{0.28} \quad (700°C) . \tag{4}$$

where x_u and x_g are in micrometers and t is in hours. The curves in Fig. 8.1.2 are generated from the respective equations. It should be noted however, that the exponents of the time term decrease as a function of time; that is, as data from longer exposures were included in the fit, the exponents decreased in each case.

The fact that the above results exhibited a different and variable time dependence compared with Eq. **(1)** can be ascribed to differing test conditions between our static capsules and those of Olson et al.[2,3] Olson's experiments were conducted in an open crucible inside a glove box

such that the nitrogen concentration was kept essentially constant throughout a particular test. In our procedure, however, the material and nitrogen-contaminated lithium are enclosed in a sealed capsule. This leads to a decreasing nitrogen concentration as a function of time as the nitrogen reacts with the stainless steel. If the corrosion process in static, nitrogen-contaminated lithium is solid-state diffusion controlled, as suggested by Olson's experiments,[2,3] then the time dependence of the corrosion depth in our particular experiments should have an exponential closed-form solution[4] rather than the form implied by Eqs. (1) through (4). We are presently analyzing our results in terms of applicable diffusion models, such as the uptake of reactants from stirred solutions. While our studies confirm that the corrosion of austenitic stainless steels is enhanced by the presence of nitrogen in lithium, they also indicate that the detrimental effects of such contaminants should be transient in a closed system.

While no definite conclusions can be drawn because we have just one data point at each temperature and the microstructure of the type 316L differed from that of the type 316 stainless steel, it is interesting to note that the type 316L was attacked to a greater extent under otherwise similar conditions. An apparent enhancement of corrosion for an L grade has recently been observed in experiments at the Colorado School of Mines,[5] where type 304L stainless steel was more prone to attack by nitrogen-contaminated lithium than type 304. This observation and the present result, if it is due to a difference in composition and not microstructure, both run counter to the explanations advanced[6] to explain the intergranular attack of austenitic stainless steels by lithium. Further work will be done to determine the controlling factor in the corrosion of type 316L relative to type 316 stainless steel.

A scanning Auger microprobe study of stainless steel surfaces exposed to pure and nitrogen-contaminated lithium has been initiated. The work is being done on a cooperative basis with R. J. Blattner of the Materials Research Laboratory of the University of Illinois. Initial examinations have been made on several types of stainless steels that were tested in relatively pure lithium. Further work will be done on

surfaces exposed to static lithium plus nitrogen and flowing lithium. Other capsule tests are planned for studying the corrosion of type 316 stainless steel as a function of the initial nitrogen concentration (0.05 to 0.30 wt %) in order to obtain a better understanding of the reaction mechanisms and kinetics.

8.1.5 Conclusions

1. The corrosion of type 316 stainless steel in Li–2.0 wt % N is severe. However, the corrosion rate decreases as a function of time such that this enhanced corrosion will be transitory in a closed system.

2. Type 316L stainless steel seems to be more susceptible to corrosion by nitrogen-contaminated lithium than type 316 because of eitner composition or microstructural differences.

8.1.6 References

1. J. H. DeVan and J. R. DiStefano, "Capsule Tests of Iron-Base Alloys in Lithium," *ADIP Quart. Prog. Rep. Jan.–Mar. 1978*, DOE/ET-0058/1, pp. 190–99.
2. R. A. Patterson, R. J. Schlager, and D. L. Olson, "Lithium Grain-Boundary Penetration of 304L Stainless Steel," *J. Nucl. Mater. 57:* 312–16 (1975).
3. D. L. Olson and W. L. Bradley, "The Corrosion of Ferrous Alloys in Nitrogen Contaminated Liquid Lithium," pp. 446–52 in *Int. Conf. Liquid Metal Technology in Energy Production, May 3–6, 1976,* ed. by M. H. Cooper, CONF-760503-P2.
4. J. Crank, *The* Mathematics of Diffusion, 2nd ed., Clarendon Press, Oxford, 1975, p. 56.
5. D. L. Olson and P. A. Steinmeyer, Colorado School of Mines, private communication, May 1978.
6. J. E. Selle and D. L. Olson, "Lithium Compatibility Research — Status and Requirements for Ferrous Materials," paper 107 presented at Corrosion '78, March 6–10, 1978, Houston.

8.2 THERMAL-CONVECTION LOOP TESTS OF STAINLESS STEEL IN LITHIUM — P. F. Tortorelli and J. H. DeVan (ORNL)

8.2.1 ADIP Task

ADIP Task I.A.3, Perform Chemical and Metallurgical Compatibility Analyses.

8.2.2 Objective

The purpose of this task is to evaluate the corrosion resistance of possible first-wall materials to flowing lithium in the presence of a temperature gradient. Corrosion rates (in terms of both dissolution and deposition) are measured as functions of time, temperature, additions to the lithium, and flow conditions. These measurements are combined with chemical and metallographic examinations of specimen surfaces in order to establish the mechanisms and rate-controlling processes for dissolution and deposition reactions.

8.2.3 Summary

Type 316 stainless steel thermal convection loops containing molten lithium are being used to investigate the effect of time on corrosion rates in lithium. Corrosion rates are initially time dependent, decreasing up to 2000 h, and constant after approximately 2000 h. Absolute weight losses among three loops were quite reproducible at short exposures (500 h) but diverged at longer times.

8.2.4 Progress and Status

As described previously,[1] two types of thermal-convection loops (TCLs) are being used to evaluate the compatibility of austenitic stainless steels with lithium. The first type is in the form of a 0.46-m by 0.64-m parallelogram that contains interlocking tab specimens of the same material as the loop. The loop is operated without interruption for 3000 to 10,000 h and is then cut open to remove tab specimens for analysis. The second type of TCL is larger (0.48 m by 0.76 m) and is designed so that tab specimens can be withdrawn and inserted without altering the

loop operating conditions.[1] In this way, corrosion rates can be monitored at selected time intervals for a given set of test specimens. At present, three of the latter type of loops are in operation, and one of the former type has recently been terminated after 3000 h (see Table 8.2.1).

In the preceding quarterly report,[2] we tabulated weight changes of specimens from loops 2, 3, and 4, which are all of the larger TCL design. These loops have continued operation to provide base-line data for comparing effects of nitrogen and aluminum additions to the lithium at a later stage of operation. Figure 8.2.1 presents plots of weight change versus time for three specimen positions in each of the loops. These three positions are denoted H2, H3, and H4 and are located within the higher temperature region of the loops, as shown in Fig. 8.2.2 (A detailed drawing of a loop can be found in ref. 1). The data for the three loops indicate that a constant corrosion rate is achieved after an initial period in which the rate constantly decreases. This linear dependence on time was observed for all the coupons that showed significant weight loss (H2, H3, H4, and H5 in Fig. 8.2.2). For loop 2 (represented by the circles in Fig. 8.2.1), the constant corrosion rate was

Table 8.2.1. Present Status[a] of Operating Loops

Loop	T_{max} (°C)	ΔT (°C)	Operating Time (h)	Test Variable
1[b]	600	175	3000	Effect of Li_3N addition to Li
2[c]	600	150	7832	Long-exposure base-line data
3[c]	600	150	3532	Time effect base-line data
4[c]	600	150	1500	Short-exposure base-line data, future Al additions to Li

[a] As of Sept. 11, 1978.

[b] Small, uninterrupted loop (terminated after 3000 h).

[c] Large loops with accessible specimens.

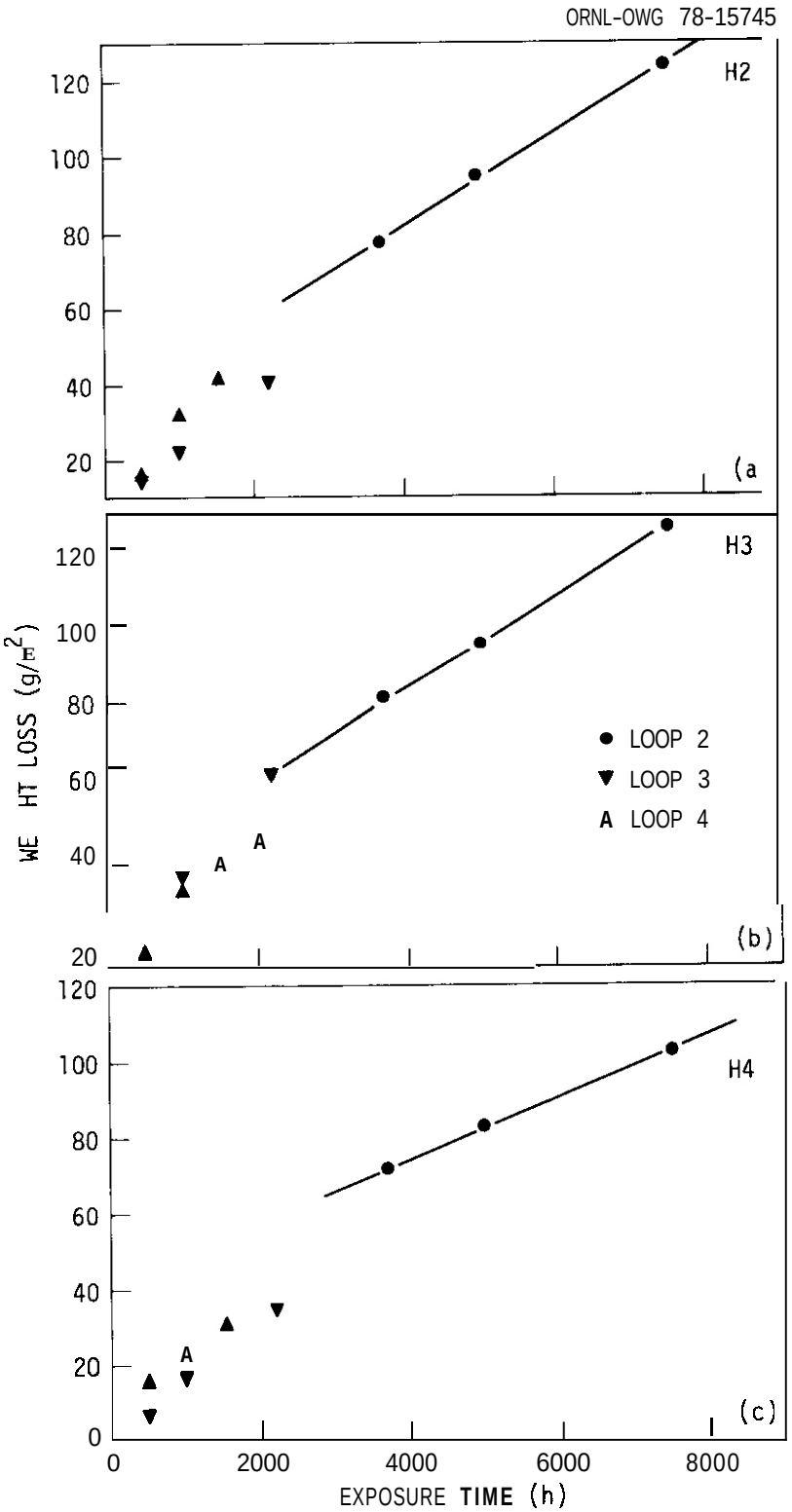

Fig. 8.2.1. Weight Change Versus Time for Three Specimen Positions in Each of Three Loops.

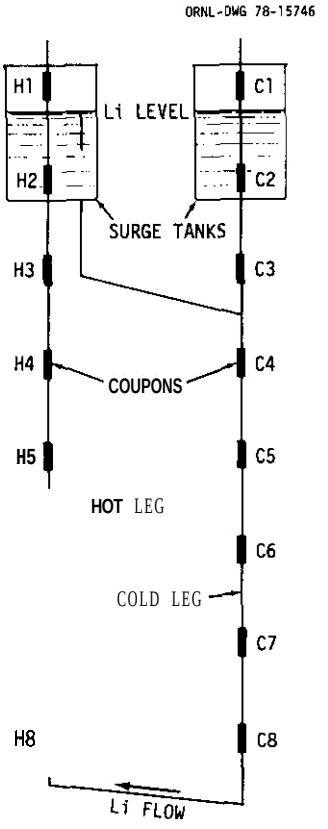

Fig. 8.2.2. Schematic Diagram of Coupon Positions in a Large Loop.

approximately 0.01 g/m^2 h (2.8 $\mu g/m^2$ s, 1.1×10^{-5} m/year, or 0.4 mil/year in terms of uniform corrosion). The absolute weight changes for loops 3 and 4 are lower than those for loop 2. However, the slope (rate) for the straight-line portions of the weight change curves of loops 3 and 4 are the same as for loop 2.

The constant corrosion rate observed above is consistent with the "steady-state, moving boundary" model[3] that was used earlier[1] to explain an observed constant ferrite thickness between 3000 and 10,000 h in flowing lithium. Nickel and chromium are preferentially leached from stainless steel when it is exposed to molten lithium under these conditions. The depletion leads to the development of a ferritic layer that is metallographically distinct from the underlying austenitic. After a transient period, which is characterized by a decreasing corrosion rate, a steady-state situation is reached whereby the iron-rich, lithium-exposed surface recedes at the same rate as the boundary between the ferrite and austenite. One of the obvious checks on this proposed model is to metallographically verify the constant ferrite layer thickness. However, we have not yet destructively examined any of the corrosion coupons.

As depicted in Fig. 8.2.2, coupons are positioned in both the heated and cooled legs of the loops. This allows us to develop a weight change profile around the loop and to determine if a mass balance is reached between dissolved and deposited material. Figure 8.2.3 is a compilation of the weight change data for coupons in loops 2 and 3 after several samplings. It is noteworthy that the locations of the balance points, that is, the positions in the loop where the dissolution and deposition processes balance (points of no weight change), do not significantly change as a function of exposure time. This type of behavior is consistent with the observation that dissolution rates in the hotter regions become constant with time.

As observed above in reference to Fig. 8.2.1, there appears to be a significant difference in the magnitude of the weight loss between loop 2 and loops 3 and 4 when the data of the latter loops are extrapolated to the longer exposure time of loop 2. Data for loops 3 and 4 at longer times will soon be available (see Table 8.2.1), and direct comparisons

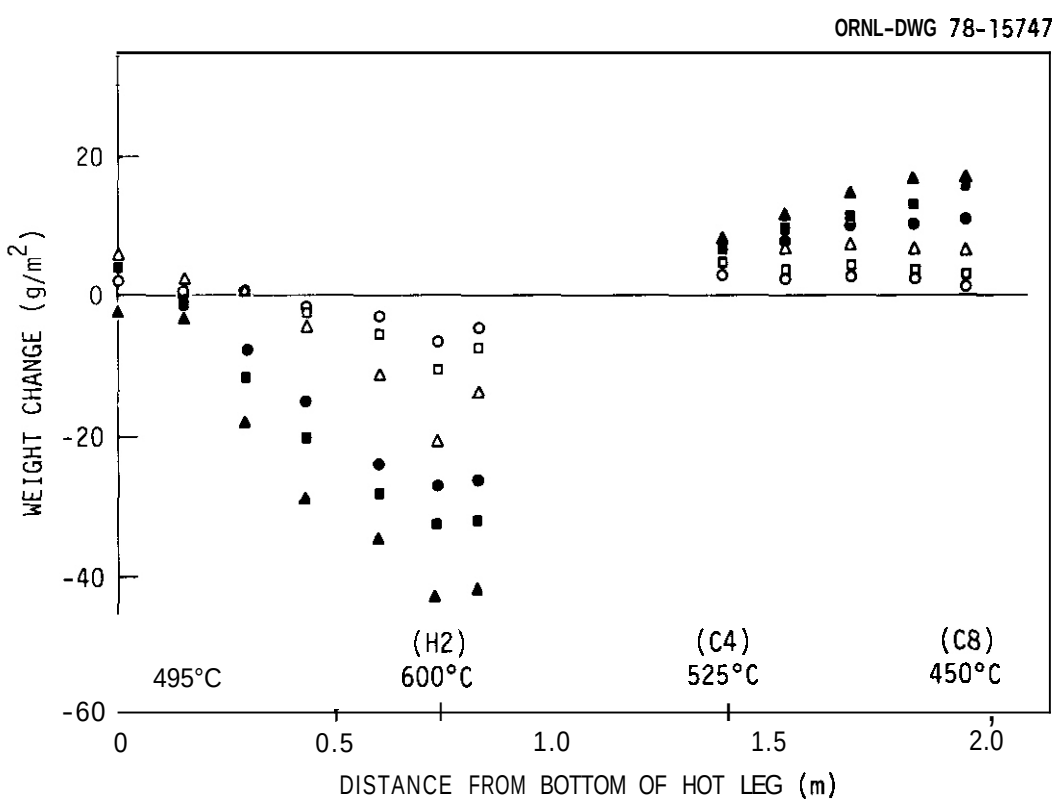

Fig. 8.2.3. Weight Change as a Function of Loop Position.

can then be made. This apparent discrepancy may be due to the fewer samplings that were made for loop 2 than for loops 3 and 4. Whereas loop 2 was not sampled until after 3700 h of operation, the coupons in loops 3 and 4 were cycled in and out at shorter intervals. As additional samplings of the present loops are completed, the effect of this variable will be better established. Another factor that we know is important is the temperature profile around the loop, which varies slightly among the three loops. This variable will also be studied in more detail by programmed changes in the cooler temperature profile in later tests. In any case, the "steady-state" corrosion rate appears to be approximately the same among the loops so that additive effects planned in later tests can be evaluated against the base-line rate of 0.01 g/m^2 h (2.8 $\mu g/m^2$ s).

Three loops are planned for start-up within the next four months, as shown in Table 8.2.2. Because of fabrication difficulties with the higher nickel alloy loops, only alloy 800 will be tested in the near future. The second loop will be constructed from a Ti–3.0 wt % Al–2.5 wt % V alloy and will contain coupons of various path C titanium alloys. The material for this loop was supplied by the McDonnell-Douglas Astronautics Company, and work has begun on its fabrication and on the preparation of the vacuum chamber that will house it. The third loop (type 316 stainless steel) will be similar to loops 2, 3, and 4 and will be dedicated from the beginning of operation to a study of the effect of nitrogen in flowing lithium on corrosion as a function of time.

Table 8.2.2. Planned Loops

Alloy	T_{max} (°C)	Test Variable
Alloy 800[a]	500	material
Ti alloy[a]	500	material
316 SS[b]	600	N additions to Li

[a]Small, uninterrupted loops.

[b]Large loop with accessible specimens.

8.2.5 Conclusions

1. After an initial period characterized by a decreasing corrosion rate, the corrosion in type 316 stainless steel thermal-convection loops becomes linearly dependent on time, with an approximate corrosion rate of 0.01 g/m^2 h (2.8 $\mu g/m^2$ s).

2. The reproducibility in weight loss among different loops at short exposure times is very good. There are indications, however, that the weight losses may be affected at longer times by sampling procedures or by small changes in the temperature difference.

8.2.6 References

1. J. H. DeVan and J. R. DiStefano, "Thermal-Convection Loop Tests of Type 316 Stainless Steel in Lithium," ADIP *Quart. Prog. Rep. January–March, 1978*, DOE/ET-0058/1, pp. 200–08.
2. P. F. Tortorelli and J. H. DeVan, "Thermal-Convection Loop Tests of Stainless Steel in Lithium," *ADIP Quart. Prog. Rep. April–June, 1978*, DOE/ET-0058/2, pp. 158–64.
3. E. G. Brush, *Sodium Mass* Transfer. *XVI, The Selective Corrosion Component of Steel Exposed to Flowing Sodium*, GEAP-4832 (March 1965).

8.3 COMPATIBILITY OF BLANKET, COOLANT, AND TRITIUM-PROCESSING SALTS — J. R. Keiser and E. J. Lawrence

8.3.1 ADIP Task

ADIP Task I.A.3, Perform Chemical and Metallurgical Compatibility Analyses.

8.3.2 Objective

Molten salts have been proposed for blanket, coolant, and tritium-processing applications in a fusion reactor. The purpose of this work is to determine the corrosion behavior of path A and B alloys in candidate molten salts.

8.3.3 Summary

A type 316 stainless steel thermal convection loop recently began operation with the proposed tritium-processing salt LiF-LiCl-LiBr. Two additional thermal convection loops are being used to study the corrosion properties of Li_2BeF_4 and $NaNO_2$-KNO_3-$NaNO_3$.

8.3.4 Progress and Status

The molten salt mixture LiF-LiCl-LiBr (22-31-47 mol %) is being evaluated at Argonne National Laboratory (ANL) as a process solvent for stripping tritium from lithium. V. A. Maroni of ANL has supplied us a quantity of this salt sufficient to determine its corrosivity in a type 316 stainless steel thermal-convection loop similar to the larger design used for lithium studies (Sect. 8.2). The loop is presently operating at a maximum temperature of 540°C and a temperature difference of 50°C. Corrosion specimens will be weighed after 500- to 1000-h intervals until a corrosion time dependence has been established.

Controlled-potential voltammetry is being employed to follow real-time changes in both the oxidation potential of the salt and the concentration of certain impurities and corrosion products. Salt samples will be taken and analyzed at regular intervals and the results can be used to help interpret the voltammetry data. After the corrosion

rate has been determined for the initial operating conditions, lithium will be added to the salt and corrosion measurements made under the new conditions.

Two other thermal convection loops are currently operating with molten salts. The status of all molten-salt loops is given in Table 8.3.1.

Table 8.3.1. Status of Molten-Salt Loops

Loop Material	Specimen Material	Salt Composition	Cover Gas	current operating Temperatures, °C		operating Time[a] (h)
				max	min	
31h stainless steel	316 stainless steel	$LiF-BeF_2$ (66-34 mol %)	Ar	650	525	22,583
Hastelloy N	316 stainless steel 12 specimens Hastelloy N 4 specimens	$NaNO_2-KNO_3-NaNO_3$ (49-44-7 mol %)	N_2	550	460	18.418
316 stainless steel	316 stainless steel	LiF-LiCl-LiBr (22-31-47 mol %)	Ar	540	490	98

[a]As of Sept. 18, 1978.

8.3.5 Conclusions

The status of thermal-convection corrosion loops with $LiF-BeF_2$, $NaNO_2-KNO_3-NaNO_3$, and LiF-LiCl-LiBr is summarized. The last of these was recently started.

8.4 HYDROGEN PERMEATION CHARACTERISTICS OF PATH A, PATH B, AND PATH C ALLOYS - E. H. Van Deventer and V. A. Maroni (Argonne National Laboratory).

8.4.1 ADIP Task

I.E.l. Hydrogen Dissolution and Permeation Effects. This task was added to the ADIP program plan during the first quarter of FY-1978. The results presented in this section contribute to Subtask I.E.l.l, Milestone I.E.1.b. The above title and assigned numbering are tentative, pending approval by the ADIP Task Group.

8.4.2 Objective

The objective of the work reported in this section is to provide base-line hydrogen dissolution and permeation data for the group of titanium-base alloys currently under examination as part of the ADIP Path C alloy development activities' . The hydrogen dissolution, out-gassing and permeation characteristics of this family of materials is vital to an understanding of their performance as first-wall and blanket structural materials for fusion devices. A further objective of this work is to begin examining methods for overcoming any serious hydrogen isotope uptake and migration problems associated with the rather strong hydride-forming nature of titanium and its alloys.

8.4.3 Summary

The hydrogen dissolution and permeation characteristics of the 5621S alloy of titanium have been evaluated. This alloy was found to have a permeability ~3000 times greater than that of conventional 300-series stainless steels. The observation of a pressure dependence somewhat greater than half-power was construed as evidence for a per-meation process that is partially limited by surface impurity effects. Roughly determined values for the solubility of hydrogen in the 5621S alloy were in the range of those reported for Ti-6%Al-4% V. The sur-face condition and mechanical integrity of the 5621S membrane appeared to be unaffected by ~2600 hours of hydrogen infiltration under typical power-reactor plasma-chamber conditions with respect to temperature,

gas pressure and gas composition.

8.4.4 Progress and Status

The hydrogen dissolution and permeation studies on titanium-base alloys initiated' during the third quarter of FY-1978 were continued through the fourth quarter. The investigation of a sample of the 5621S alloy' (Ti-5%Al-6%Sn-2% Zr-1%Mo-0.25% Si), supplied by J. W. Davis (MDAC), has been completed. The knife-edge-type gasket-sealed sample assembly described in the preceeding progress report' held up without failure during the ~16 weeks of study, despite periodic temperature cycling over the range from 500 K up to 920 K. The measured permeability of the sample (see Fig. *8.4.1)* was upwards of 3000 times greater than that of typical 300-series stainless steels at comparable temperatures and hydrogen driving pressures. The observed dependence on pressure, P, over the pressure range from 10^{-1} *to* 10^{2} Pa and temperature range from *687* to *920* K was near $P^{0.7}$ as shown in Fig. *8.4.2* (although the data in Fig. *8.4.1* were actually forced to fit a $P^{0.5}$ dependence for purposes of comparison with 316-SS). This result implies that surface impurity interactions are at least partially affecting the results, but to a lesser extent than in prior studies[3,4] of a-titanium, where a $P^{\sim 1.0}$ dependence was reported. Furthermore, we observed permeation rates that are 20 to 30 times greater than those measured previously for α-titanium.[3,4] This may be due either to a reduction of surface impurity influences on our results (compared to earlier work[3,4]) or a higher solubility and/or diffusivity of hydrogen in the 5621S alloy (than in a-titanium).

Transient data taken during the early stages of a permeation run on the 5621S alloy give evidence of the dissolution of large amounts of hydrogen in the alloy, as expected. Although refinement and analysis of the transient data are incomplete, the magnitudes of the hydrogen-solubility values are in the range anticipated for titanium-base materials,[5] and the derived diffusion coefficients are consistent with a partially surface-limited permeation process. In addition, following the first series of permeation measurements (A in Fig. 8.4.1), wherein

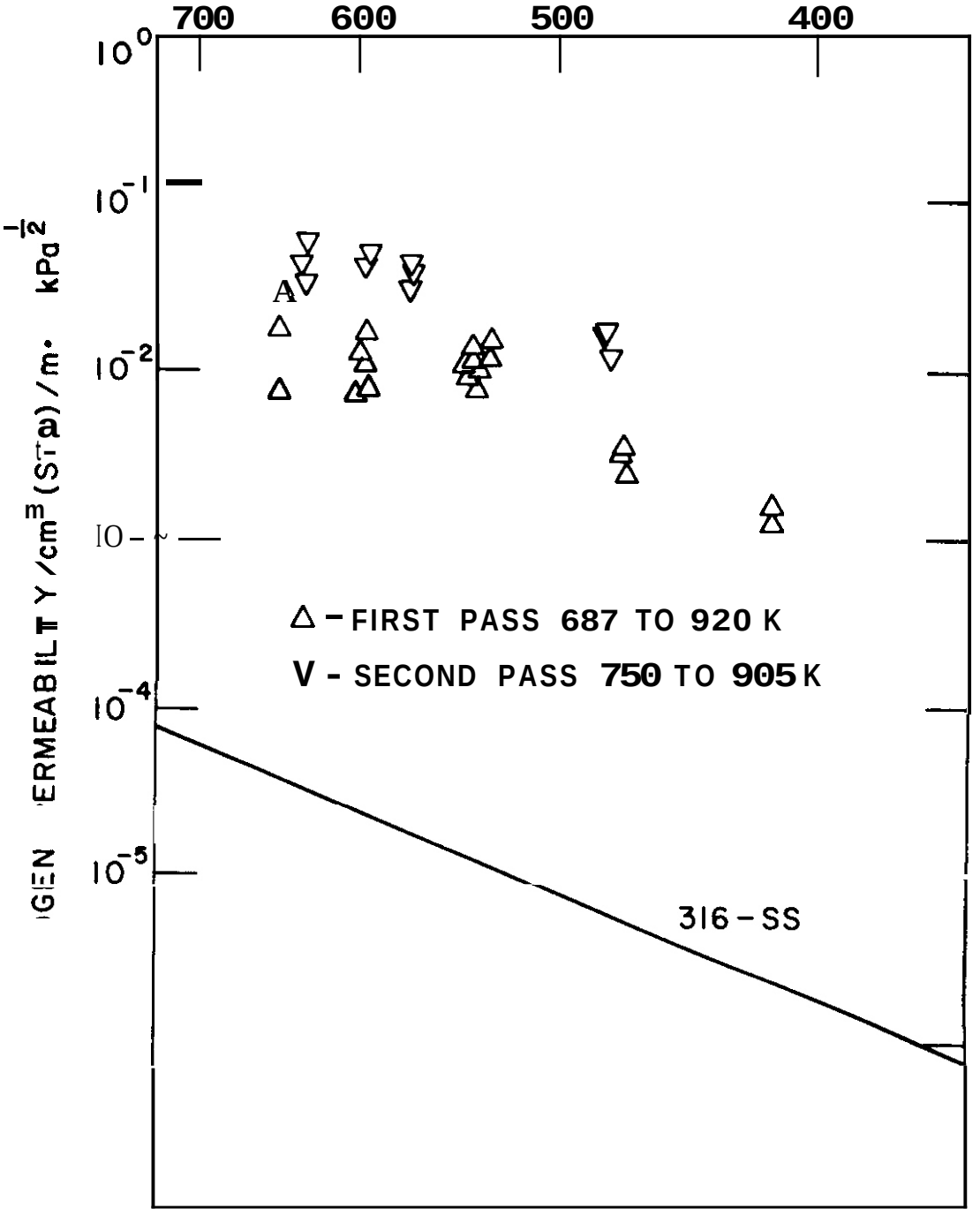

Fig. 8.4.1 Hydrogen permeability *versus* temperature for titanium alloy 5621S.

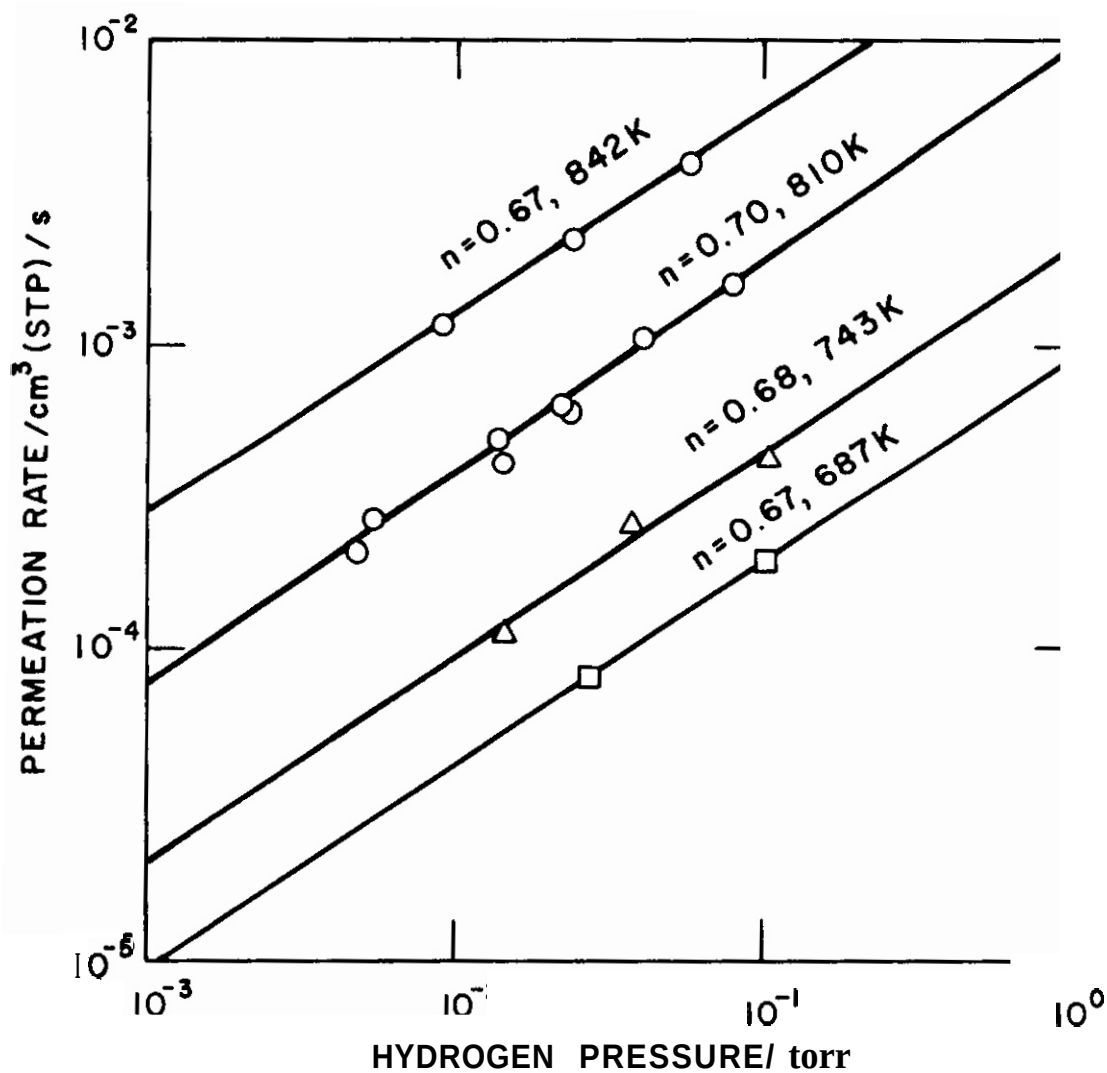

Fig. *8.4.2* **Hydrogen permeation rate** ***versus*** **hydrogen pressure at** *687, 743, 810,* **and** *842* **K** for **titanium alloy** 5621S.

the sample temperature was gradually increased from 687 to 920 K, a second series of measurements (∇ in Fig. 8.4.1), yielded higher peamea-tion rates in the 650 to 900 K range. This increase could be due in part to bulk-phase transformations that occurred when the alloy was at 920 K during the first series.

Following completion of the study discussed above, the sample holder was disassembled and the 5621S alloy specimen was removed for inspection. There was no visual evidence of change in the appearance or mechanical integrity of the specimen despite the fact that it had been subjected to ∿2600 hours of hydrogen infiltration. In particular, there was no doming of the membrane surface (which is usually indicative of hydrogen diffusion induced creep) and absolutely no discoloration of either surface which reflects favorably on the purity of the gas environment in our apparatus during the permeation measurements. The permeation specimen and a sample of the as-received 5621S alloy are being prepared for comparative micro-scopic and microprobe analyses.

From the brief description given above and the two attached figures, it is clear that in titanium-base alloys we will be dealing with materials that are susceptible to relatively high levels of hydrogen retention and permeation. (This should come as a surprise to no one.) Purthermore, in the environment of our experiments, which is representative of post-burn plasma-chamber gas environments, we observe no evidence of long-term re-ductions in permeability due to surface passivation or aging.

In preparation for follow-up work, we have received a sample of the 6-4 titanium alloy (Ti-6% A1-4% V) from J. W. Davis and have fabricated several specimens for permeation study. A nitride coating has been applied[6] to the surface of one of these specimens, using methods, pro-cedures and equipment described in reference 7. We plan to investigate the permeation characteristics of an as-received specimen, the nitrided specimen, and possibly an anodized sample in the coming months.

In order to insure that as much useful information as possible is derived from the present campaign to evaluate the hydrogen-interaction characteristics of titanium-base alloys (in the context of fusion reactor applications), a memorandum eliciting recommendations for pro-cedures and conditions to be applied during the campaign has been for-

warded to selected members of the ADIP community. The memorandum requests specific recommendations and suggestions on (1) sample selection and pretreatment, (2) experimental conditions for the dissolution/permeation studies, and (3) post-measurement analysis procedures. As an adjunct to our present work, which will be guided by the recommendations we receive, specimens of each titanium-alloy sample (normally 33 mm in diameter and 1-mm thick) subjected to hydrogen dissolution/permeation tests will be made available to members of other laboratories supported by the DOE/OFE Materials and Radiation Effects Branch upon request. The actual quantity and configuration of each specimen will be limited by sample size and user demand.

8.4.5 Conclusions

The 5621S alloy of titanium exhibits a permeability roughly 3000 times greater than that of ordinary 300-series stainless steels at temperatures (700 to 900 K) and hydrogen pressures (10^{-1} to 10^{2} Pa) in the range of interest for fusion power reactor first-wall applications. The observation of a pressure dependence somewhat greater than half-power indicates that the permeation process was partially controlled by surface impurity effects. Roughly determined values for the quantity of hydrogen dissolved in the alloy under the conditions of our experiments are near those reported for Ti-6%Al-4% V under similar conditions. Exposure of the 5621S alloy to ∿2600 hours of hydrogen infiltration in a typical plasma chamber environment (with respect to temperature, gas composition, and pressure) does not appear to have adversely affected its surface condition or mechanical integrity.

8.4.6 References

1. J. W. Davis *et at.*, *Microstructure of Titanium Scoping Alloys Prior to Irradiation*, Alloy Development for Irradiation Performance Progress Report for the Period Ending June 30, 1978, U. S. Department of Energy Report DOE/ET-0058/2 (1978) pp. 85-99.
2. E. H. Van Deventer and V. A. Maroni, Hydrogen *Permeation Characteristics of Path A, Path B, and Path C Alloys*, Alloy Development for

Irradiation Performance Progress Report for the Period Ending June 30, 1978, U. S. Department of Energy Report DOE/ET-0058/2 (1978) pp. 169-174.

3. D. L. Johnson and H. G. Nelson, "Determination of Hydrogen Permeation Parameters of Alpha Titanium Using the Mass Spectrometer," *Metall. Trans. 4:* 569-573 (1973).
4. K. K. Shah and D. L. Johnson, "Effect of Surface Pre-oxidation on Hydrogen Permeation in Alpha Titanium," Proceedings of the International Conference on the Effects of Hydrogen on Materials Properties, September 23-27, 1973, Champion, PA.
5. See J. W. Davis and G. L. Kulcinski, *Assessment of Titanium for Use in the First Wall/Blanket Structure of Fusion Power Reactors,* Electric Power Research Institute, EPRI ER-386, 1977, pp. 53-55.
6. Work performed in collaboration with D. M. Gruen (Argonne National Laboratory), G. O'Donnel and G. L. Kulcinski (University of Wisconsin).
7. M.-B. Liu, D. M. Gruen, *et al.,* "Ion Nitriding of Titanium and Zirconium by a D. C. Discharge Method," *High Temp. Sci. 10:* 53 (1978).

*U.S. GOVERNMENT PRINTING OFFICE : 1979 0-281-704/44